Proteomic Host Responses and Growth Properties of Highly Pathogenic H5N1 and Novel H7N9 Avian Influenza Strains

by

Philippe François Simon

A thesis submitted to the Faculty of Graduate Studies of

The University of Manitoba

In partial fulfillment of the requirements of the degree of

Doctor of Philosophy

Department of Medical Microbiology

University of Manitoba

Winnipeg

Abstract

Influenza viruses cause significant mortality and morbidity worldwide due to seasonal oubreaks as well as occassional, and sometimes devastating, pandemics. Estimates state that approximately 5% of the adult and 20% of the child population is infected yearly, leading to approximately a half-million deaths and three million severe infections in non-pandemic years. Aside from globally-circulating strains, zoonotic outbreaks caused by avian strains are a constant threat. In 1997, the first human cases of H5N1 infections occurred and since then strains of this subtype have killed approximately 700 people causing a severe disease with as high as 60% lethality rate. In March 2013, a strain of the H7N9 subtype started an epizootic in China causing a severe respiratory disease reminiscent of H5N1 infections and with a 20% case fatality rate. In this thesis, we have studied the host responses as well the viral replication kinetics of H5N1 and H7N9 strains and compared then to those of mild H1N1 seasonal and 2009 pandemic strains. During early infections of A549 cells, we have shown that the H5N1 virus induced a more profound and functional change to the host proteome. All viruses induced the NRF2-mediated oxidative stress responses and the H7N9 and H5N1 strains downregulated fibronectin, a host protein vital to infection for human strains. Using mathematical modeling and extensive growth kinetic analysis, we showed that the H5N1 and H7N9 strains had higher peak titers and faster growth kinetics. This was due to an higher infection rate for the H7N9 strain and an higher production rate for the H5N1 strain, compared to the human viruses. Conversely, the 2009 pandemic H1N1 strain had the poorest replication kinetics, longest eclipse phase and lowest infection rates. These results point towards the higher level of cellular disruption during infection with highly pathogenic strains of influenza, which may be indicative

of the more profound changes required to support growth of viruses with faster kinetics to higher titers. Furthermore, the greater changes in the cellular proteome that we have characterized *in vitro* may be connected to the significantly greater virulence associated with infection by avian viruses *in vivo*, opening a novel and productive avenue of investigation to understand viral virulence mechanisms.

Dedication

À toi Papa, je t'aime

À Mr. Hervé, pour avoir ouvert la porte de la science à plusieurs générations d'élèves. Merci.

Acknowledgments

Comme pour tout ce que je réussi à accomplir, la première personne que je souhaite remercier est ma blonde, Marie-Krystel pour son support infaillible au cours des épreuves des dernières années. Sans toi, je n'aurais jamais réussi à garder le moral et passer au travers de ce périple parfois houleux. On dit que derrière chaque grand homme il y a une femme encore plus forte. Je ne sais pas si je suis un grand homme, mais je suis convaincu que tu es la plus forte et formidable des femmes! Ensemble nous formons une équipe incroyable et jamais je ne pourrais suffisament te remercier pour tout le support, la patience et l'amour que tu me donne ;-)

À Jules, ta naissance quelque peu chaotique m'a servi de catalyseur pour réussir à terminer ce Doctorat et m'a montré quelles étaient les choses réellement importantes dans la vie.

Many thanks to my advisor, Darwyn Kobasa, for granting me the freedom and ressources to satisfy my curiosity. You have provided me with a unique, stringent and demanding vision of science, never stopping or slowing down until a problem is thoroughly and completely solved.

I also wish to warmly thank Kevin Coombs who went above and beyond his duties and became my mentor. You have made a significant contribution to my PhD and I will always be grateful for your help, advice and wisdom.

Steve, thank you for the positive energy and encouragements throughout the years. Your input, support and perspecitve on science have been a source of inspiration since day one.

To the NML Mass Spectrometry and Proteomic Core (Garrett, Stu, Patrick) you guys provided me with all the technical expertise I could have hoped for and de-mystified those big, expensive machines. Thanks also to Mike Carpenter for his patience in teaching me basic proteomics.

To the folks in the Respiratory virus and Zoonotics labs (Robin, Mike, Donnie, Mark, Nathalie, Maya, Antonia, Kristina, Laura) thanks for helping me set up in Level 3 and all the Flu reagents. Thank you Shaffy for letting me use that awesome cell culture robot!

To Catherine Beauchemin, Laura and Éric at Ryerson. After 7 years of collaboration, I finally start to understand the meaning of “infecting time”. Thank you for your patience in dealing with experimental error and explaining the model over and over again. Working with you has been a priviledge and I value our collaboration as a great example of what can be achieved when different fields finally decided to work together.

To my Brothers and Sisters at 17 (Winnipeg) Field Ambulance, you guys have been family from the day we moved to Manitoba. Tuesday night at the mess have played a pivotal role in maintining some measure of sanity ☺.

Merci à Léanie pour la FLEUR.

Also many thanks to the Theodore Roberts Association for the Advancement of Science and Healthcare for continous and excellent support. The high intellecual calibre of each of your distinguished members has been a source of inspiration and motivation throughout my PhD.

Un merci au Fonds de la Recherche en Santé du Québec pour m’avoir accordé une bourse de Doctorat de 3 ans qui à couvert mon salaire de 2011 à 2014. Thanks also to the Public Health Agency of Canada for allowing me to use the world-class facilities of the National Microbiology Laboratory. Finally, many thanks to the Department of Medical Microbiology and especially Angie for piloting me through all the paperwork and formalities of the PhD.

List of tables

List of Figures

Table of Contents

Chapter One – Introduction

1.1 Influenza virology

1.1.1 General virology

Influenza viruses are enveloped [1], [2], negative single-stranded RNA viruses with a segmented genome and are part of the *Orthomyxoviridae* family [3]. Three types of influenza viruses (A, B and C) are distinguished with types A and B causing most human infections. Type A influenza is the most prevalent and causes both epidemics and pandemics whereas type B only causes seasonal epidemics. Type C influenza causes a mild respiratory illness and only rarely infects human [4][5]. This Thesis focuses only on influenza type A viruses. Virions are pleomorphic and typically exhibit a spherical morphology with diameters of 80-120 nm although more elongated and even filamentous particles have been observed [1], [6], [7]. The surface of the virions is composed of a lipid bilayer derived from the host cell cytoplasmic membrane [2]. On this envelope, two major viral proteins are present: the hemagglutinin (HA or H) and the neuraminidase (NA or N) [8]. These two proteins are the major antigenic determinants of the virus and are used to categorize them based on their sub-type [2]. To date, 18 subtypes of HA and 11 subtypes of NA have been described with any combination representing a different subtype of virus (e.g. H1N1, H3N2, H5N1 and H7N9) [5]. The H17N10 and H18N11 subtypes have been found exclusively in bats [9] while all other combinations are found in wild waterfowls [10], [11]. The HA and NA proteins will be discussed further in this Chapter. A third protein is present at the surface of virions, the M2 ion channel protein. Its major role is to enable the acidification of the virions upon internalization in the host cell [12]

and with M1 it also plays an important role in shaping the morphology of the virions [6]. The virus envelope is supported by the M1 (or Matrix) protein that acts as a scaffold and drives the budding of new virions [13]. The negative-sense single-stranded viral RNA segments are coiled around several monomers of the Nucleoprotein (NP) and also carry the viral RNA polymerase complex composed of the PA, PB1 and PB2 proteins (Protein Acid, Protein Basic 1 and 2) [14]–[18]. This ensemble is termed the Ribonucloprotein (RNP) complex. The genome of types A and B influenza viruses is composed of 8 RNP segments while type C influenza only has 7 [2]. Figure 1.1 illustrates the typical morphology of influenza A virion and shows an actual image obtained by electron microscopy. The traditional model of influenza virion structure suggests that infectious virions must be composed of the 8 RNPs and that any lack of segments leads to non-infectious particles [2]. However, fascinating recent research suggests that incomplete or even multi-partite viral particles are more common then previously thought [19]. Recent studies have also highlighted that influenza [20]–[23] (and enveloped viruses in general [24]–[28]) have the ability to capture host proteins in their matrix and/or their envelope and carry them during replication in a specific and functional capacity.

Figure 1.1 - Influenza virion

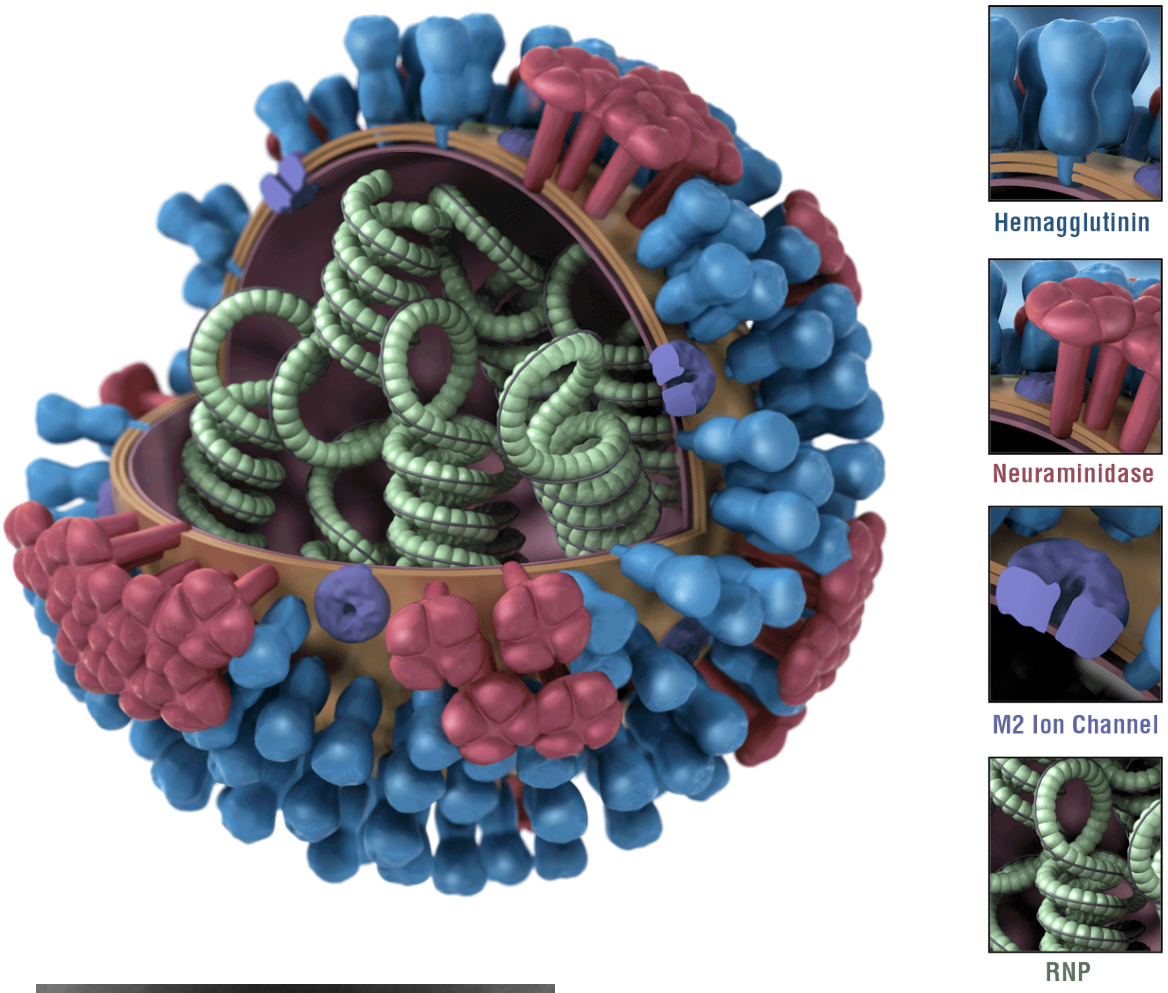

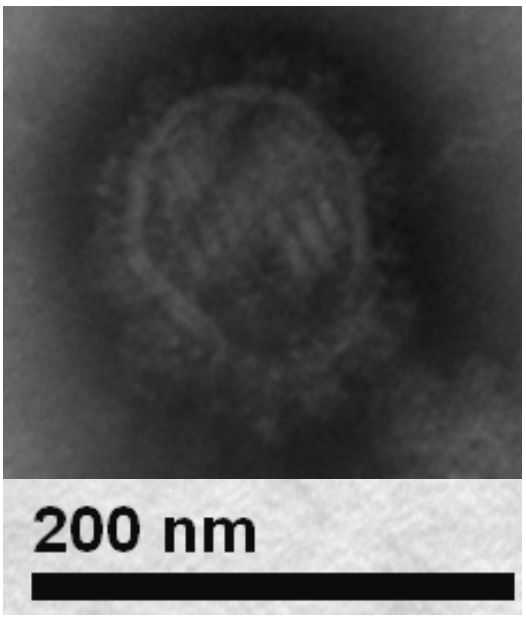

Representation of a typical influenza A virion. The typical spherical virions are approximately 100 nm in diameter. The Hemagglutinin (blue) and Neuraminidase (red) glycoproteins are readily observable by electron microscopy as are the RNPs inside the virions in thin sections preparations. Colored Image from [29]. Electron micrograph © Philippe Simon, 150,000x magnification of an H3N2 stain counterstained with phosphotunstic acid.

1.1.2 HA and NA subtypes and viral tropism

As mentioned previously, HA and NA are the major antigenic determinants of influenza viruses. This is a convenient classification method that dates back to antibody typing. Type A influenza viruses are further divided into subtypes. Accordingly, one is familiar with the nomenclature of H1N1, H3N2 and H7N9 viruses, each representing virions with different combinations of HA and NA on their envelopes. The ratio of HA to NA in virions has been shown to be approximately 4:1 [2]. Importantly, HA has been identified as the major virulence determinant in the H1N1 strain that caused the Spanish Flu pandemic of 1918 [30].

In the replication cycle of the virus, the roles of HA and NA can be thought as antagonists and a delicate balance of their respective activities is required for optimal viral replication [31]. HA is a glycoprotein whose major role is binding to cellular receptors while the role of NA, also a glycoprotein, is to cleave the moiety on cellular glycoproteins that HA uses to link to the host cell which enables budding virions to detach from the cell [2], [31]. On the viral surface, HA arranges itself in trimers [32] while NA forms tetramers [33]. In order to mediate the membrane fusion necessary for infection HA needs to be cleaved by host proteases. HA cleavage occurs at a specific site (the HA cleavage site, see Figure 1.2) on the inactive HA precursor (HA_0) and leads to the membrane-fusion capable HA_1-HA_2 linked by di-sulfide bridges [32], [34]–[36]. The amino-acid sequence of the HA cleavage site is a crucial marker of virulence. Low virulence strains have a monobasic cleavage site composed of one Arginine (R) residue or, rarely, a single lysine (K). In humans, monobasic sites are enzymatically cleaved by specific trypsin-like host proteases found in the respiratory epithelium such as tryptase Clara, mini-plasmin, and tryptase TC30 as well as TMPRSS2 and HAT (Reviewed in [37]). Strains

possessing a polybasic HA cleavage site have a consensus R-X-R/K-R motif that can be cleaved by a much wider number of host protease including ubiquitously expressed furin or PC5/6 proteases (Reviewed in [37]). From a pathogenicity perspective, this means that viruses harboring a polybasic cleavage site in their HA can be cleaved (and thus activated) in almost any cell type in the body, enabling them to replicate systemically [4], [37]. It is not surprising that the polybasic cleavage site is one of the best studied molecular markers for highly pathogenic influenza A viruses.

Figure 1.2 - Hemagglutinin protein

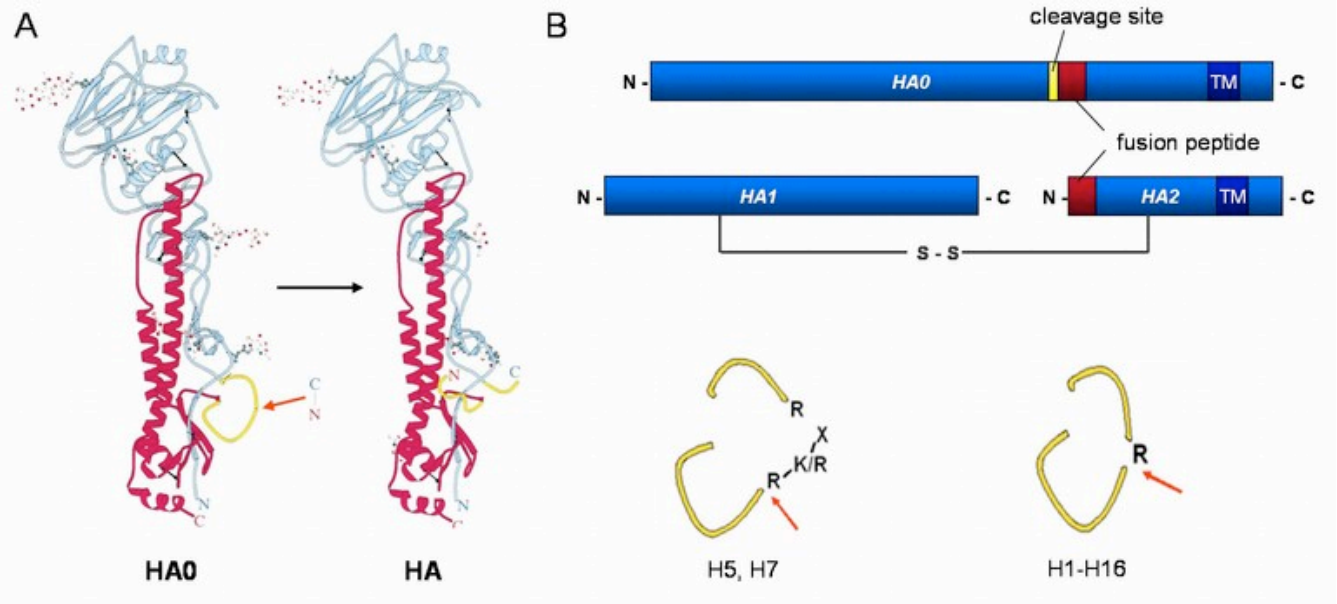

A. Hemagglutinin protein and its cleavage site and glycosylation sites. B. Schematic representation of the HA_0 and HA_1-HA_2 as well as a monobasic and polybasic cleavage site. Image taken from [38] based on a study by [36].

Following HA cleavage by a host protease and internalization of cell-attached virions into acidified endosomes, the lowering of the pH will trigger a conformational change in HA_1-HA_2 that will lead to the fusion of the viral envelope with the endosome membrane [39][40] and release of the RNPs in the host cell cytoplasm. In parallel with its cleavage HA also directs viral

tropism. Influenza viruses do not have specific receptors. Rather, they use sialic acid (SA) moieties linked to galactose on cell surface glycoproteins as initial attachment points. HA is responsible for this attachment. Human influenza A viruses (IAV) typically have a preference for sialic acids linked to galactose by an α(2,6) linkage while avian viruses normally target α(2,3)-linked sialic acids [41]. This is clinically relevant as in the human the epithelial cells of the upper airways generally harbour α(2,6)-linked sialic acids while the deeper airways have a mix of α(2,6) and α(2,3) moieties [37], [42], [43]. Low pathogenicity human seasonal IAV will therefore usually infect the upper airway, with consequently less severe illness, than viral replication deeper in the lungs as seen by infection with highly pathogenic viruses. In this Thesis, both low pathogenicity human strains as well as highly pathogenic avian strains are studied. An understanding of key virulence determinants such as the HA polybasic cleavage site and the different tropisms of these strains is important.

1.1.3 Viral life cycle and evolution

As mentioned in the previous section, HA mediates the attachment of the virions to host cells. The interaction between SA and HA is thought to be of relatively low affinity, requiring multiple bonds to be formed to properly anchor virions at the cell surface [41]. The major mechanisms leading to the entry of virions in the cell is thought to be clathrin-dependent endocytosis [44] although other clathrin-independent mechanisms have been described [45] including macropinocytosis [46]. Once inside an endosome, the lowering of the pH will trigger conformational changes of HA, membrane fusion [47] and the release of the RNPs in the cell [41]. Upon release in the cell, the nuclear localization signals on NP target the RNPs to the nucleus [48], [49] where viral RNA is synthesized through a complementary cRNA intermediate

by the PB1, PA and PB2 polymerase proteins. These proteins are also responsible for the cap snatching of cellular messenger RNA (mRNA) which allows the virus to highjack the cellular protein synthesis machinery to translate viral proteins [50].

Inherently, RNA polymerases are more error-prone then DNA polymerases and thus RNA viruses usually have higher mutation rates than DNA viruses. In the case of influenza viruses, the mutation rate ($\mu_{s/n/c}$) is estimated to 2.3×10^{-5} substitutions per nucleotide changes per cell infection (range: 7.1×10^{-6} to 4.5×10^{-5} $\mu_{s/n/c}$). [51]. These point mutations caused by single nucleotide changes lead to what is called genetic drift. This relatively slow evolution of virus strains can be responsible for anti-viral resistance as well as vaccine escape mutants [4]. However, due to its segmented genome another, more drastic form of evolution has been observed in IAVs. Upon co-infection of a cell by viruses of two (or more) different subtypes the RNP segments of the incoming virions can be mixed and re-assortment to produce many hybrids of the two incoming viruses. This is called genetic shift and is the phenomenon at the origin of influenza pandemics [52]. The major danger with reassortant viruses is that there will be no pre-existing immunity and the virus, if it possesses high transmissibility and high virulence, can rapidly spread globally. This was partially the case in 2009 when several strains of human (H1N1 and H3N2), swine (H1N1, H1N2, H3N2) as well as avian (unknown subtype) reassorted and led to the emergence of a novel H1N1 reassortant (See figure 1.3). Within months this new virus was disseminated worldwide [53]. Pandemics have been documented in 1918, 1957, 1968 and 2009 (See Figure 1.4) with the 1918 H1N1, the 1968 H3N2 and the 2009 H1N1 strains still in circulation today [54], [55]. A major public health threat with influenza is the possibility for reassortment between a highly transmissible strain (such as any of the human

seasonal viruses) with a highly pathogenic avian strain currently circulating in birds (see following section).

Figure 1.3 - Reassortment of seasonal strains

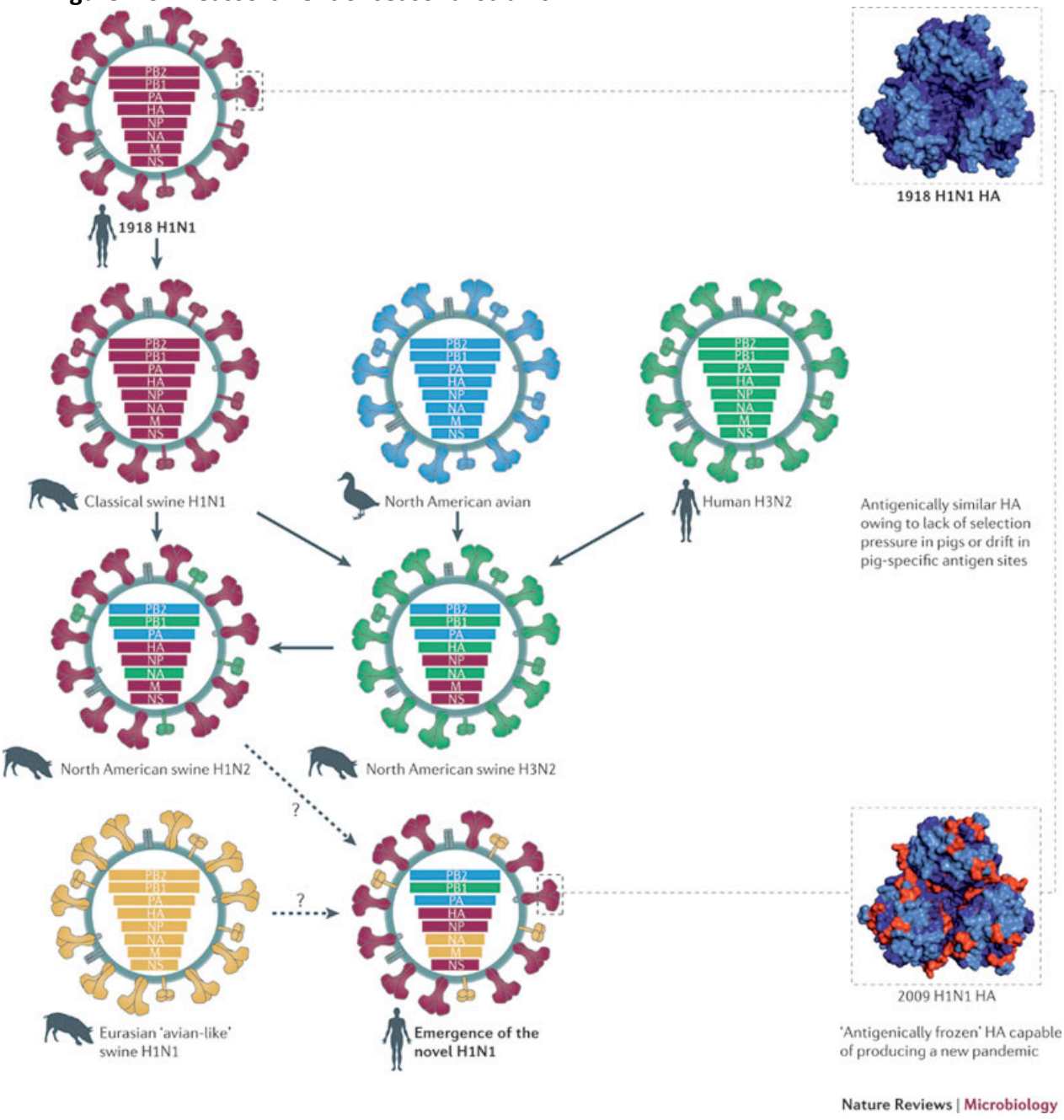

Reassortment events leading to the emergence of the 2009 pandemic H1N1 strain. The common ancestor derived from the 1918 H1N1 Spanish Influenza pandemic reassorted with avian and swine strains over the last century leading to the emergence of the novel 2009 H1N1 pandemic strain. Image from [53].

Figure 1.4 - Influenza pandemics

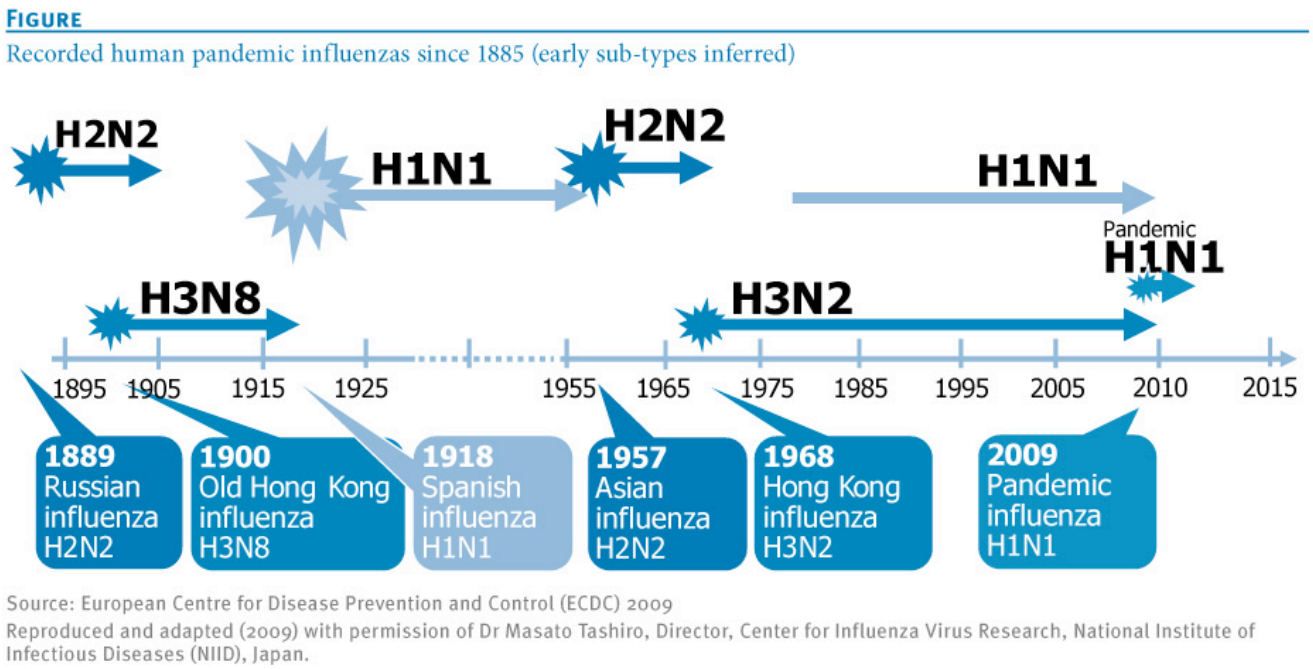

Influenza pandemics of the late 19th, 20th and 21st centuries. In post-pandemic periods, the causative strains became attenuated and circulated for several years causing seasonal outbreaks. Starburst are proportional to the number of deaths. Image from [56].

1.2 Clinical and pathophysiological aspects

1.2.1 Public health impact and spread of avian and human strains

In our sterile labs, we often forget the devastating impact of infectious diseases on sick patients in hospital beds. From a clinical and a public health perspective, influenza is one of the most important respiratory infections. Estimates from the World Health Organization for seasonal influenza quotes approximately 500,000 yearly deaths and around 3,000,000 severe infections due to influenza [4], [57]. It is estimated that 5% of the worldwide adult population and as much as 20% of the child population gets infected annually by either type A or B influenza viruses [57]. Accurately measuring the number of cases is challenging, as patients with mild or moderate flu symptoms may not seek treatment in hospitals and clinics whereas

patients with more severe symptoms will [58]. Beyond seasonal influenza, pandemics can result in millions of deaths. It is estimated that between 20 and 50 million people died from the 1918 Spanish Influenza, although this may also reflect secondary bacterial infections and the absence of antibiotics and poorer hygiene measures [59]–[61]. More recently, the 1957 H2N2 and 1968 pandemics each caused approximately one million deaths [59] while the best estimate for the 2009 H1N1 pandemic is at 300,000 deaths worldwide [62]. Finally, as influenza viruses can infect virtually all mammals as well as most bird species [4], it is highly unlikely that it will ever be eradicated. Seasonal influenza viruses are attenuated descendants of the H1N1 Spanish Influenza of 1918 and are of H1N1, H2N2 and H3N2 subtypes [63], although the H2N2 viruses only circulated between 1957 and 1968. Since the Mexican pandemic of 2009, a new H1N1 subtype has also become a seasonal strain.

1.2.2 HPAI and LPAI strains of influenza in their reservoir, in humans and in poultry – It's complicated

With the exception of the H17N10 and H18N11 subtypes only found in bats [9][64], wild waterfowls and aquatic birds are the reservoir for all subtypes of IAV [10], [11]. Specifically, Anseriformes such as ducks, geese and swans and Charadriiformes such as shorebirds and gulls form the natural reservoir species and are responsible for infections to other avian and mammalian species [10]. For all subtypes of IAV – including those causing severe disease in humans and poultry – viral replication in their wild bird reservoir is asymptomatic. Importantly, the distinction of Highly Pathogenic Avian Influenza (HPAI) and Low-Pathogenic Avian Influenza (LPAI) is primarily a veterinary consideration: HPAI strains are those causing mortality in domestic poultry. The criteria for a given IAV strain to be classified as HPAI is that it either has

an intravenous pathogenicity index (IVPI) greater than 1.2 in 6-week-old chickens or causes at least 75% mortality in intravenously-infected 4-to 8-week-old chicken [65]. IVPI is a standardized method for testing pathogenicity of IAV in chicken. Briefly, it relies on intravenous infection in groups of 4-to-8 week old chickens. Those are observed every 24h hours and scored whether they are normal (0), sick (1), paralysed (2) or dead (3) [66]. For H5 and H7 subtypes, molecular characterization can also be used to ascertain whether they contain the polybasic cleavage site in their HA [65] and see section 1.1.2. To be classified as LPAI, an H5 or H7 strain will therefore be non- or low-pathogenic in chicken and will not possess a polybasic cleavage site. To date, only a few H5 and H7-subtyped strains have be classified as HPAI strains while the majority of those subtypes exhibit LPAI properties. Human infection with LPAI strains usually leads to a mild or asymptomatic disease. A notable exception is the infection with the recent H7N9 strain from China. That strain has all the characteristics of an LPAI virus (low pathogenicity in poultry, no polybasic cleavage site) yet causes severe disease in humans. The term HPAI can be confusing as highly pathogenic strains refer to infection in poultry. Human infection with several HPAI strains of H7N7 [67] or H7N3 [68] subtypes leads to mild symptoms. Figure 1.5 illustrates the multiple possibilities of cross-species infections by IAVs.

Figure 1.5 - Influenza reservoir and interspecies transmission

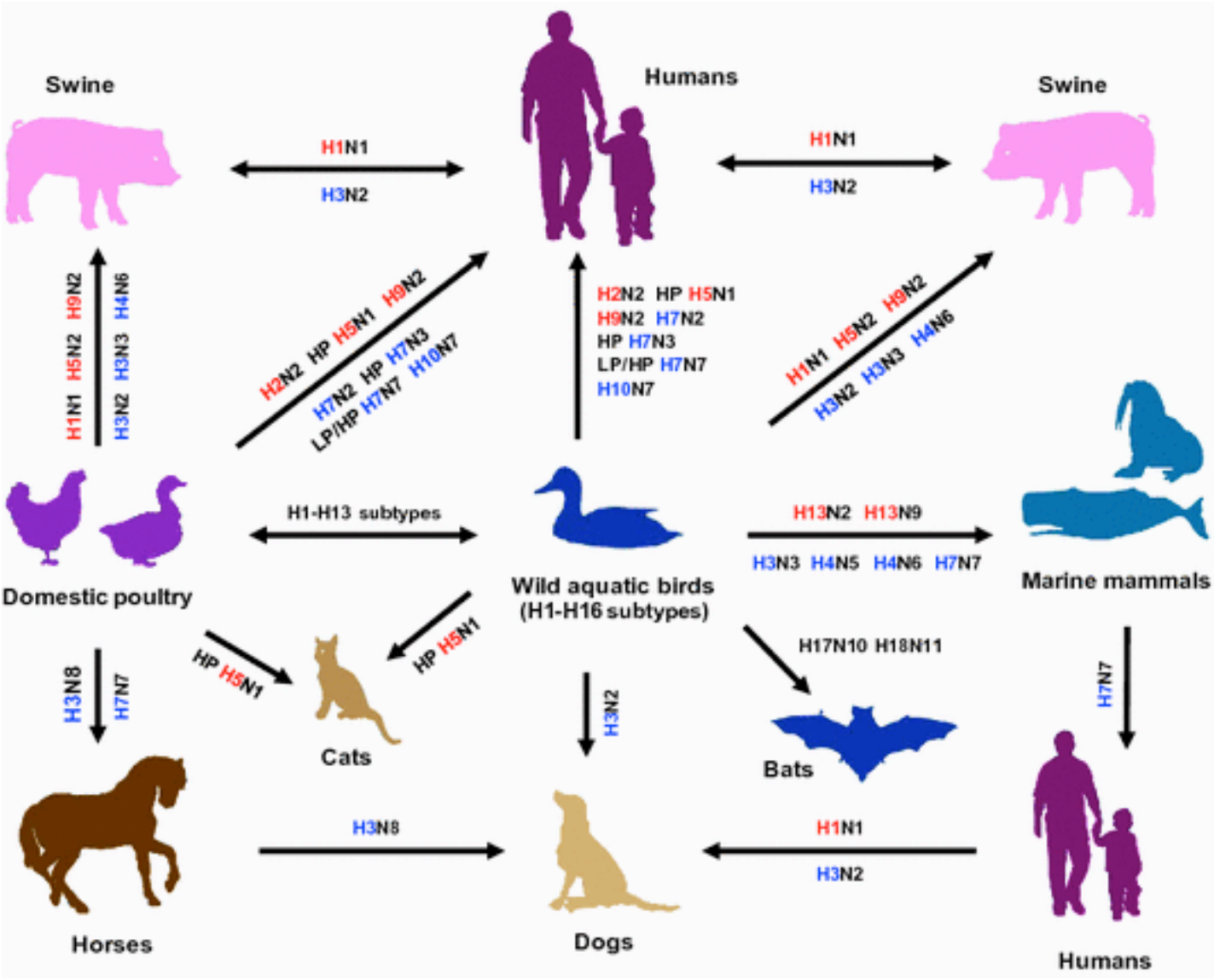

Host range of influenza A viruses. Wild waterfowls are the natural reservoir of almost all subtypes, excluding the H17 and H18 subtypes only found in bats. They can then infect domestic poultry, humans, swines as well as several other mammalian species with several different subtypes. LP : Low pathogenic and HP : Highly pathogenic. Figure from [10].

Of all circulating HPAI strains, the one that is most worrisome for humans is the H5N1 strain that emerged in 1997 and re-emerged in 2003 in south-east Asia. In humans, it causes Acute Respiratory Distress Syndrome (ARDS) with lethality rates as high as 60% [69]. Despite high lethality, it typically does not show any significant human-to-human transmission [69]. In 1997, the first cases of infection by H5N1-subtyped HPAI were reported in humans [70]. Since then, this subtype has been in circulation in migratory birds and has caused large-scale poultry outbreaks as well as fatal isolated human infections. Between 2003 and May 1st, 2015, 840 infections have been document with 447 deaths, resulting in a lethality rate of over 50% [71]. In January 2014, a traveler returning from China died of an H5N1 infection in a Canadian hospital. This was the first human case in North America [72]. In March 2013, a new H7N9 strain emerged in China and has, as of February 2015, infected over 500 people with a 20% lethality rate [73], [74]. As with the H5N1 virus, two imported cases of H7N9 have been documented in North America [74]. Clinically, H7N9 infections are similar to those by H5N1 (reviewed in [75]) yet that strain lacks the polybasic cleavage site in its hemagglutinin surface protein, a hallmark and well-described molecular marker of HPAI viruses [75][76]. The continued spread and high lethality of those HPAI or HPAI-like strains continues to pose a serious public health risk. Figures 1.6 and 1.7 respectively illustrate the geographical spread of the H5N1 and H7N9 subtypes.

Figure 1.6 - Spread of the H5N1 HPAI strain

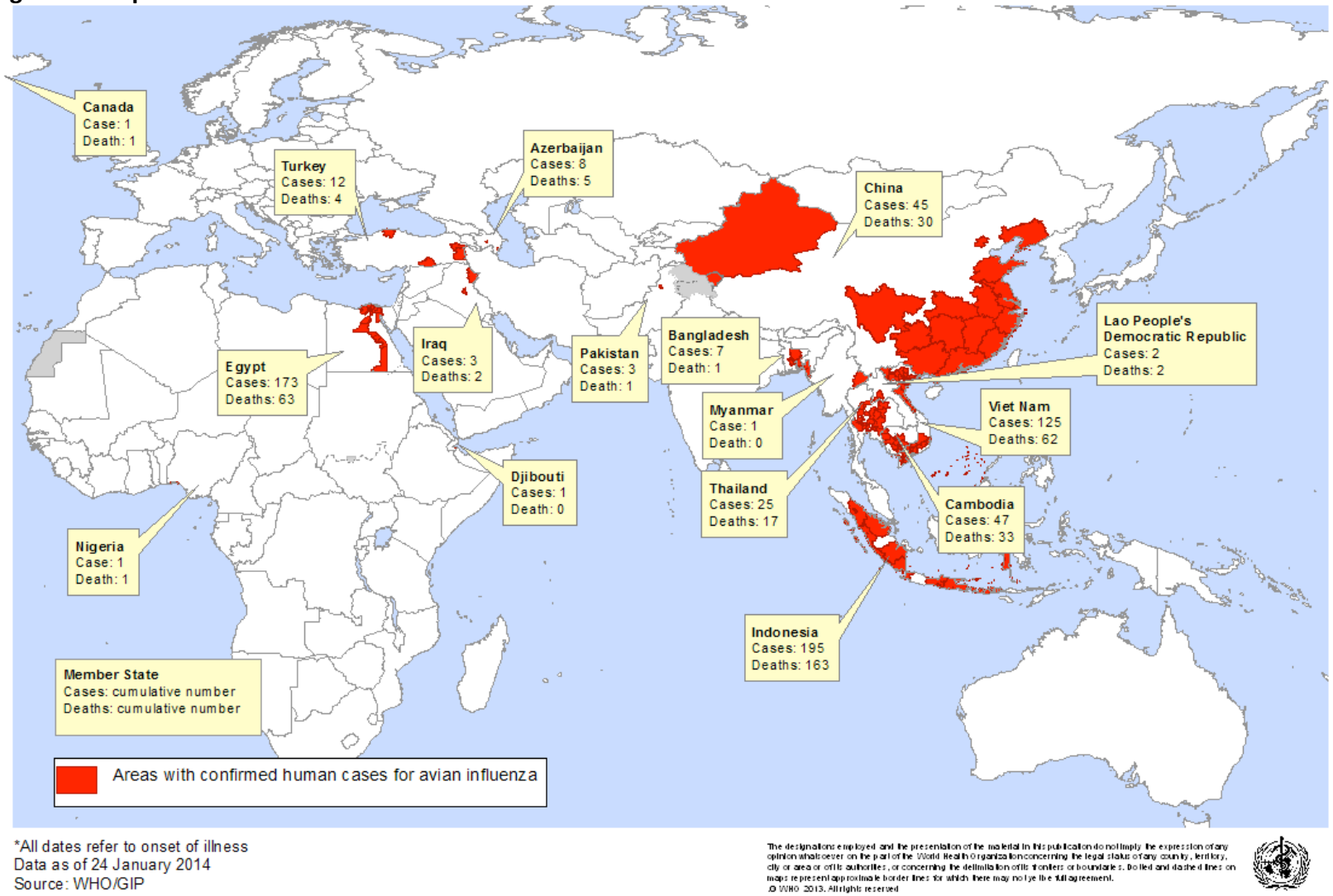

Spread of H5N1 virus in humans since 2003. The first human infections with H5N1 strains were reported in 1997. That outbreak waned and the virus re-emerged in 2003. It currently infects birds across Asia, Europe and Africa and has caused fatal human infection in over 16 countries. Image from [77].

Figure 1.7 - Spread of H7N9 LPAI strains

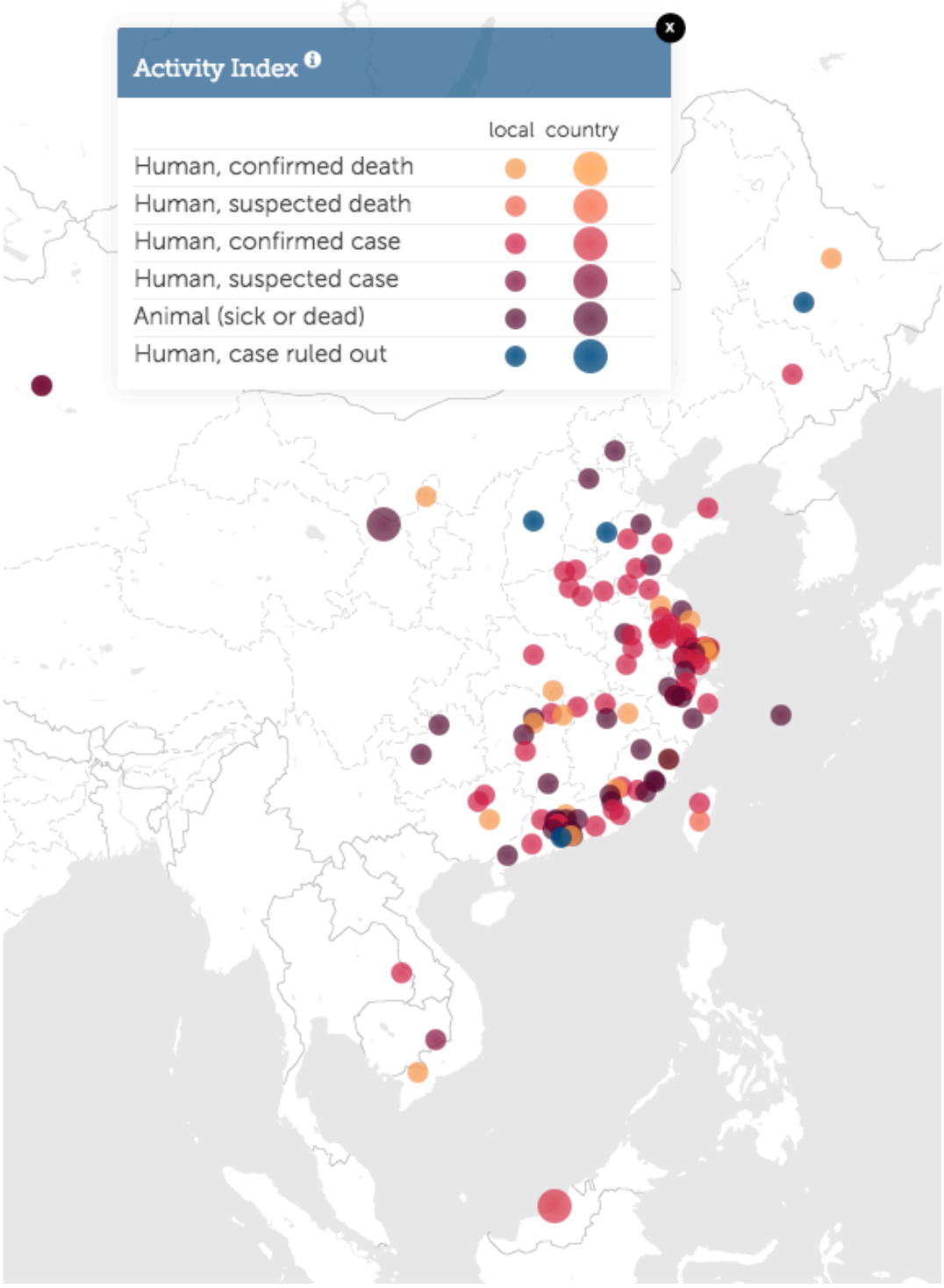

Spread of a novel H7N9 strain in China and South-East Asia since March 2013. This strain is classified as a low pathogenicity avian influenza virus yet causes severe disease in humans with a case fatality rate of over 20%. Small dots indicate the localized alerts while large dots indicate country-wide alerts. Map from [78], two fatal cases in Canada not shown.

1.2.3 Clinical and pathological aspects of seasonal influenza

Typical symptoms of mild or moderate seasonal Flu include headache, chills and cough followed by fevers as high as 40°C that can last up to six days. Myalgia and generalized malaise are also common [4][79]. Figure 1.8 lists the most common symptoms for pediatric, adult and elderly patients.

Figure 1.8 - Symptoms of seasonal influenza

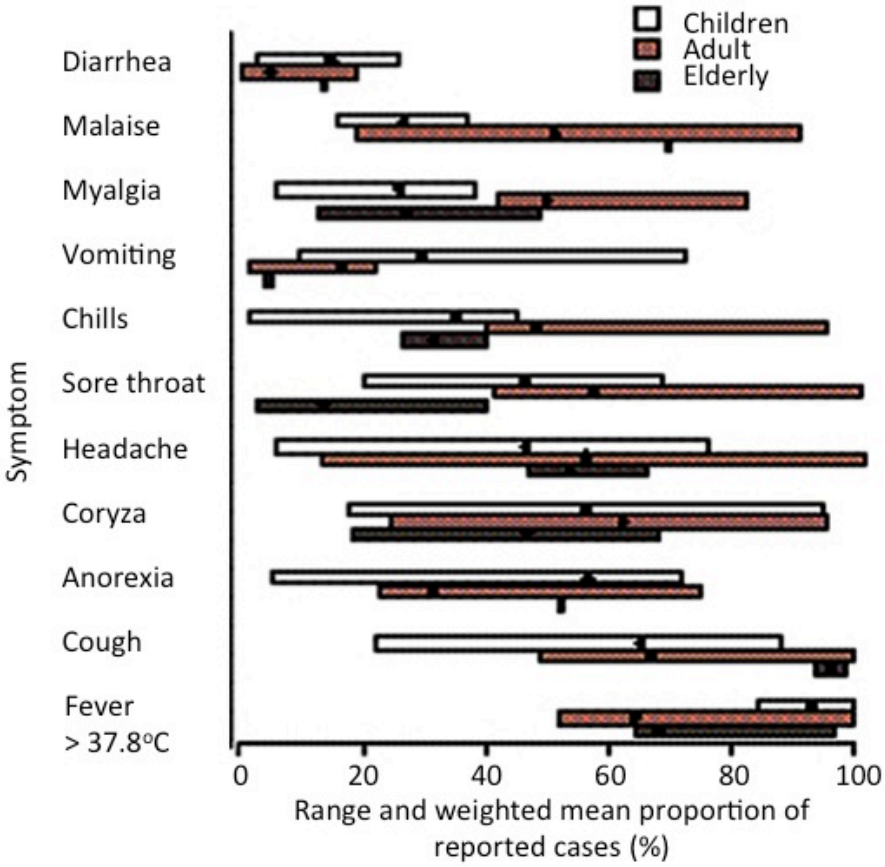

Symptoms of seasonal influenza for children, adults and the elderly. Most common symptoms for all age groups include fever, cough, coryza and headache. In healthy individual, seasonal influenza is usually a mild, self-limiting disease. Figure adapted from [79].

One of the challenges of seasonal influenza is that, as a respiratory virus targeting the upper airways it can readily be transmitted by aerosols and very low doses of virus (0.3 to 6 TCID50) are sufficient to cause an infection [80]. The incubation period varies between one and five days [81] and an infected individual can shed the virus for up to one week following infection [4][82] although children can shed virus up to 15 days post infection [83]. In the majority of cases, the disease is self-limiting with healthy individuals recovering within one or two weeks. In uncomplicated cases, viral replication and inflammation occurs mostly in the upper airways (trachea, larynx, bronchi) where superficial epithelial cells are infected. As mentioned in the previous section, this is largely due to the distribution of alpha(2,6)-linked sialic acids in the upper airways in human [42]. Young children [79], the elderly [84], pregnant women [85] as well as patients with comorbidities such as cardiopulmonary disease or compromised immune systems [86] are more likely to be hospitalized for severe and complicated symptoms than adults. Three types of severe complications can happen upon infection by seasonal influenza: primary viral pneumonia, combined viral-bacterial pneumonia and a secondary bacterial pneumonia [4]. All of these involve the lower respiratory tract. The primary viral pneumonia is similar to non-complicated illness with the addition of bronchiolitis and alveolitis [4], [87], thereby severely compromising gas exchanges in the lungs. This can lead to death by hypoxia in 1 to 4 days and can take up to 4 months to affect complete recovery [4], [88]. The combined viral-bacterial pneumonia is symptomatically indistinguishable from the primary viral pneumonia and is predominantly caused by co-infection with *Streptococcus pneumonia*, *Staphylococcus aureus* and *Heamophilus influenza* [79][89]. The fatality rates for an *S. aureus* co-infection can be as high as 42% [90] and bacterial co-infection is thought to have played a

significant role in the high mortality observed during the 1918 Spanish Influenza pandemic [91]. At a 7% fatality rate [4], secondary bacterial pneumonia is a complication that can at least be treated with antibiotics yet causes significant issues in elderly patients [92]. Other very rare complications following seasonal influenza infection includes viremia [93], cardiac involvement, Reye Syndrome [94] and encephalopathies (Reviewed in [95]).

1.2.4 Clinical and pathological aspects of avian influenza in human

Certain subtypes of avian IAV are documented as causing severe and fatal Infection in humans as well as in chickens. The classification of Highly Pathogenic or Low Pathogenicity Avian Influenza (HPAI, LPAI) is derived from the lethality of a strain in chickens. HPAI infection in human is a mirror image of seasonal influenza. Where seasonal influenza infects millions annually only very few patients (only 840 for H5N1 HPAI since 2003) have been infected by HPAI strains. Where seasonal influenza mortality rates are so low as to be difficult to accurately measure, HPAI mortality rates can be as high as 60%. Where the disease caused by seasonal influenza is usually self-limiting and restricted to the upper airways, HPAI cause severe and acute disease involving the whole lung and can spread to other organs such as the intestine and brain. Figure 1.9 illustrates the major pathological differences between human and H5N1 HPAI infections.

Figure 1.9 - Seasonal and avian influenza

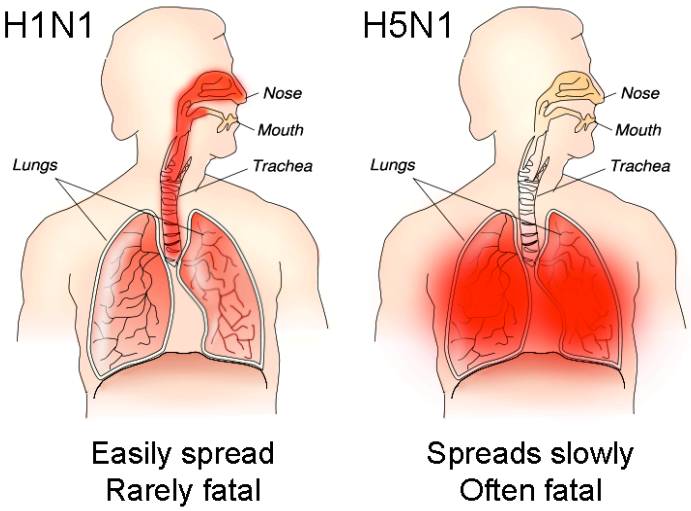

Differences in H5N1 highly pathogenic avian influenza and seasonal H1N1 infections in human. Seasonal strains of influenza primarily replicate in the upper airways, are easily transmissible and cause mild, self-limiting disease. Conversely, H5N1 infections are characterized by replication in the lower airways, a very severe disease and poor-if-nonexistent human-to-human transmission. Image from [96] based on [97].

As mentioned previously, viral replication in the respiratory tract of a patient infected by an HPAI strain occurs deeper in the lungs. This is largely due to the virus preference for alpha(2,3)-linked sialic acids which are found deeper in the human respiratory tract [42]. HPAI viruses cause an Acute Respiratory Distress Syndrome (ARDS) similar to a primary viral pneumonia but that also involves a detrimental inflammatory response termed a cytokine storm [98], [99]. The combination of high viral load, broadened lung tropism and inflammatory damage leads to severely reduced gas exchanges in the alveoli and death by hypoxia within a few days. Viral replication occurs not only in lung epithelial cells but also in type II pneumocytes and alveaolar macrophages [100], [101]. Unlike seasonal flu, replication can occur beyond the lungs including in the intestines, brain and placenta [99], [100], [102]. Infected macrophages can also spread the virus to the lymph nodes. Sustained human-to-human transmission of HPAI strains has

never occurred and most infected individuals have been highly exposed to the virus while handling sick or dead poultry [103]–[107].

1.3 Proteomics

1.3.1 Proteomics 101

Compared to genomics, proteomics is still in its infancy and has yet to reach its full potential. Nonetheless, the concept of studying proteins in a high throughput manner is ultimately what proteomics set out to do, as mRNA expression does not always correlate with protein expression [108]. From a systems biology perspective, the information from both approaches is complementary and has greatly assisted our understanding of complex cellular phenomena.

1.3.1.1 Mass spectrometry

Modern proteomics relies on the identification (and quantitation, see section 1.3.2) of proteins using mass spectrometry [109],[110]. Mass spectrometers are instruments that measure the atomic masses of gas-phase ions, from atoms to complex molecules such as peptides and proteins. The first mass spectrometer is credited to J.J. Thomson at the turn of last century [111]. Initially, this method was first used to study the nature of cathode rays and then pioneered by Francis Aston and Arthur Dempster to study isotopes. Figure 1.10 illustrates the basic composition of a simple mass spectrometer. Until the 1990s', mass spectrometry was mostly used for analytical chemistry. It then became a major tool for biologists with the development of soft ionization techniques such as matrix-assisted laser desorption ionization

(MALDI) [112] and electrospray ionization (ESI) [113] that enabled peptides to be ionized without being destroyed and thus made them measurable in a mass spectrometer.

Figure 1.10 - Basic mass spectrometer

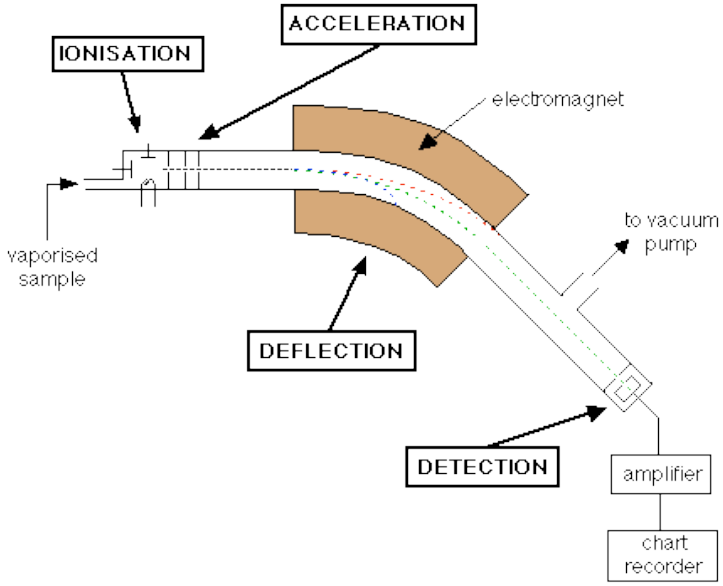

A sample in gas phase is ionized at the source and accelerated in the instrument. Ions are deflected in a magnetic field. Based on their mass and charge (m/z) they will either reach the detector or be lost. Their m/z can then be determined based on the properties of the magnetic field and type of detector used. Image from [114].

A brief description of the inner working of a mass spectrometer is useful to properly appreciate the work carried out in this project. First, the analyte is ionized by the source. In the case of peptides, a common technique used is called Electrospray Ionization (ESI) where a strong electric current is applied to the ion source (in our case a nano liquid chromatographic column, see 1.3.1.2) [113]. This ionizes the peptides in the buffer solution, giving them a charge that allows them to "fly" in the mass spectrometer. The ions enter the mass spectrometer through a series of lenses that adjust and direct the beam toward several detectors. Modern instruments can then detect the mass of entire peptides but these need to be further broken down to allow for their sequence to be determined. Using a combination of electric and radio

waves, the instrument will automatically select an ion population of a given mass (i.e. a specific peptide) and will then fractionate it using collisions with a gas (usually Nitrogen, Helium or Argon). While the initial identification of the analyte is called MS, this fractionation of a given analyte is called MS/MS. This will break the peptidic bonds and sequentially release individual amino acids whose mass (and therefore identity) will be measured by the instrument. Much like contig assembly in DNA sequencing, the fragmented peptides can be aligned and their overall sequence can be determined by looking at the masses of each of the amino acids composing them [109]. Figure 1.11 shows a chromatographic elution profile followed by MS followed by MS/MS of a single peptide. This is performed several hundred thousand times to generate peptide sequence information that will be used to identify the proteins.

Figure 1.11 - Peptide fragmentation

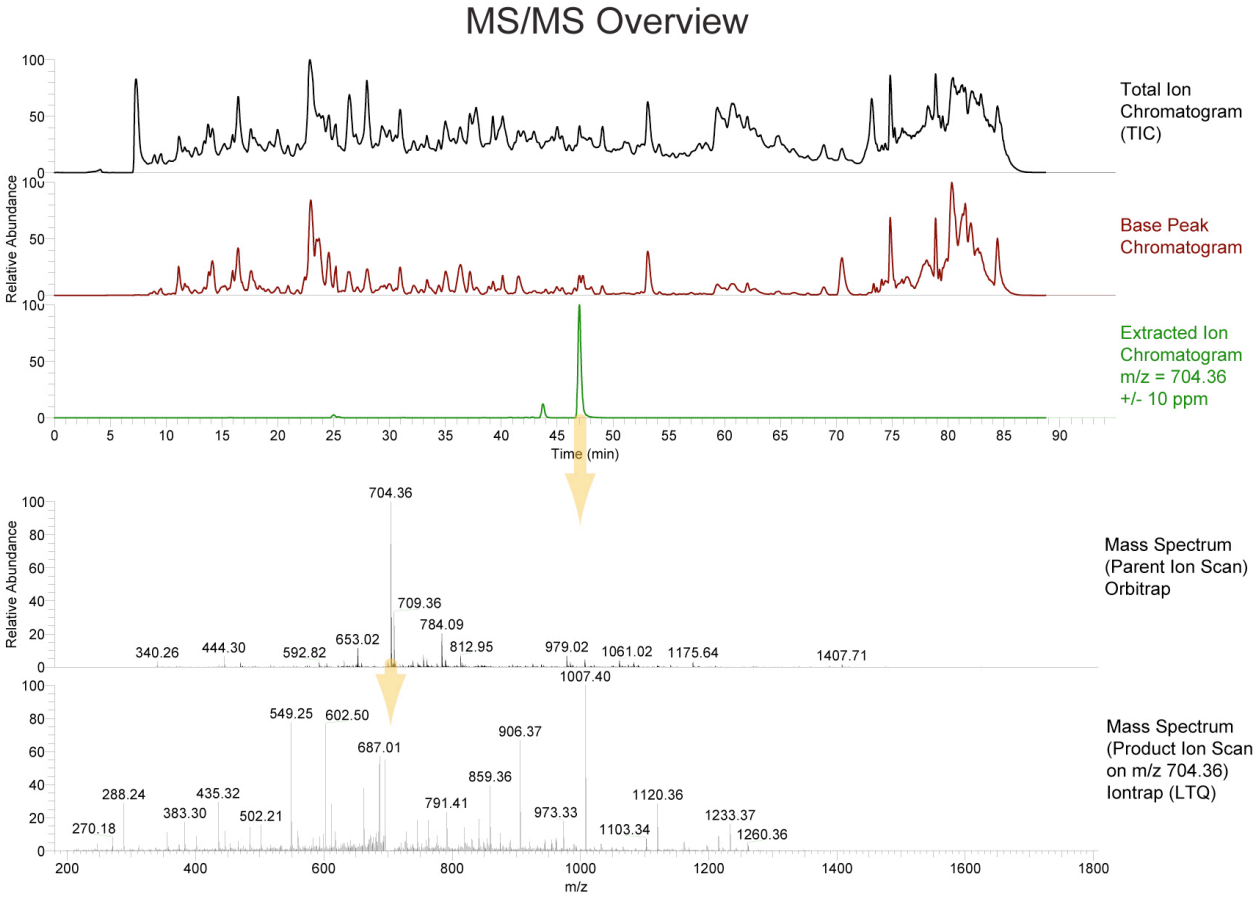

The black and red chromatograms (top) measure the samples entering the mass spectrometer over time. A specific population of peptides, eluting at approximately 47 minutes is analyzed by MS. The most abundant species at 704.36 m/z is further selected for MS/MS and its amino acid sequence can be determined from its fragmentation. Image from [115].

1.3.1.2 Offline fractionation systems

There is a significant complexity when analyzing a whole cellular extract for its entire proteome. This has prompted the development of several methods to simplify the mixture to enable optimal sequencing and quantification by mass spectrometry. These are termed offline methods as they are carried out independently of the mass spectrometer, as opposed to inline methods where the end product is directly injected in the instrument. For historical consideration, we will briefly describe two-dimensional differences in gel electrophoresis (2D-

DIGE) and then focus on two-dimensional reverse-phase high performance liquid chromatography (2D RP-HPLC). In 2D DIGE, complex cell lysates are applied to a two-dimensional gel where the first fractionation is done based on isoelectric -focusing of proteins. A second dimension of separation is then achieved by making the ioselectrically-focused proteins migrate in an SDS-PAGE gel of set concentration (or gradient), separating proteins with similar isoelectric points based on their sizes. Dyes can be used to label samples and up to three samples can be run on the same gel. By analyzing the migration pattern and the relative sizes of the protein spots, quantitative information can be obtained even prior to MS or MS/MS. To identify the differentially-abundant proteins, the bands are excised, digested with trypsin and the peptidic mixture can be sequenced by MS/MS (see previous section) [116], [117].

This technique has the advantage of showing protein isoforms and certain post-translational modifications yet severely lacks reproducibility and is less than optimal when dealing with large, complex mixtures [118]. Newer approaches rely on orthogonal fractionation by High Performance Liquid Chromatography (HPLC) [119]. A complex peptide mixture is first fractionated offline using a hydrophobic gradient with an organic solvent such as acetonitrile and a sample in a buffer at an alkali pH. The resin (i.e the stationary phase) most often used is called C-18 which consists of beads of set diameters coated with 18-carbon alkyl chain, acting as a highly hydrophobic matrix. The high pH deprotonates peptides, giving them a set charge and then separates them based on hydrophobicity from least hydrophobic to most hydrophobic by increasing the amount of organic solvent over time. Figure 2.2 (see section 2.6.3) shows a typical elution and fraction collection profile for the offline HPLC. Fractions are collected sequentially and can then be subjected to a second round (or dimension) of HPLC, this time

using a low, acidic pH. This second HPLC is called an in-line nano Liquid Chromatography (nLC) and is connected directly with the ESI source of the mass spectrometer. This enables the immediate ionization and sequential injection in the instrument for identification and quantitation. The goal of using first a high and then a low pH is to have as much of an orthogonal separation as possible, thus optimally simplifying the peptide mixture at both steps. Figure 1.12 shows the concept of orthogonal separation.

1.3.2 Quantitative shotgun proteomics

Identifying the proteins present in a cell is the first step of proteomics. Another crucial aspect is to obtain quantitative information on their abundance. As mentioned, this has been historically done by 2D DIGE however newer methods are available. Broadly speaking, this can be achieved using two approaches: by labeling the samples in such a way that they can be tracked in the mass spectrometer or by using advanced computational methods to compare the MS spectra of two samples injected sequentially in the instrument. The former is the method we employed while the latter is undoubtedly the one that will become more mainstream as the computational tools to acquire the data and the speed and mass accuracy of the instruments will improve.

Figure 1.12 - Orthogonal separation

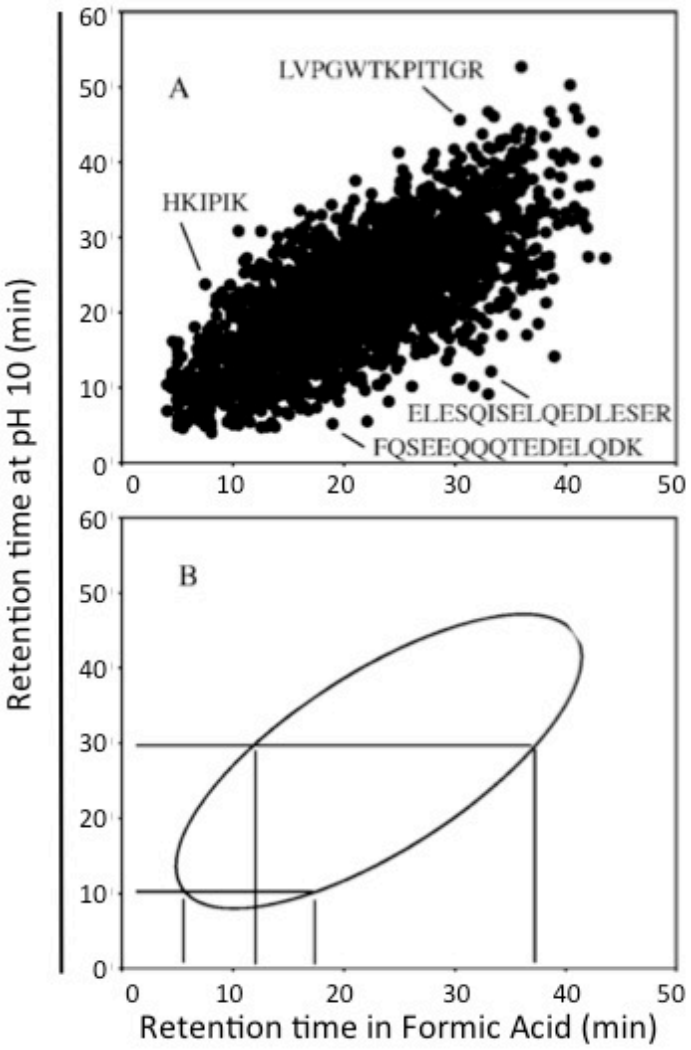

A. Each dot represents a different peptide plotted based on its retention time in high pH (y axis) or formic acid (low pH, x axis) buffers during HPLC. B. Orthogonal separation is achieved in 2 dimensions, as peptides eluting at any given time in one of the two conditions will elute at different times in the other. Adapted from [119] © ACS 2015.

1.3.2.1 iTRAQ and SILAC

There are several types of labeling strategies used for quantitative proteomics. We chose to use iTRAQ (isobaric Tags for Relative and Absolute Quantitation [120]) but other methods such as SILAC (Stable Isotope Labeling of Amino acids in Cell culture [109]) or ICAT (Isotope-coded affinity tags - [121]) are commonly used, each with their advantages and limitations. In SILAC,

cells are grown in media enriched with a stable-isotope-labeled amino acid, such as Arginine containing only C_{13} carbon. Upon treatment, one group will have proteins with C_{12} while the other one will have proteins that incorporated C_{13} (and potentially Nitrogen 14) in all their arginine residues. Upon analysis by mass spectrometry, this difference in mass for the peptides of one group to another can easily be measured. In iTRAQ, tags of identical overall masses but with reporter groups of known different masses are chemically linked to lysine side-chains and the n-terminus of peptides [120], [122]. iTRAQ kits enable the simultaneous analysis of up to 8 samples, whether from cell culture or animal tissues. After fractionation for MS/MS, the intensity of each of the tags – differing by a mass of only 1 Da – is measured. The relative intensity of the tags are reported for all peptides which then enables the deduction of the relative abundance of proteins. Figure 1.13 shows a typical iTRAQ workflow. The advantages of iTRAQ is that it can be used in any animal or cell culture system and complexities of 4- or 8-plex are routinely feasible to allow simultaneous comparison of 4 or 8 different samples, respectively. From a mass spectrometry perspective, one peptide is fractioned in MS/MS to yield quantitative and sequence information whereas in SILAC two peptides (isotopically labeled) need to be identified and quantified.

Figure 1.13 – Typical iTRAQ workflow

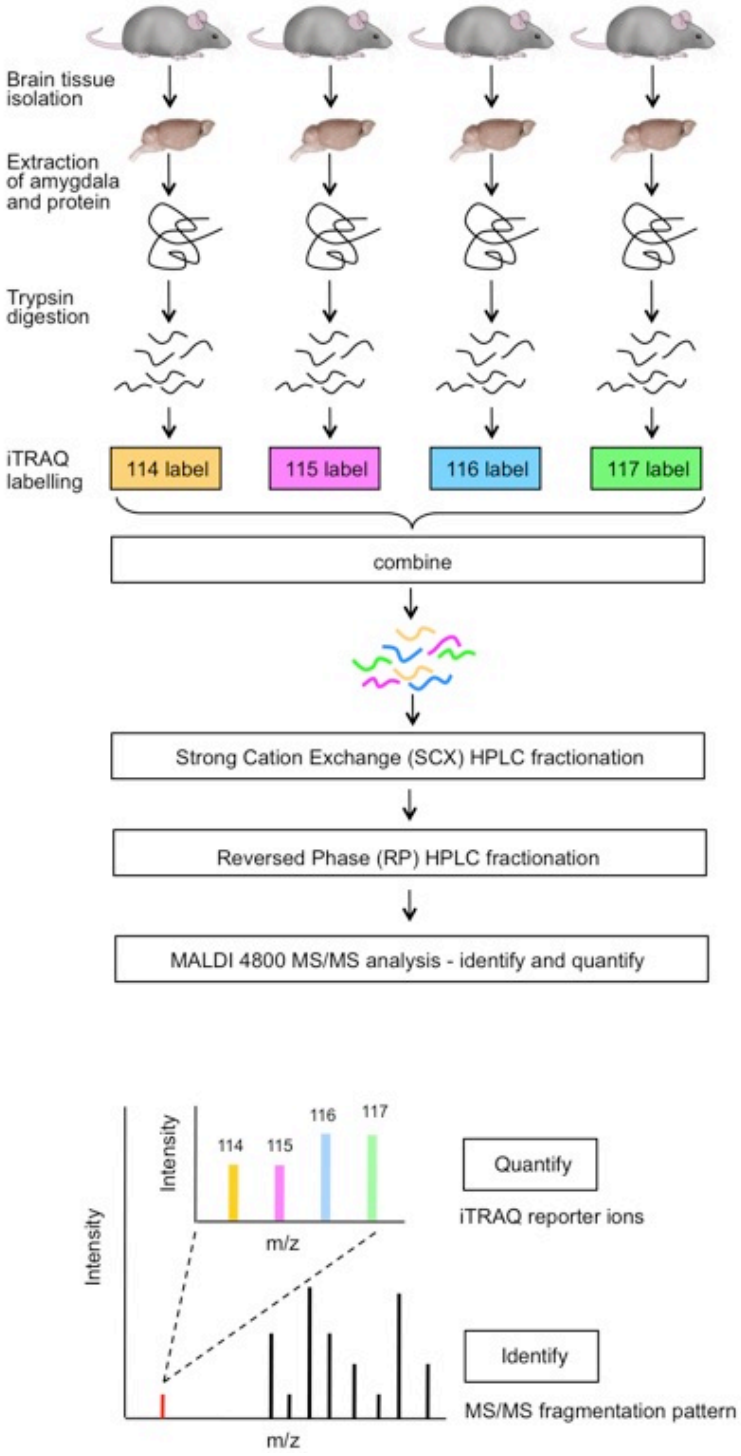

Proteins from four different samples are extracted, digested with trypsin and chemically labeled with one of the four iTRAQ tags. iTRAQ-labelled tryptic peptides are then combined in a 1:1:1:1 ratio and this complex mixture is fractionated by two dimensional chromatography and injected in a mass spectrometer. The relative abundance of each peptide is determined based on the ratio of each iTRAQ reporter ions as measured by MS/MS. Image from [123].

1.3.3 Proteomics studies of influenza virus

A few studies have been conducted on the host response to influenza infection in *in vitro* model systems. Some of those used A549 cells, the same model used in this thesis [124]–[128]. The study by Dapat et al. [124] focused on the phosphoproteomic response during infection by a strain of the 2009 pandemic H1N1 virus using iTRAQ labeling and phosphopeptide enrichment. By 24h post-infection, they identified 366 phosphorylation sites on 283 proteins of which 43 were up-regulated and 35 were down-regulated. Based on their results, the major functions modulated by infection involved RNA regulation (splicing, translation initiation, nuclear localization). Another pioneering study by Coombs et al. [128] using the lab adapted PR8 H1N1 strain in A549 cells and SILAC labeling examined the sub-cellular proteomic host response by 24h post-infection. They used both 2D HPLC and SDS-PAGE LC fractionation and identified host modulation in both nuclear and cytoplasmic fractions. The top biological functions involved with infection were related to protein localization and transport. In two sister studies, Wu et al. [125], [126] infected A549 cells with a swine-origin H3N2 strain and used 2D-DIGE to study the proteomic responses in sub-cellular fractions. While both the Dapat and Coombs studies used an MOI of 7, the Wu studies used only MOIs of 1. This would theoretically mean that only about 60% of the cells were infected. They also harvested their samples for proteomic analysis at 24h. The low MOI they use impacts their results as by 24h their sample would have contained a distribution of cells in various stages of infection. Nonetheless, their findings show that Apolipoprotein 2 was found to be up-regulated by infection in the mitochondria. We have also observed this in our own results. In their subcellular fractionation experiments, they found that a large portion of proteins – both in the

cytoplasmic and the nuclear fractions – were involved in cellular death. All these studies have been conducted using A549 cells for infection and low pathogenicity strains of influenza virus. One study used A549 cells and a H5N1 highly pathogenic avian influenza strain. Liu et al. [127], similarly to the Wu studies, used an MOI of only 0.5 which translates into less then 40% of infected cells, weakening any potential conclusions. They used 2D-DIGE on membrane-enriched protein extracts and sampled their infected cells at 6, 12 and 24h post-infection but only used a single biological replicate. Interestingly, they found the viral NS1 protein in their membrane fractions and also several keratin proteins, indicative of potential contamination during the sample preparation. Two more studies examined the proteomic host responses to highly pathogenic avian influenza strains but they used other cell lines than A549. Using Calu3 cells, a human lung adenocarcinoma cell line, Menachery et al. compared the host responses of a low pathogenicity 2009 pandemic H1N1 strain, several H5N1 strains as well as the SARS and MERS Coronaviruses at several time points from 0h to 24 or 48h post-infection [129]. They used an impressive combination of proteomics and genomics microarray technology to highlight the different modulation strategies used by these viruses to circumvent the interferon-stimulated genes triggered during the innate anti-viral response. For the influenza viruses, they showed that the H5N1 strain was able to rapidly modulate interferon stimulated genes (ISGs) while the low pathogenicity 2009 pandemic H1N1 strains was not, suggesting this modulation of the host response was an important aspect contributing to the severity of symptoms. Finally, a small study by Cheung et al. examined the comparative host responses to infection by a low pathogenicity H1N1 strain and a HPAI H5N1 strain in primary human macrophages [130]. Their study showed that by 1h post infection, a significant host response was present in the H5N1-

infected cells while nothing significant had occurred in the H1N1-infected cells. Strangely, the initial response to H5N1 infection had faded by 3h and 6h post infection (see Figure 1.14). They also showed that several members of the eukaryotic initiation factor (EIF2) family and ribosomal proteins were strongly modulated by the H5N1 infection. To our knowledge, the Menachery and Cheung studies are the only ones that attempted to compare host responses to low and highly pathogenic influenza strains. However, in our opinion they suffered from a suboptimal experimental design and lacked for sufficient controls and reproducibility. In the Menachery study, the MOI for the different infections was not constant and was between 1 for the H5N1 and 3 for the 2009-H1N1 and in the Cheung study the MOI was of 2. Furthermore, in the Cheung study while a strong response was seen very early upon infection it disappeared by 3h and 6h. However, as this was the only study using primary human cells it is possible that it carries a different and higher physiological relevance when compared to immortalized cell lines such as A549 and Calu3. It is also possible that macrophages would react rapidly and aggressively to infection with a highly pathogenic H5N1 strain as they have also been shown to react very rapidly to infection with both inactivated and live Ebola virus as measured by microarrays [131].

From this review of existing proteomic studies of influenza infections, it is quite apparent that more work is needed to fully characterize the host response during infection by HPAI and seasonal strains. This is one of the major themes presented in this thesis.

Figure 1.14 - H5N1 and H1N1 proteomic host response

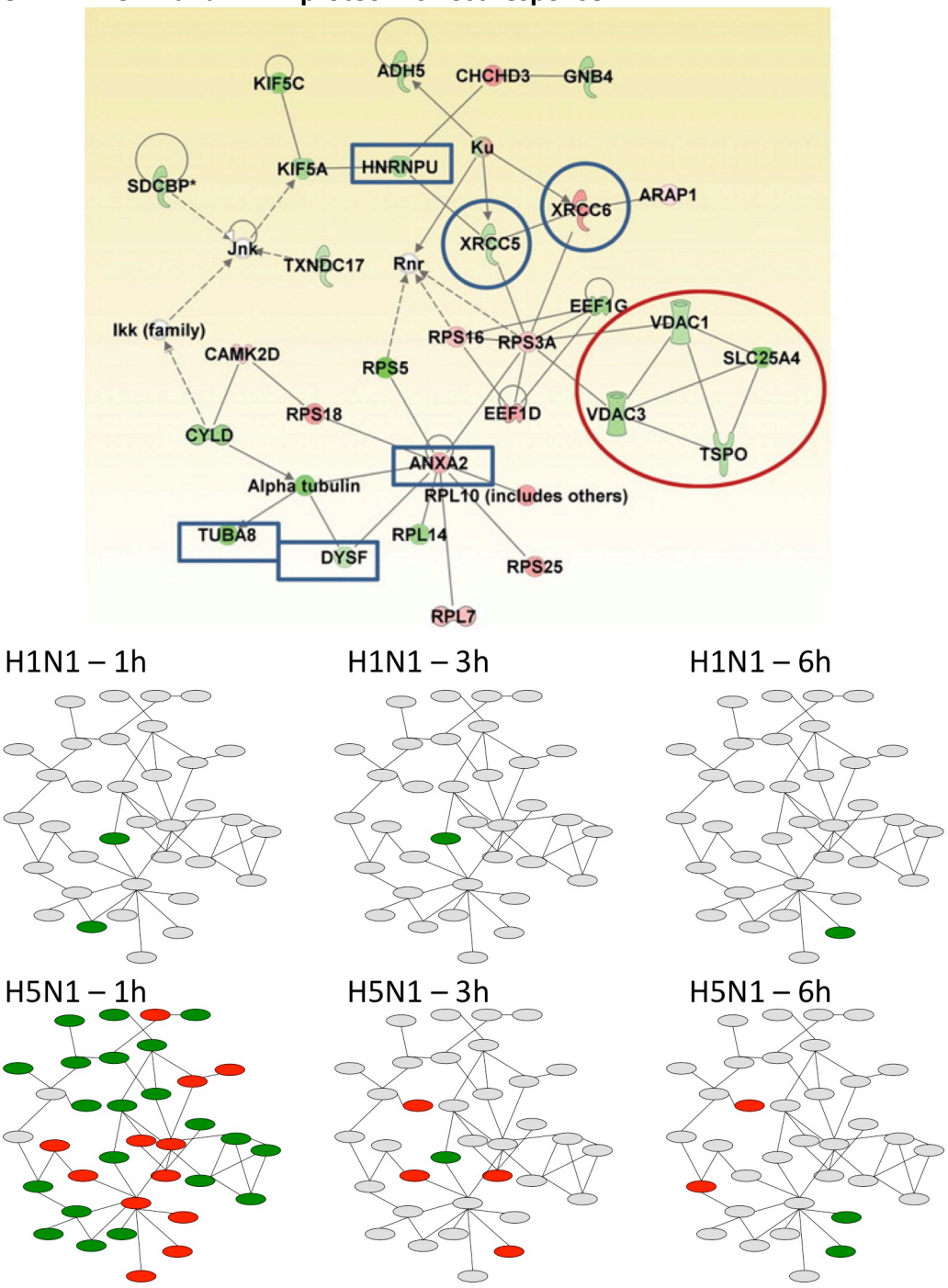

Comparative host-response in primary human monocytes during H1N1 and H5N1 infection. In their study, Cheung *et al.*, identified a network of proteins (large image) that was highly modulated at 1h post infection upon infection by an H5N1 strain. Green indicated down regulation and red indicates up regulation. Adapted from [130], the small network at the bottom represent the changes of the same network observed at each time points for both the H1N1 and H5N1-infected macrophages.

1.4 Mathematical modeling of in vitro infections

In an effort to better understand each step of viral replication, a portion of the work presented in the thesis is the result of an inter-disciplinary collaboration with physicists that have developed a mathematical model of influenza virus infection processes. While the full description and theoretical basis of computer simulations of viral *in vitro* growth kinetics fall out of the scope of this thesis, a short introduction to the relevant literature will be useful to better understand and appreciate our results.

From the point of view of a virologist, a mathematical model works as a detailed, quantified description of a viral replication cycle where the model-generated data fits with the experimentally-generated or clinically-observed data. The replication is described by several parameters with quantifiable values that, when combined in mathematical equations, should mimic the growth curves observed experimentally. A more detailed description of the parameters and assumptions underlying the model used in this study is available in the methods section (2.9). Once a good fit is obtained, the range of values of the variables for each parameter are extracted, giving in-depth information on the viral replication kinetics. A particular strength of mathematical modeling is that it can dissociate and quantify early and late events of viral replication, a difficult, if not impossible, task to address experimentally. The input values for our model consist of RNA concentrations and viral titers at various time points and the output are values such as the length of the eclipse phase, the decay rate of viral particles, the time it takes for a cell to become infected and the amount of viral particles released by a cell.

Surprisingly, the first use of mathematical modeling of viral infections was done *in vivo* to better understand viral replication in patients treated under different drug regimens. This approach has been used in both Human Immunodeficiency Virus (HIV) (reviewed in [132]) and Hepatitis C virus (HCV) (reviewed in [133]) research to monitor the effectiveness of antiviral therapy. In both cases, it was used to understand the effect of different drug regimens on viral clearance. The results of those studies were used to modify and improve treatment modalities. Specifically, early studies modeling HIV replication dynamics have shown that over 10^9 virions can be produced each day, accurately predicting the rapid replication of this virus. It also showed that the half-life of virions in plasma was 6 hours or less, prompting the idea that viremia could be cleared rapidly by antiviral therapy [134]. This and other studies conducted in the 1990s also helped in our understanding of HIV replication to not be one long latent event where viral activity was relatively low but rather as an active process where virions actively replicated and decayed at very high rates. Early on, this was recognized as important for viral evolution and the emergence of mutations involved in drug resistance [135]. Using mathematical models of viral replication, the effect of different doses of drugs [136], [137] as well as different drug regimens can also be assessed [132]. Using a similar model in human infections with HCV, the steady-state viremia during latent, untreated infection was found to be caused by an even more rapid production (over 10^{12} virion/day) combined with a more rapid decay (3 hours of half life) [138]. These results were all obtained using a very similar modeling approach (see Figure 1.15) where the mathematical variables define each of a series of discrete steps that each occur at a defined rate in the infectious process; uninfected (target) cells were infected at a certain rate, and produce a certain number of virions daily. Additional parameters

define the rate at which cells die and the rate of clearance of virions. The elegance of this approach is that much more complex phenomena (e.g. immunological pressure) do not need to be understood for their effect to be measured.

Figure 1.15 - Basic Model of Infection

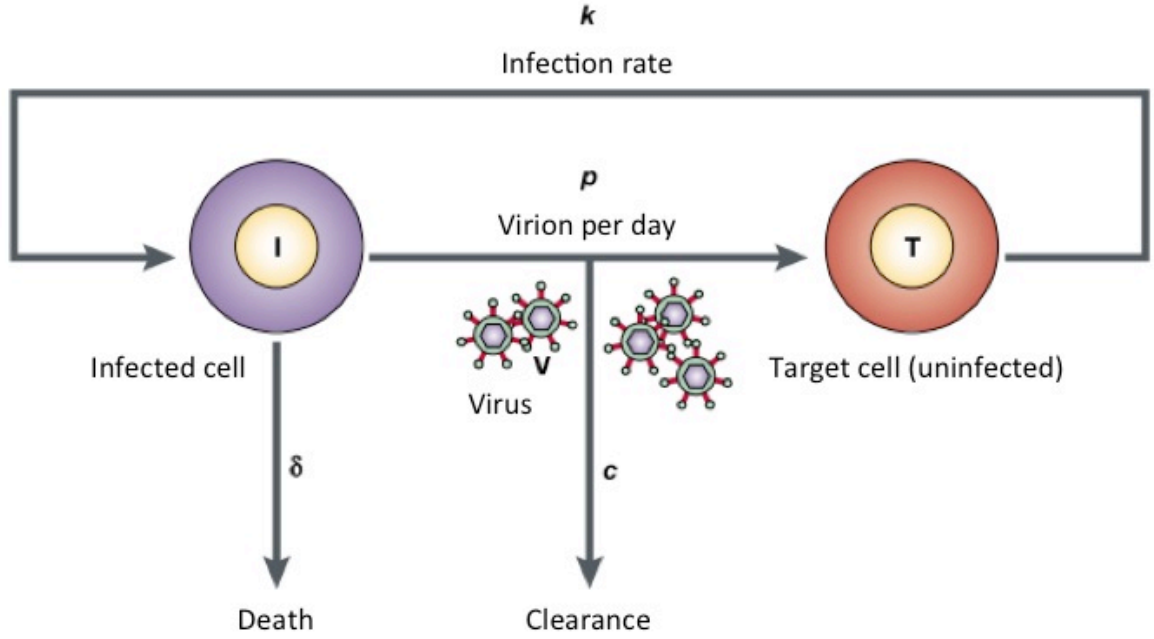

The basic concept of infection is that virions can infect cells at a certain rate. Infected cells will produce a certain quantity of virions at a definable rate within a measureable length of time before dying. Virions will also degrade and loose infectivity. Mathematical modeling aims at quantifying those steps. Figure from [132].

The portion of the work involving a mathematical model presented in this study builds upon prior collaborative work between the Beauchemin Lab at Ryerson and the Boivin Lab at Université Laval. In those studies, efforts were made to understand the differential replication kinetics of oseltamivir-resistant strains of influenza. A first study used plaque growth rates, as a measure of cell death defined by cellular lysis, as well as viral titres for virological input [139]. In that study, we showed the apparent lack of difference in fitness between a wild-type and an

oseltamivir-resistant strain of H1N1 IAV was in fact due to two competing mechanisms. The wild-type strain had a shorter eclipse phase but a longer infecting time while the oseltamivir-resistant mutant had a longer eclipse phase but a shorter infecting time. This provided an elegant mechanistic explanation to the global spread of the oseltamivir-resistant A/Brisbane/59/2007 (H1N1) strain in the 2008-2009 season even in the absence of drug pressure [140]–[142]. This study also pioneered the use of the combination of low MOI multi-cycle of viral replication experiment and a high MOI single cycle assay to provide the basic values needed for the model. Indeed, the high MOI experiment conducted in that study was used as independent experimental validation of our simulation data. A similar approach was used to study wild-type and oseltamivir-resistant strains of the 2009 pandemic H1N1 virus. In that project, qRT-PCR was introduced to measure viral RNA and also to track virus production during competition experiments with the two strains, both *in vitro* and in ferrets [143]. Similar to the seasonal H1N1 strain, the H275Y NA mutation conferring resistance to oseltamivir increased the length of the eclipse phase. In a refinement of the model, the burst size was also quantified as being larger for the wild-type strain.

Our understanding of biology constantly relies on the conceptualization of complex phenomena into simple, easier to comprehend and visualize models. The basic assumption that a virus infects a cell, produces progeny, eventually kills the cell and moves on to spread the infection could be considered the most basic of virology models. The modeling portion of this thesis simply refines and quantifies the steps of infection in a model that accurately conforms to experimentally-observed values.

1.5 Study rationale, hypothesis and objectives

The central hypothesis of this thesis is that the more highly pathogenic strains of influenza virus will induce a more profound host response in A549 cells and will exhibit significant differences in their replication cycles compared to less pathogenic strains. By studying the differences in cellular dysregulation between strains of low and high pathogenicity we hope to generate knowledge that can be used to develop new treatment strategies. Because of speed with which drug resistance develops in viral infections (see section 1.1.3), designing therapies modulating host pathways crucial to viral infection is a promising approach to augment a fairly limited arsenal of anti-viral strategies [144].

Specific objectives are:

1. Obtain proteomic datasets from A549 cells infected by low and highly pathogenic strains of Influenza virus at different early time points
2. Use bioinformatics tools to study the global impact of infection at early time points, contrasting these measured values between each of the viruses that are studied.
3. Validate interesting targets to confirm initial proteomic data and develop for potential follow-up as novel targets for further study and evaluation as targets for therapeutic intervention.
4. Confirm infection in A549 cells and study the viral replication kinetics of low and highly pathogenic strains
5. Use mathematical modeling to understand the differences in replication kinetics of low and high pathogenicity strains

Chapter Two – Material and methods

2.1 Virus strains

The following strains of influenza A viruses were used throughout this work: A/Canada/RV733/2007 (sH1N1 - a seasonal A/New Caledonia/20/1999-like clinical isolate), A/Mexico/INDRE4487/2009 (pH1N1 – a 2009 Pandemic H1N1 strain), A/Indonesia/05/2005 (H5N1 – a strain originating from a large outbreak in Indonesia in 2005 [145]) and A/Anhui/1/2013 (H7N9). Both H5N1 and H7N9 viruses are classified as biosafety level 3 risk organisms and therefore were handled in a Containment Level 3 (CL3) facility at the National Microbiology Laboratory in Winnipeg, Canada following all approved guidelines and SOPs.

2.1.1 Stock generation by ultracentrifugation

To generate sufficiently concentrated stocks of viruses, low passage isolates of each strains were grown on 10-12 T150 flasks (Corning) of 90%-confluent MDCK cells in Minimum Essential Medium (MEM) containing 0.1% of bovine serum albumin (BSA) and 1 μg/ml of Tosyl phenylalanyl chloromethyl ketone (TPCK)-treated typsin. MOI for infection was approximately 0.001 and supernatants were collected at 48h post infection. Infectious supernatants were pooled and clarified of larger cell debris by a first low-speed centrifugation at 2,400 g for 15 minutes at 4^{o}C. Supernatants were then ultracentrifuged in a Beckman-Coulter L90-K with a SW-32 Ti rotor at 28,000 RPM for 2 hours at 4^{o}C. This speed corresponds to a maximum of 133,907 x g and an average of 96,281 x g. Supernantants were discarded and 35 ml of fresh MEM containing 0.1% BSA was added to the centrifuge tubes. This was done without disturbing the pellets to wash away any remaining soluble contaminants. These were then submitted to a

second round of ultracentrifugation for 1h at 28,000 RPM. Supernatants were again carefully removed and 200 µl of MEM containing 0.1% BSA was added to each pellet. This was left to incubate overnight at 4^{o}C and the next day dissolved pellets were gently mixed and pooled prior to being distributed in 40 µl aliquots and frozen at -80^{o}C.

2.2 Tissue culture

2.2.1 Classical tissue culture

2.2.1.1 A549 culture

Human lung adenocarcinoma cell line A549 was used for all infections with influenza viruses. These were cultured in Ham's F12 media with Kaighn's modification (F12K - Hyclone, GE Healthcare) supplemented with 5% fetal bovine serum (FBS - Sigma). Typically, they were passaged by rinsing confluent monolayers with sterile PBS prior to trpysinization with a solution of 0.25% Trypsin (Sigma) for approximately 10 minutes. The usual split ratio was 1:4 (based on surface area of the flask) to obtain confluent monolayers within 48h. To obtain accurate cell counts, an automatic optical counter (Countess – Life Technologies) was used to count live/dead cells stained in a 0.4% trypan blue solution.

2.2.1.2 MDCK culture

Madin-Darby canine kidney cells (MDCK) were used for the preparation of virus stocks, for plaque assays and measuring infectivity by Tissue Culture Infectious Dose 50% (TCID50). These were cultured in Minimal Essential Media (MEM – Life Technologies) supplemented with 5% FBS and 1X L-Glutamine. As these cells are quite adherent, the following procedure was used to passage them: they were washed with PBS and then with a 0.25% trypsin solution which was

then replace by fresh 0.25% trypsin solution. They were then incubated at 37^{o}C between 30 and 45 minutes or until the monolayer was completely detached. Typically, a 1:6 dilution (based on surface area of the flask) enabled a new monolayer to reach 90-99% confluence within 48h. For both A549 and MDCK cells, low-passage samples were kept frozen in liquid nitrogen in a 9:1 mixture of FBS:Dimethyl sulfoxide (DMSO).

2.2.2 Robot-assisted cell culture

To obtain more constant growth conditions for A549 cells, we had access to a SelecTCompacT cell culture robotic instrument (TAPBiosystems). This essentially consists of a robotic arm inside a sterile laminar flow hood connected to a carousel incubator along with various peristaltic pumps to dispense media via sterile tubules. It also has a built-in confluence reader that can be programmed to take regular measurements. The robot can be programmed to automatically passage the cells upon reaching certain confluence threshold. These features were used extensively to passage the cells for the proteomic experiments of Chapter Three. Cells were grown in standard F12K + 5% FBS media and their confluence was measured automatically every 6 hours. Upon reaching 70-75% confluence they were automatically passaged in a 1:4 ratio based on surface area of the flask. After a minimum of 3 cycles of this passage scheme the cells where then used for the proteomic experiments.

2.2.3 Virus titration on MDCK cells

2.2.3.1 Plaque assay

For plaque assays, we used the Avicel overlay methodology developed by Matrosovich et al. [146] that I successfully used previously [139]. Confluent MDCK cells in 6- or 12-well plates

(Corning) were washed and maintained in MEM + 0.1% BSA in CL2 and brought into CL3. Once in CL3, maintenance media was removed and infection media added. Ten-fold dilutions of samples covering the range from 10^{-3} to 10^{-9} were made in MEM + 0.1% BSA + 0.5 µg/ml TPCK-treated trypsin. Serial dilutions were adsorbed on the cells for 1h at 37^{o}C with gentle rocking every 10 minutes. For 6-well plates, 500 µl of each dilution was used whereas 200 µl was used in 12-well plates. After the adsorption, infection medium was removed and a 1:1 mix of 2x MEM and 2.4% Avicel RC-831 (FMC Biopolymers) in cell-culture grade water and containing final concentrations of 0.1% BSA and 0.5 µg/ml TPCK-treated trypsin was added (3ml/well of a 6 well plate or 1ml/well of a 12-well plate). Plates were incubated between 48h and 72h and the semi-solid overlay was then pipetted out. Cells were fixed – and virions inactivated – with a cold 4% paraformaldehyde solution in MEM for at least 30 minutes and then a 1% Crystal Violet solution in 20% Methanol:water was used to stain the wells. This was left for 10 minutes in the plates before rinsing them and counting the plaques which was then used to calculate the virus yield in plaque forming units (PFU) per ml of the undiluted sample.

2.2.3.2 Tissue Culture Infectious Dose method

A standard TCID50 method was used to measure infectivity. MDCK cells were grown to approximately 80-90% confluency in 96-well plates (Nunc) and washed with 100 µl of MEM + 0.1% BSA in CL2. They were then brought into CL3. To allow us to process large batches of samples, we used 96-well 2ml dilution blocks to process either 8 or 12 samples simultaneously across a wide ten-fold dilution range. Samples were serially diluted in the block and added to at least four 96-well plates in identical format. Infection media was MEM + 0.1% BSA + 0.5 µg/ml TPCK-treated trypsin. Infected plates were incubated for at least 72h or until the difference in

cytopathic effect (CPE) was easily distinguishable between non-infected and infected wells. We used an Excel file available at http://www.klinikum.uni-heidelberg.de/fileadmin/inst_hygiene/molekulare_virologie/Downloads/TCID50.xls which calculates TCID50s based on the Spearman and Kärber algorithm.

2.2.4 A549 infections

For both the Proteomics study of Chapter 3 and for the Kinetic study of Chapter 4, A549 cells were infected at high MOIs while the low MOI infection was used only for Chapter 4. For the proteomic study we used an MOI of 10 PFU/cell and for the Kinetic study MOIs of 3 and 0.01 PFU per cell. A549 cells were cultured either by the traditional method (see 2.2.1.1) for the kinetic experiments and by the robotic method (see 2.2.2) for the Proteomics experiments. Prior to infection, cells were trypsinized and counted on an automatic cell counter (Countess – Life technologies) and 1,000,000 live cells were plated with 7ml of F12K medium in T25 flasks. These were incubated for 48h and at least two spare flasks where kept, typsinized and counted on the Countess the morning of the infection to ensure accurate MOI calculations. Flasks were washed with F12K in CL2 and brought in CL3 where the wash media was removed and 1 ml of infection media (F12K + 0.1% BSA + 0.5µg TPCK-treated Trypsin) containing the adequate MOI was adsorbed for 1h at 37^{o}C. Following adsorption, maintenance medium was added for the duration of the subsequent experiment. In the case of the proteomic experiment, cell lysates were collected at 1, 3 and 6h post-infection using an SDS lysis buffer (see 2.3.1). For the kinetic experiments, 500 µl of supernatant were harvested at set time points (see Chapter 4) and replenished with fresh medium. In the case of the high MOI infection of the kinetic experiment, the high background was removed by rapid washes with a 0.9% NaCl solution at pH 2.2

followed by several rapid washes with F12K media, similar to what we had previously used in other high MOI experiments [139].

2.3 Level 3 sample inactivation

Stringent inactivation protocols are in place at the National Microbiology Laboratory to ensure proper inactivation of infectious samples exiting high-containment laboratories. This section describes the protocols used for sample preparation in CL3 containment that meet the requirements for sample inactivation for removal from CL3.

2.3.1 SDS

To obtain protein lysates either for western blots or for iTRAQ labeling, the preferred method is to scrape the cells in a 2% SDS buffer in 50 mM Tris and boil the samples for a minimum of 10 minutes twice. This satisfies the biosafety requirements for inactivating CL3 agents. It also produces protein lysate that contains an equal distribution of membrane, cytoplasmic and nuclear proteins [147].

2.3.2 AVL

The AVL buffer (560 µl containing the chaotropic denaturant guanidinium isothiocyanate) supplied in the Qiagen ViralRNA kit is first mixed with sample (140µl) in the recommended ratio. When subsequently combined with 560µl of ≥95% ethanol the sample is ready for the first step of the extraction of RNA and is fully inactivated. The method has been approved as a safe to inactivate viral pathogens for both CL3 and CL4 work. We used this method to obtain RNA samples from supernatant for qRT-PCR (see 2.10).

2.4 Western blotting

For western blot analysis, we relied on the Odyssey System (Li-Cor). It uses a near-infra-red (NIR) detector and tagged secondary antibodies for NIR detection and allows the simultaneous detection in two channels (designated red and green). Samples prepared in CL3 were kept in at least 2% SDS solution and 5% Beta-mercaptoethanol (BME) was added prior to boiling and loading on the gels. Most of the SDS-PAGE gels were done using the BioRad Mini-Protean system typically with a 4% Acrylamide-Tris stacking gel and a 10% Acrylamide-Tris resolving gel. We also used some 4-12% gradient Bis-Tris pre-cast gels (Novex, life Technologies). Typical voltage settings for the gels were 100-130 V for 60-80 minutes. The best results for transfer in preparation for Western blotting were by using a slow (40 mA) overnight wet transfer onto Nucleon membranes. These were block with Odyssey-supplied blocking buffer for 1h at room temperature. Primary antibodies used were anti-Ferritin (3F8 and H-53, abcam ab134276 and H-52 ab7332) and anti-fibronectin (abcam ab2413). For confirmation of infection, we used a mouse anti-NS1 monoclonal antibody (7D11) produced by the Coombs lab [148]. Densitometry analysis was performed with the ImageStudio Lite 4.0 software from Li-Cor. Ladder was Thermo Scientific PageRuler NIR ladder or MagicMark (LifeTechnology).

2.5 Protein quantitation

For protein quantitation for both western blot and to prepare the lysates for iTRAQ labeling we used the Pierce Microplate BCA Protein Assay kit (Life Technologies). The advantage of this kit is that it tolerates up to 5% SDS as well as 5mM DTT and therefore allows the quantitation of CL3-removed samples. It also requires only 9 µl of sample. The colorimetric reaction relies on the reduction of Cu^{2+} ions by peptides to Cu^{+} in the presence of bicinchoninic acid. The

bicinchoninic acid then chelates the Cu^{+} and changes color from green to purple. This takes place in 96-well round-bottom plates that can be read in any standard plate readers at a wavelength of 562 nm. A standard of serially diluted BSA is used to determine the protein concentration of each samples using a linear regression linking absorbance at 562 nm to the know protein concentration of the standard.

2.6 Quantitative proteomics

For the Proteomic portion of this project I received expert help and advice from the Mass Spectrometry and Proteomics core facility at the National Microbiology Laboratory as well as from Dr. Michael Carpenter who optimized the Filter-Aided Sample Preparation (FASP) technique.

2.6.1 Filter-Aided Sample Preparation

Throughout this project, we used an improved version of the Filter-Aided Sample Preparation (FASP) method described previously [118], [149]. It relies on denatured protein lysates being adsorbed on a filter, washing off the SDS, alkylating the cysteine residues and digesting them to peptides on that same filter. Using the optimized protocol, described below, an experienced individual can recover the peptides in 75% yield. After protein quantitation (see 2.5), 200 µg of protein was mixed with DTT to a final concentration of 20mM, boiled and adsorbed to Nanosep 10 kDa filters (Pall Corporation). These are centrifuged, the filtrate is discarded and the filter is washed several times with an 8 M Urea buffer to remove the SDS and proteins are then alkylated on cysteine residues using 0.05M of iodoacetamide in 50 nM HEPES buffer. After 30 minutes, this is washed with 50 mM HEPES buffer and 1 µg of trypsin (MS-

Grade, Promega) in 50 mM HEPES is added per 100 µg of protein lysate. The filters are incubated overnight in a humid chamber at 37^{o}C. Tryptic peptides are eluted the next day by spinning the filters at 14,000 g x 10 min with 50 µl of 50mM HEPES followed by 50 µl of water. Samples are then dried on a SpeedVac (medium setting for 2h) and frozen at -80^{o}C until ready for iTRAQ labeling.

2.6.2 iTRAQ labeling

For the quantitative portion of the proteomic work, we chose to use isobaric Tags for Relative and Absolute Quantitation (iTRAQ) (AB Sciex). At the time of ordering them, our group was most familiar with the 4-plex kit but an 8-plex is also available. Peptides were labeled following the manufactures instructions [150]. Briefly, each iTRAQ label is reconstituted with 70 µl of pure ethanol and 100 µg of each peptide sample (reconstituted in MilliQ water) is added to the tube. The chemical labeling of the amino group is carried over 1h at room temperature and the reaction is quenched by adding 100 µl of MilliQ water. After labeling, the liquid is evaporated in a speedvac and the iTRAQ-labeled peptides are suspended in 30 µl or 100 mM HEPES buffer pH 8.

To ensure no labeling bias for the large number of samples and replicates we had to process, we used a simple label-swapping method so that no sample from the three biological replicates was labeled twice with the same tag (see Table 2.1).

Table 2.1 - iTRAQ label swapping

Replicate	iTRAQ Label	Samples				
1	**114**	sH1N1-1h	pH1N1-1h	H5N1-1h	H7N9-1h	Nothing
1	**115**	sH1N1-3h	pH1N1-3h	H5N1-3h	H7N9-3h	Mock-3h
1	**116**	sH1N1-6h	pH1N1-6h	H5N1-6h	H7N9-6h	Mock-6h
1	**117**	Mock-1h	Mock-1h	Mock-1h	Mock-1h	Mock-1h
2	**115**	sH1N1-1h	pH1N1-1h	H5N1-1h	H7N9-1h	Nothing
2	**116**	sH1N1-3h	pH1N1-3h	H5N1-3h	H7N9-3h	Mock-3h
2	**117**	sH1N1-6h	pH1N1-6h	H5N1-6h	H7N9-6h	Mock-6h
2	**114**	Mock-1h	Mock-1h	Mock-1h	Mock-1h	Mock-1h
3	**117**	sH1N1-1h	pH1N1-1h	H5N1-1h	H7N9-1h	Nothing
3	**114**	sH1N1-3h	pH1N1-3h	H5N1-3h	H7N9-3h	Mock-3h
3	**115**	sH1N1-6h	pH1N1-6h	H5N1-6h	H7N9-6h	Mock-6h
3	**116**	Mock-1h	Mock-1h	Mock-1h	Mock-1h	Mock-1h

2.6.2.1 Pre scan normalization

Besides stringent infection conditions, normalization of samples was done at the protein level by protein quantitation (see 2.5). However, our experience has shown that the preparation can have some variability between samples. Bias can be somewhat corrected by the Scaffold software (see 2.6.5) but having 1:1:1:1 ratio of labeled samples is an excellent way to improve the quality of our results. To achieve this, the MSP Core has developed a method called *Pre Scan normalization*. Once the samples were labeled with iTRAQ tags, 2 µl of each samples (across a 4-plex) were mixed together. This achieved a 1:1:1:1 ratio based on volume.

The 4-plex were then run on a short 2h gradient on the mass spectrometer (see 2.6.4) and a distribution of the labeled peptides was obtained. The median was then used to assess whether the 1:1:1:1 ratio was maintained or whether volume adjustments were required to achieve the desired 1:1:1:1 ratio. Scaffold can apply computer-normalization to samples that have as high as a 20% labeling bias but for the purpose of this study we tried to keep the bias under 5%. Figure 2.1 shows a histogram for two prescans. The left shows a mostly adequate labeling bias while the right one requires further volume adjustment to achieve the desired null ratio.

Figure 2.1 – Labeling bias histograms

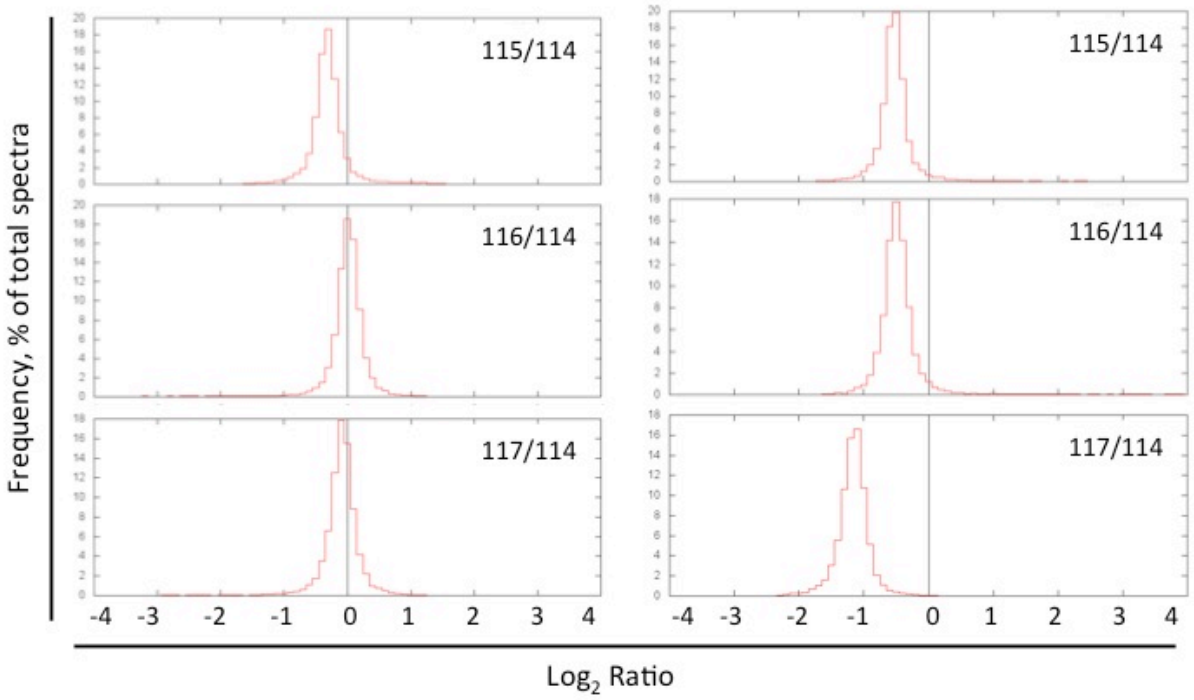

By mixing equal volumes of labeled peptides and running the mixture on the mass spectrometer for a short run any labeling bias can be addressed for the major proteomic experiment. The histograms on the left show a 4-plex with a mostly well-balanced 1:1:1:1 ratio while the histograms on the right show a mixture where the 1:1:1:1 ratio will need to be further adjusted prior to definitive mixing of the iTRAQ labeled peptides.

2.6.2.2. iTRAQ multiplexing strategy

A challenge with this study is that we needed to obtain quantitative proteomic information on 4 viruses in three independent biological replicates at three different time points. We also need time-matched mock controls. In total, this amounts to 45 samples that should, ideally, all be directly comparable to each other. To achieve this, we used a within-replicate common control. Therefore, a 4-plex consisted of the Mock-1h samples and the 1, 3 and 6h-virus-infected samples. This was done across each replicate and as the Mock-1h sample was the same within each replicate it allowed for direct comparison of differential abundance of each of the infected samples both across different viruses (and including the Mocks) as well as across all time points. Figure 2.2 represents this strategy.

Figure 2.2 - iTRAQ multiplexing strategy

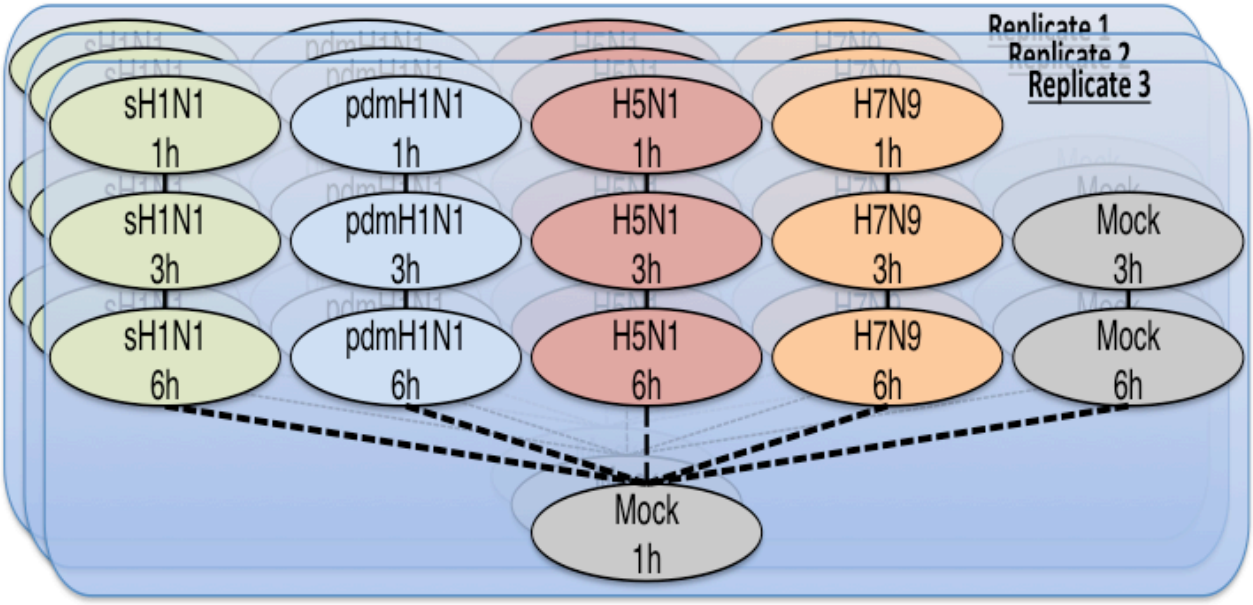

Multiplexing strategy for the iTRAQ 4-plex. A. Identical Mock 1h sample is added to all 4-plexes within each biological replicate allowing direct comparison of all data from infections with each virus at each time points.

2.6.3 HPLC fractionation and concatenation

To reduce the complexity of the peptidic mixture we used 2 dimensional liquid chromatography fractionation [118], [119]. A first fractionation step was conducted at pH 10 on an offline Agilent 1200 HPLC system using an XBridge C18 column (Waters). Buffer A was 20mM ammonium formate (pH 10) and Buffer B was 90% acetonitrile (ACN) in 20 mM ammonium formate, pH 10. The gradient was from 3% to 95% buffer B over 170 minutes at a constant flow rate. A total of 34 fractions were collected across the peptide elution profile (15-60 min) and concatenated into 12 fractions by mixing early and late fractions together. This was determined to be a balanced compromise between too many fractions - which gives excellent identification and quantitation but takes too long on the mass spectrometer – and too few where, while more quickly processed, the peptide complexity is such that identification is poor. Figure 2.3 shows a typical elution profile along with the fractionation and concatenation scheme used. Early fractions (of low hydrophobicity) were mixed with middle and late fractions, respectively of high and higher hydrophobicity. The goal of this is to achieve an orthogonal mixture of peptides that will easily be separated in the 2^{nd} dimension chromatography (see 2.6.4).

Figure 2.3 - Offline fractionation and concatenation

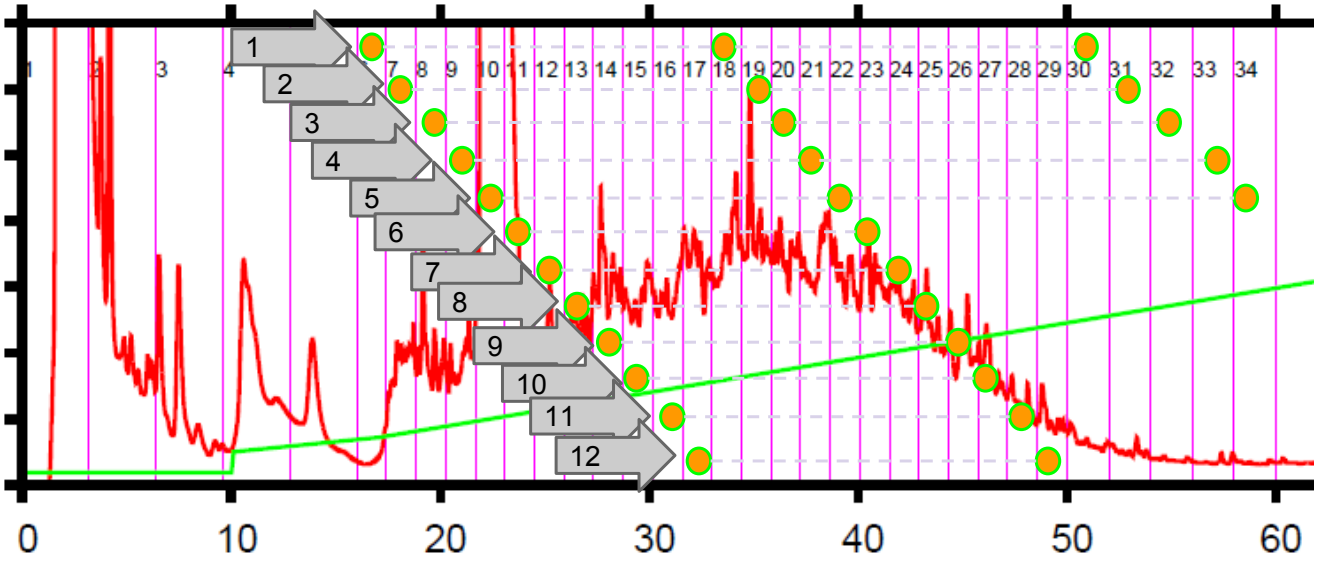

A total of 34 fractions were collected between 15 and 60 minutes within the 70 minutes gradient. These were then concatenated into 12 fractions (grey arrows and orange dots). The intent was to combine early and late fractions to mix peptides with as wide a range of hydrophobicity as possible.

2.6.4 nLC-MS/MS

The 12 fractions (per biological replicate) generated on the offline HPLC were dried in a SpeedVac and reconstituted into nano-LC buffer A (2% acetonitrile, 0.1% formic acid). For each fractions, 1.5 µg of protein injected into our LTQ Orbitrap Velos mass spectrometer (Thermofisher) using the Proxeon Easy-nLC system with a 15 cm analytical column (id=75 µm) packed with 2.4 µm ReproSil-Pur C_{18}-AQ resin (Dr. Maisch GbmH). A 2-32% buffer B (98% acetonitrile, 0.1% formic acid) linear gradient was applied over 120 min at a constant flow rate of 250 nl/min. This was injected in the mass spectrometer using a nanoelectrospray ion source at 2.3 kV. Mass spectra were acquired in an LTQ Orbitrap Velos using data-dependent acquisition. Ionized peptides were fragmented in the HCD cell (40% normalized collision energy) for identification and quantitation. The survey scans were acquired in the Orbitrap using a mass

window of 300–1700 m/z at a target resolution of 60 000. The work involving the mass spectrometer was expertly performed by Stuart McCorrister from the Mass Spectrometry and Proteomics Core Facility at the National Microbiology Laboratory.

2.6.5 Data acquisition and protein identification

Spectra were processed in Mascot Distiller 2.4.3 (Matrix Sciences) using the Swissprot 2013_09 database for mammals as well as a standard contaminant database (Matrix Science) and a custom influenza virus database with sequences retrieved from Global Initiative on Sharing Avian Influenza Data (GISAID) on all 4 strains used in this study. Table 2.2 identifies the sequences used in our custom influenza database. A decoy database to measure false discovery rates (FDR) was created by inverting the Swissprot database. Mascot search results were imported into Scaffold Q+ 4.1.1 (Proteome Software [151]) and only proteins with a minimum of 2 peptides at 80% confidence and an overall confidence of over 90% for their identity were kept for analysis. This translated to a false discovery rate (FDR) of < 1% as calculated by Scaffold.

Table 2.2 - GISAID etiquette compliance

Segment ID	Segment	Country	Collection date	Isolate name	Submitting Laboratory	Authors
EPI105013	PB2	New Caledonia	1999	A/New_Caledonia/20/1999 (H1N1)	Not specified	Not specified
EPI105015	PB1					
EPI105017	PA					
EPI105019	HA					
EPI105021	NP					
EPI105023	NA					
EPI105024	MP					
EPI105027	NS					
EPI178279	PB2	Mexico	2009	A/Mexico/InDRE4487/2009 (H1N1)	Not specified	Not specified
EPI178281	HA					
EPI178284	MP					
EPI178287	NA					
EPI178290	NP					
EPI178293	NS					
EPI178296	PA					
EPI178299	PB1					
EPI376534	PB2	Indonesia	2005	A/Indonesia/5/2005 (H5N1)	Not specified	Herfst,S. et al.
EPI376535	PB1					
EPI376536	PA					
EPI376537	HA					
EPI376538	NP					
EPI376539	NA					
EPI376540	MP					
EPI376541	NS					
EPI439503	PA	China	2013-03-20	A/Anhui/1/2013 (H7N9)	WHO Chinese National Influenza Center	Yang, Lei
EPI439504	PB2					
EPI439505	NP					
EPI439506	MP					
EPI439507	HA					
EPI439508	PB1					
EPI439509	NA					
EPI439510	NS					

2.7 Statistical analysis of significantly modulated proteins

Several statistical approaches can be used to extract meaningful information from high throughput results, yet there is no absolute consensus on which is the best approach. Importantly, the statistics alluded to in this section refer to the quantitation results (i.e. whether a protein is up- or down-regulated). The identification of a protein by mass spectrometry has already been covered in the previous section. This section focuses on the statistical approaches used to generate lists of proteins considered to be significantly modulated. Historically, we have used the z-score distribution of protein abundance as an indicator of significance. Mathematically, $\log_2$ fold changes for each protein were converted into z-scores, which is a measure of the standard deviation of the value from the mean. In the resulting z-distribution, by definition values of under -1.96 and over 1.96 sigmas represent proteins that are either of lower (<-1.96) or higher (>1.96) abundances at a 95% confidence level. This also represents a two-tailed p-value of at most 0.05. From the three biological replicates, we kept only proteins where the p-value was <0.05 for at least 2 replicates and tolerated a third replicate to be non-significant [128], [152], [153]. These criteria are simple to implement and simple to understand for biologists; however, newer and more modern approaches can be used. To ascertain that we had the most up-to-date statistical method for our quantitative proteomic study, we collaborated with a biostatistician (Dr. Pingzhao Hu, University of Manitoba). He first used a batch correction to eliminate unwanted and non-relevant replicate effects [154], [155]. Filtered results were then analyzed with a Bayesian model fitted to a Linear Model for Micro Array (LIMMA) package in R (a major open-source statistics software), similar to what has been used in recent work by the Kawaoka group [129].

A Benjamini-Hochberg multiple comparison correction of the p-value was performed [156] and only proteins with a corrected p-value of <0.05 were considered for subsequent analysis. This generated 2 lists of proteins: the LIMMA list and the z-score list. To get as broad a search as possible, we used the combination of these two lists for the subsequent bioinformatics analysis while we only relied on the stringent LIMMA list for individual target for follow-up. Two-way hierarchical clustering of rows and columns was performed using a correlation-based distance measure and ward linkage [157]. This unbiased approach aims at grouping proteins with similar expression values in clusters. This is done both on rows (individual proteins) and on columns (each samples). The resulting dendrogram is a measure of how similar each column is in terms of protein dysregulation. Similar samples will cluster together while dis-similar samples won't. This work was performed by Dr. Hu in collaboration with this project.

2.8 Bioinformatic analyses

2.8.1 Global overview in IPA

Lists of statistically-significant proteins for each triplicate infections were imported into Ingenuity Pathway Analysis (IPA), a cloud-based bioinformatics pathway analysis tool (Qiagen). IPA possesses a built-in suite of analytical tools that were pivotal to better understand the functions involved with our dataset. We first ran a Core Analysis for each infection subset (i.e. Mock1h-sH1N1:1h-sH1N1:3h-sH1N16h) and followed this with a Comparison Analysis of all the infection and mock subsets (i.e Mocks vs sH1N1 vs pH1N1 vs H5N1 vs H7N9). From each core analysis, we were able to extract the "Disease and Function" heat maps. These represent individual IPA-defined biological pathways or functions that are modulated by the dysregulation

of the proteins of the dataset of each subset, giving us a broad overview of the outcome of infection in the cells with each virus and at each time point (See Chapter 3). From the "Comparison Analysis" we were able to extract the top modulated biological pathways when looking at all the viral infections simultaneously.

2.8.2 FLEUR analysis

To illustrate the regulation of interesting proteins found in our screen, we developed a novel analysis tool termed "FLEUR". This stands for Focused Layout of Entities with Unbiased Relations. To build a FLEUR network in IPA around a protein of interest, one sequentially probes user-defined datasets (in this case each infection 4-plex and the mock) for interacting partners. This generates individual, experimentally-derived clusters of proteins/genes that have interactions with a central protein. The amount of overlap can be readily visualized, giving valuable information on potential regulatory mechanisms involved in the expression of the central protein. Theoretically, this could be used for any datasets with 2 or more subsets.

2.9 Lay overview of mathematical modeling

Chapter 4 of this Thesis deals with the growth properties of four strains of influenza A virus. This was the result of a collaborative study with Dr. Catherine Beauchemin, a physicist developing a model to describe influenza infection, from Ryerson University. While I dealt with all the aspects of virological experiments in the laboratory, her group developed and implemented the mathematical model. A complete and detailed description of the inner workings of the model is beyond the scope of this work as, from my perspective, it was used as a tool rather than as an expansion of the development of the model itself. However, a

simplified explanation of the concept is warranted. The model is built on a set of parameters that, together, can be combined to define the *in vitro* growth properties of – theoretically – any *in vitro* infection by any lytic virus. The virology-relevant parameters are defined in Table 2.3 and a schematic representation of the model is given in figure 2.4.

Table 2.3 - Parameters of the Infection Model

Parameter	Unit	Description
Clearance	1/hr	Rate of loss of infectivity
Production rate	TCID50/cell/hr RNA/cell/hr	Output of virions (either in TCID50 or RNA) per cell per hour
Infection rate	ml/(TCID50 x hr)	Ability of virions to infect cells
Infectious lifespan	hr	Duration of continuous virion production by an infected cell (in hours)
Eclipse phase	hr	Time between cell infection and virion production (in hours)
Infecting time	min	Time between initiation of virus production in one cell and the infection of another cell (in minutes)

Figure 2.4 - Model of infection

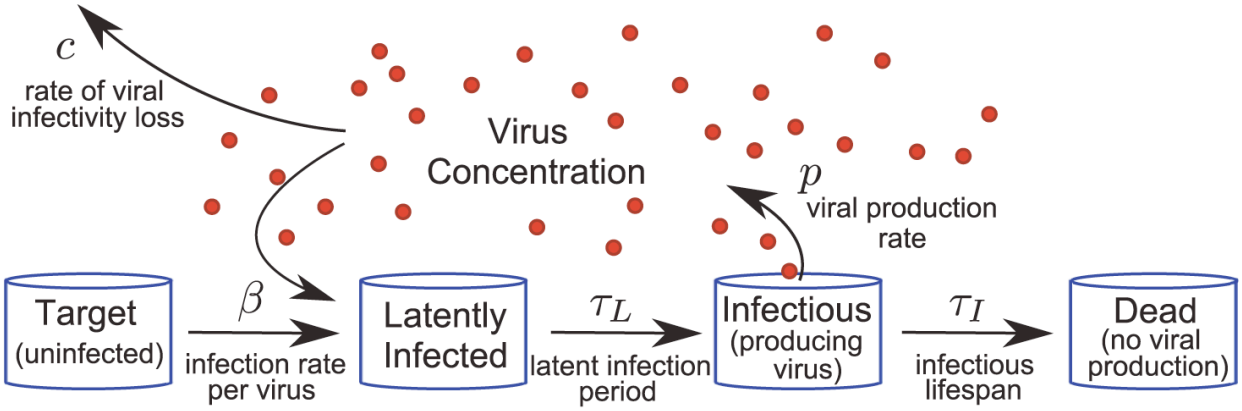

This model builds on the well-established model presented in the introduction (figure 1.14) and has been used to characterize *in vitro* infections with influenza in previous studies. Figure from [139].

The value of each parameter is modulated and an independent computer simulation is run to see how the resulting growth curve fits with the experimental data provided. This is repeated independently in over 600,000 iterations, which yields a distribution of values for each parameter where the model meets the experimental data. Comparative statistics can then be used to assess the parameter distribution between the viruses studied in the present experiments.

2.10 Quantitative PCR

For quantitative reverse transcription-PCR (qRT-PCR), we used a Roche LightCycler 480 (software version SW 1.5.1) and the Roche RNA Master Hydrolysis Probe 480 kit. The RNA was extracted as mentioned in section 2.3.2. Primer-probe sets directed to the M gene (all viruses) and HA and NA genes (pH1N1 only) were used. Primer and probe sequences are given in table 2.4. The HA and NA set for the pH1N1 virus were designed in-house and a kind gift from Laura Hart. The M set is from a CDC diagnostic kit ordered from IDT and has been described previously [158]. In all sets, the fluorophore was 5-Carboxyfluorescein (FAM) and we used Black Hole Quencher 1 (BHQ1) as quencher. The standard curves for the quantitation where done using the entire M, HA or NA segments for each respective strain cloned into a pPol vector. Purified plasmid preparations were quantified using a Nanodrop instrument. Based on the DNA content and overall length of the plasmid and the inserted gene, the copy-number can be inferred using free online tools available at http://cels.uri.edu/gsc/cndna.html. Ten-fold dilutions spanning 10^{10} to 10^{-2} (acting as negative controls) copies/µl are used as standards and inputted into the LC480 software. These produced linear regressions with r^2 values always superior to 95%. During the amplification cycles, the CP values (Crossing point values – the

Roche equivalent to Ct values) for each sample are determined by the instrument and the copy number is automatically calculated based on the standard curve. Several methods can be used to calculate copy-numbers based on a standard curve. Roche recommends the use of the Second Derivative Maximum analysis method, which is the method used throughout this study.

Table 2.4 - Primer-Probe Sets for Quantitative PCR

Target	Primers (F/R)	Probe*
M	5-GACCRATCCTGTCACCTCTGAC-3 5-AGGGCATTYTGCACAAAKCGTCTA-3	F-TGCAGTCCTCGCTCACTGGGCACG-B
HA	5-TGGCTGGATCCTGGGAAATC-3 5-CGATGAAATCTCCTGGGTAACAC-3	F-CACTCTCCACAGCAAGCTCATGGTCCTAC-B
NA	5-TTAACATCAGCAACACCAACTTTG-3 5- CCATCCACTAACAGGGCAGAG-3	F-CACTCTCCACAGCAAGCTCATGGTCCTAC-B

* F – 5-Carboxyfluorescein (FAM); B – Black Hole Quencher 1 (BHQ1)

2.11 Nuclear Fractionation

For nuclear fractionation, A549 cells in T75 flasks were infected at MOI of 10 with each strain and incubated for 6h. We used the Cayman Chem nuclear fractionation kit (Cayman Chemical, Ann Arbor MI) following the manufacturer's instructions. We also used the Rapid, Efficient And Practical (REAP) method described elsewhere [159]. For both methods, cells are washed with ice-cold PBS and harvested with cell scrapers. They are then swelled in hypotonic buffers to release the cytosolic content while maintaining nuclear integrity. The cytosolic fractions are harvested and the nucleus are washed. The main differences are that the Cayman method uses fast centrifugation at 14,000 g while the REAP method uses a slow centrifugation

(300 g) to harvest the nuclear fractions. The Cayman method uses 10% Nonidet P-40 (NP-40) to solubilize the nuclear fractions while the REAP method uses a milder buffer at only 0.1% NP-40 in PBS. Both worked well but the REAP was faster and cheaper. Loading controls of histone (H3 - Abnova MAB10253) and Mitochondrially encoded cytochrome c oxidase subunit II (MTCO2- Abcam ab3298, [160]) were used as nuclear and cytoplasmic markers, respectively. We tested two anti-NRF2 antibodies (Abcam ab137550 and Santacruz sc-722) and found that the Abcam antibody yielded good results when used at a 1:500 dilution in PBS containing 0.1% tween-20.

Chapter Three – Host responses to low pathogenicity human and low and highly pathogenic avian influenza viruses

3.1 Introduction, rationale and productivity

The work presented in this Chapter focuses on the proteomic responses during infection by strains of influenza A virus causing a continuum of illness in human patients. Low pathogenicity seasonal (sH1N1) and 2009 pandemic H1N1 (pH1N1) strains are compared to two strains causing severe disease in humans: an H5N1 HPAI strain as well as the novel H7N9 LPAI virus. Both of these latter viruses are currently causing human cases in Asia with case fatality rates of approximately 60% (H5N1) and 20% (H7N9). The A549 human lung adenocarcinoma cell line was chosen as our experimental model to study the host response to infection at early time points (1, 3 and 6h post infection). These cells represent a good compromise, balancing biological relevance of human lung cell lines with the technical ease of an immortalized cell line used extensively in influenza research. We used bottom-up quantitative shotgun proteomic approach with isobaric tags for relative and absolute quantitation (iTRAQ) labeling and to obtain un-biased quantitative information on relative protein abundance in A549 synchronously infected at a high MOI. To our knowledge, this is the first study comparing the host responses to sH1N1, pH1N1, H5N1 and the novel H7N9 strains of influenza.

The work presented in this Chapter is currently under final revisions for publication in the Journal of Proteome Research. Part of it have also been presented at the 2014 meeting of the International Congress of Virology in Montréal, QC as well as several other local and regional conferences including the Prairie Infectious Immunology Network conference in Hecla, MB.

3.2 Hypothesis and objectives

The central hypothesis of this project is that the host response to infection with mild or highly pathogenic strains of influenza virus will be different at the cellular level. We further hypothesize that pathogenic strains will modulate pathways not modulated by infection with the mild strains or modulate pathways to a great degree compared to that observed with the mild strains and that this differential effect on host pathways will contribute to the distinct ability of each virus to cause disease

Objectives for this study are as follow:

1. Obtain clean (free from cellular proteins and nucleic acid), high titre stocks of all viruses
2. Establish the optimal growth conditions of A549 cells
3. Confirm that A549 cells can be infected by the four strains of influenza studied here
4. Obtain a high-quality proteomic dataset of early infection of A549 cells
5. Mine the data using bioinformatics tools to understand the differences in global and specific host response to each strains
6. Validate potentially-interesting targets using independent methods

3.3 Results

3.3.1 Virus stock generation

The 2-step ultracentrifugation approach I used to generate virus stocks enabled me to concentrate them approximately 10-fold. For each virus, approximately fifty individual 40 µl aliquots were frozen for single use, avoiding any loss of infectivity due to freezing and thawing. Figure 3.1 shows the efficacy of the concentration method we used.

Figure 3.1 - Viral stocks

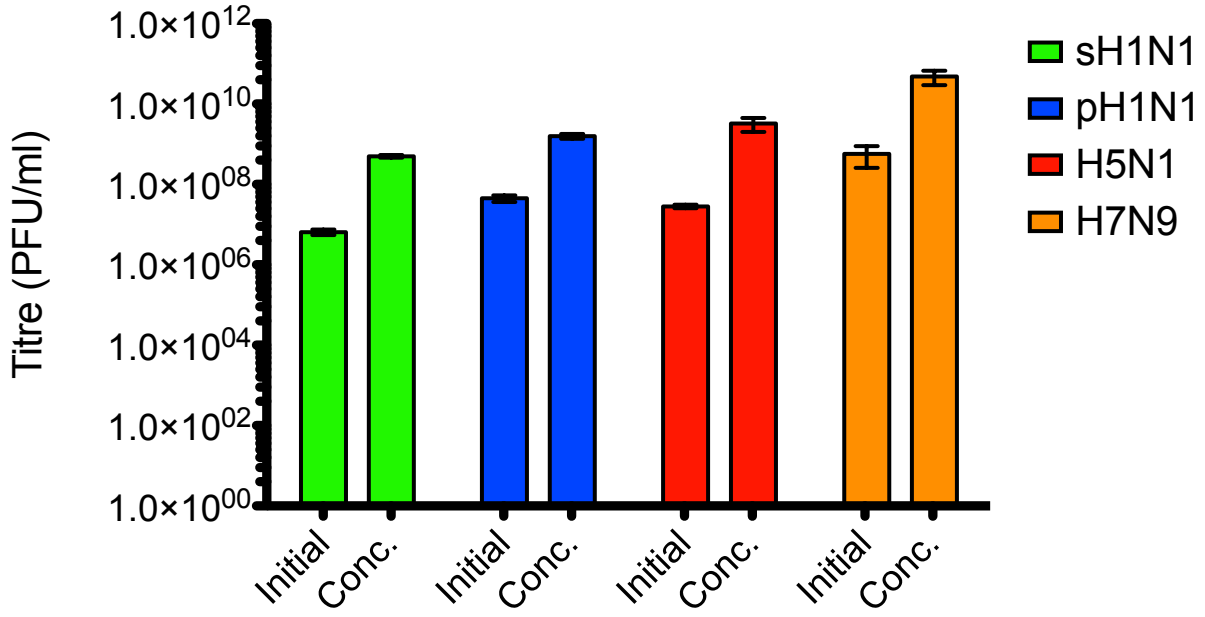

Stocks of each strain was produced in MDCK cells and concentrated using a two-step ultracentrifugation approach. The goal was to have stocks as concentrated as possible while eliminating as many soluble mediators from the infectious supernatant as possible.

3.3.2 Cell passage in CompacTSelecT cell culture robot

In an effort to keep the conditions between the replicates as consistent as possible, we cultured our A549 cells in an automated, robotic cell culture system (the CompacTSelecT – TAP biosystems). This systems uses the same media (F12K + 5% FBS) and the same growth conditions ($37^{o}C$, 5% CO_2) and the same cell passaging technique (PBS wash + 3 ml trypsin per flasks) as the standard cell culture. But it does all steps of cell maintenance and setting up cells for assays automatically. Furthermore, it has a built-in cell counter and the robot can be programmed to read the confluence of cells at any given interval and to passage them upon reaching certain thresholds. In this experiment, we used a 1:4 dilution at the cell passage and programmed the cell counter to read their confluence every 6h. The robot as programmed to split the cells 1:4 upon reaching 70% confluence. We used this passage scheme for at least 3 cycles prior to using the cells for the proteomic experiment. As can be seen in figure 3.2, the growth curves of 12 flasks in three biological replicates show very reproducible and robust growth rates of cells.

Figure 3.2 - A549 growth

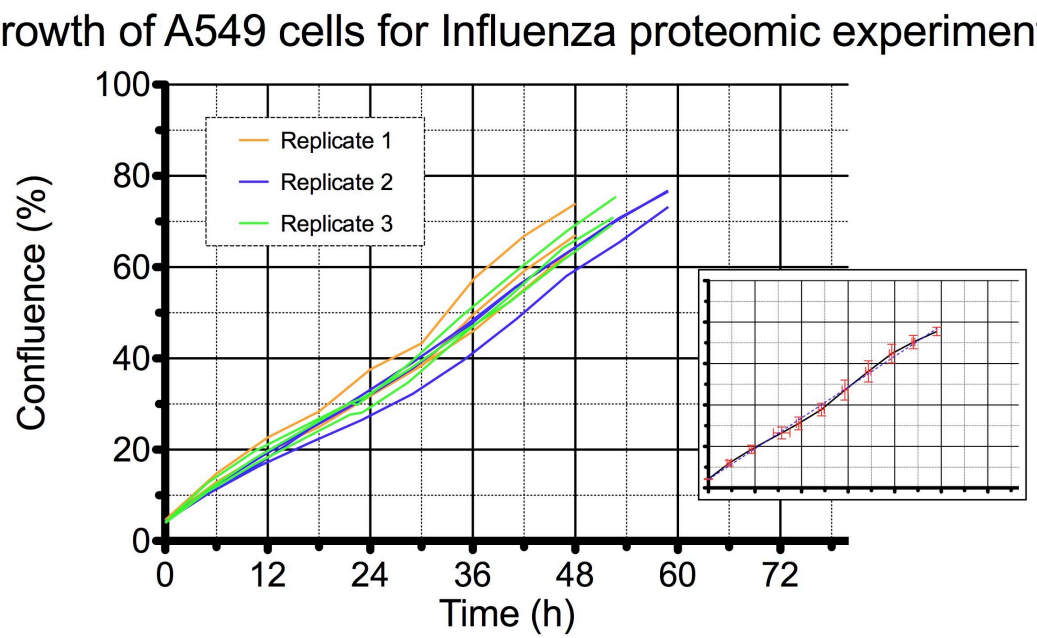

A cell culture robot was programmed to automatically read the confluence of A549 cells growing in T150 flasks every 6h. Upon reaching 70% confluence it would automatically passage the cells in a 1:4 ratio into new T150 flasks. The large graph shows the growth of three T150 flasks for three biological replicates used to generate the cells for the proteomic experiment. The small insert shows the average confluence over time along with the extent of the variability in the cell culture conditions.

3.3.3 Confirmation of infection in A549 cells

To confirm that the cells we used were infected by all 4 strains of influenza, we verified the expression of viral non-structural protein NS1 by Western Blot (Figure 3.3). NS1 expression was detected in cells infected by all four viruses. In cells infected at an MOI of 10, NS1 was detected as early as 3h post infection (for the sH1N1, H5N1 and H7N9) and at 6h for pH1N1 infection. Viral proteins were also readily identified as being strongly up-regulated in infected cells as shown in the mass spectrometry results (Table 3.1). We also performed extensive growth kinetics studies (see Chapter 4) that further confirmed that A549 supported replication of the four strains we studied.

Figure 3.3 - Confirmation of infection

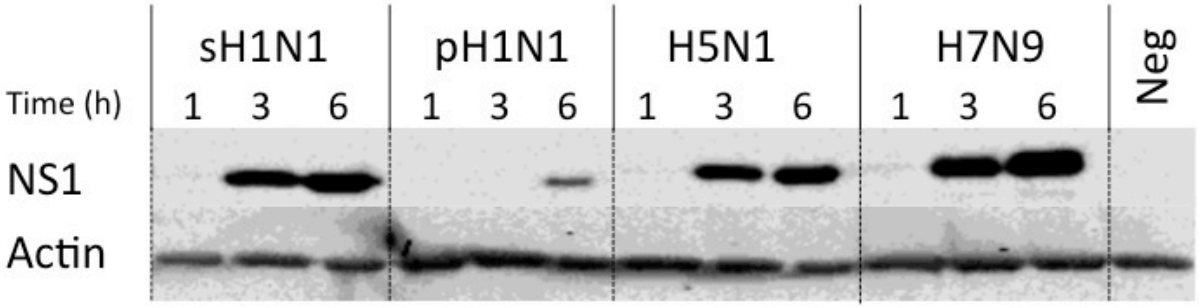

Infection in A549 cells was confirmed by measuring the expression of the NS1 protein for all four strains at 1, 3, and 6h post-infection. This viral protein is only expressed during de novo infection and serves as a marker of infection. Monoclonal antibody 7D11 to NS1 has been previously described [148] and was a kind gift from the Coombs lab at University of Manitoba.

Table 3.1 - Viral proteins identified by mass spectrometry

Virus	Protein ID	Segment	1h			3h			6h		
			Log_2FC	p-value (non adj)	p-value (adj)	Log_2FC	p-value (non adj)	p-value (adj)	Log_2FC	p-value (non adj)	p-value (adj)
sH1N1	EPI178290	NP *	0.13	9.42E-01	1.00E+00	2.87	1.38E-01	5.61E-01	9.00	5.50E-04	3.21E-02
sH1N1	EPI178279	PB2 *	0.43	9.36E-01	1.00E+00	9.67	9.93E-02	5.28E-01	16.50	1.15E-02	1.66E-01
sH1N1	EPI105024	MP	0.33	8.85E-01	1.00E+00	3.07	2.04E-01	6.02E-01	8.40	4.17E-03	9.58E-02
sH1N1	EPI105017	PA	1.70	8.27E-01	1.00E+00	19.43	2.90E-02	3.75E-01	38.13	5.83E-04	3.21E-02
pH1N1	EPI178279	PB2	0.80	7.53E-01	1.00E+00	1.50	5.58E-01	7.81E-01	11.43	1.16E-03	6.19E-02
pH1N1	EPI178287	NA	3.60	7.47E-01	1.00E+00	4.00	7.20E-01	9.47E-01	46.60	1.88E-03	8.29E-02
pH1N1	EPI178293	NS	0.27	9.09E-01	1.00E+00	0.67	7.76E-01	1.00E+00	10.50	1.20E-03	6.31E-02
pH1N1	EPI178296	PA	0.50	8.94E-01	1.00E+00	2.37	5.32E-01	7.62E-01	18.80	5.60E-04	4.29E-02
pH1N1	EPI178299	PB1	0.37	7.31E-01	9.89E-01	1.03	3.43E-01	6.35E-01	8.43	1.68E-05	7.77E-03
H5N1	EPI376541	NS	1.27	1.34E-05	1.21E-02	2.63	9.67E-09	1.42E-05	4.03	1.10E-10	1.62E-07
H5N1	EPI376538	NP	1.13	1.64E-05	1.21E-02	2.57	5.01E-09	1.10E-05	3.97	5.13E-11	1.13E-07
H5N1	EPI376534	PB2	1.47	6.94E-09	3.06E-05	2.90	5.18E-12	2.28E-08	4.07	1.39E-13	6.12E-10
H5N1	EPI178293a	NS*	0.30	6.94E-01	8.69E-01	0.40	6.01E-01	8.48E-01	1.60	5.49E-02	3.00E-01
H5N1	EPI178290	NP*	0.00	1.00E+00	1.00E+00	1.57	6.51E-07	5.73E-04	3.07	6.63E-10	6.04E-07
H5N1	EPI178284a	MP*	0.00	1.00E+00	1.00E+00	-0.03	9.15E-01	1.00E+00	0.57	9.21E-02	3.71E-01
H7N9	EPI178290	NP*	0.20	6.29E-01	8.73E-01	5.13	2.50E-07	6.43E-04	10.73	2.67E-10	4.01E-07
H7N9	EPI439505	NP	1.70	5.74E-01	8.35E-01	12.10	2.22E-03	1.39E-01	21.70	2.92E-05	2.92E-03
H7N9	EPI439508	PB1	1.70	4.40E-01	7.51E-01	7.13	7.49E-03	2.59E-01	13.43	1.01E-04	7.48E-03
H7N9	EPI439510	NS	15.50	2.30E-01	6.51E-01	32.13	2.50E-02	3.47E-01	45.53	4.02E-03	6.98E-02

* The asterisks indicate proteins identified as belonging to a different strain. This is due to incomplete protein sequencing by the mass spectrometer as well as high sequence homology between the strains.
The ratios are measured against the mock-infected sample at 1h post infection. This sample does not contain any viral protein so the background of the report ion is used instead.
Both the Bonferonni-Hochberg adjusted p-values and non-adjusted p-values are provided (highlighted in blue). Red indicates an increase in protein abundance compare to the mock-1h sample.
Log2FC – Log_2 Fold Change

3.3.4 Broad proteomic results

As we needed to compare multiple viruses at multiple time points and also use time-matched controls, we used a simple multiplexing strategy to extend the capacity of standard 4-plex iTRAQ labeling. We added the mock-1h sample in each 4-plex, which enabled us to directly compare the results for each virus at every time point as they were all standardized to an identical sample for each MS run. Figure 2.2 shows the overall experimental layout. Within each 4-plex (Mock-1h / Virus-1h / Virus-3h / Virus-6h), over 3,600 proteins overlapped within each infection group (sH1N1, pdhmH1N1, H5N1 and H7N9) and across three biological replicates. When combined together, over 7,000 proteins in total were quantified across all our samples and replicates with 2,916 proteins overlapping in all experiments for all viruses, replicate and time point. A list of statistically significant proteins showing differential abundance was generated using a double-pronged statistical approach (see section 2.7) and analyzed in IPA. Figure 3.4 shows volcano plots for the infection with each virus. Infections by H5N1 and H7N9 viruses induced the largest number of significantly dysregulated proteins (154 and 206 respectively). For all viruses, we observed the largest numbers of dysregulated proteins at 6h post-infection (see Table 3.2).

Figure 3.4 - Volcano plots

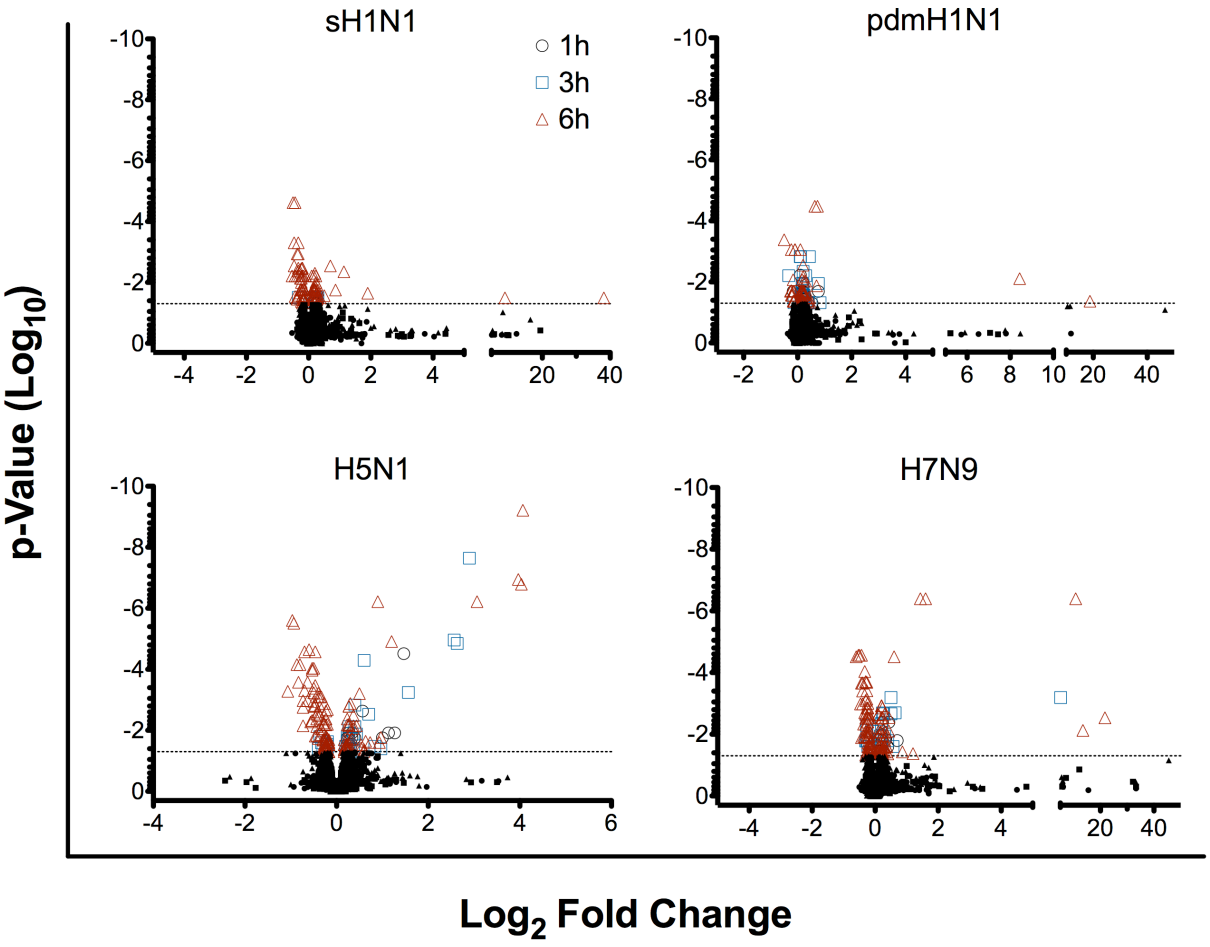

Volcano plots showing the $\log_2$ fold changes (x axis) and the significance (y axis) for all viruses at all time points. Most changes occur at 6h post-infection. The dotted line indicates p = 0.05, showing the minimum value for significance. P-values are corrected for multiple hypotheses using the Benjamini-Hochberg method.

After batch correction, cluster analysis revealed that the 1h and 3h responses were not readily differentiable from the mock infections in the cells infected by the sH1N1 and pH1N1 strains (Figure 3.5). Conversely, in the H5N1 and H7N9 infected cells, the 1h mock samples clustered together. For each infection, the proteomic responses clustered together by 6h. Table 3.3 gives a summary of the top ten most dysregulated proteins for each virus.

Table 3.2 - Total and unique significantly modulated proteins

Strain	1h	3h	6h	Total proteins
sH1N1	8 (2)	10 (2)	110 (99)	**114**
pH1N1	25 (5)	60 (28)	69 (38)	**105**
H5N1	9 (0)	33 (10)	144 (119)	**154**
H7N9	9 (1)	25 (2)	201 (180)	**206**

The numbers in parenthesis indicate how many unique proteins are found at each time point while the total number reflects proteins found to be modulated at more then one time point. The total number of unique proteins is greater than the sum of the numbers in parenthesis as several proteins are found to be significantly modulated at more than one time point.

Figure 3.5 - Cluster analysis

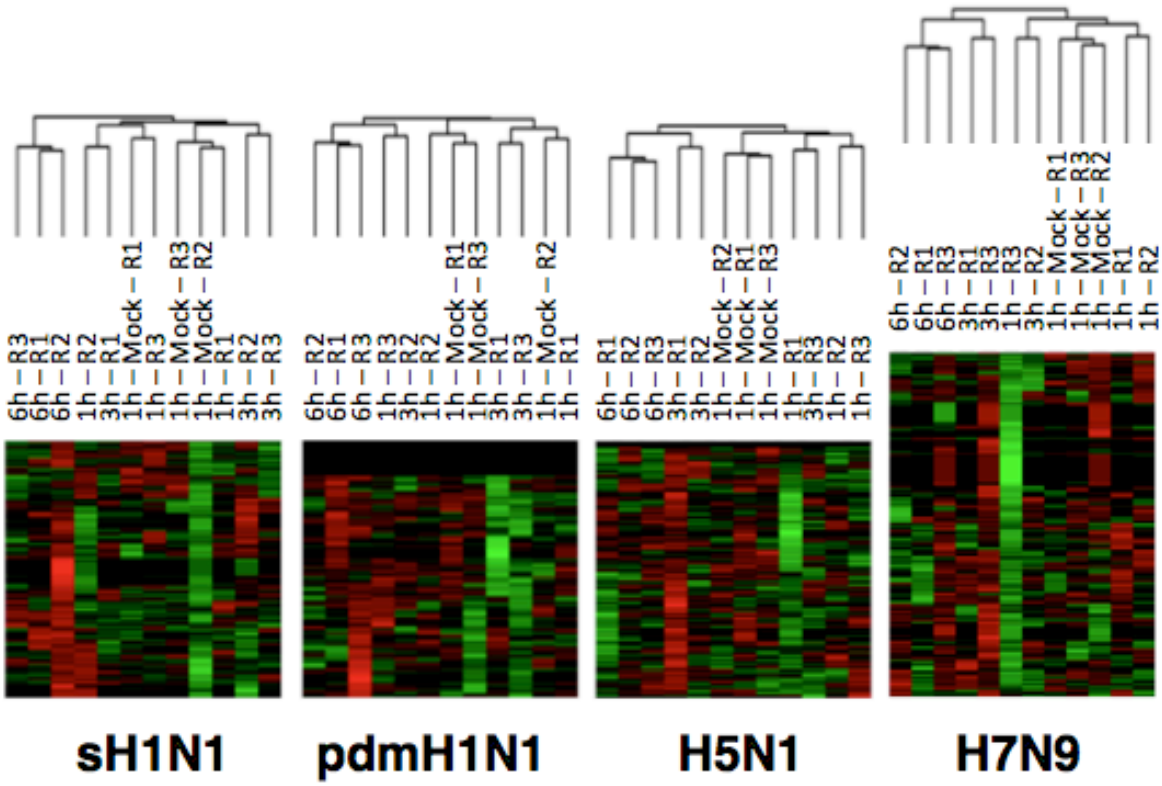

Hierarchical clustering was performed on the rows (proteins) and columns (samples) on the batch-corrected data sets of each triplicate 4-plex. The responses at 1 and 3h post infection show poor clustering while those at 6h post-infection cluster together, suggesting that the host proteome becomes more similar later in infection.

Table 3.3 - Top-ten dysregulated host proteins

Virus	Protein ID	Time point					
		1h		3h		6h	
		Log_2FC	p-value	Log_2FC	p-value	Log_2FC	p-value
sH1N1	ALDOC_PANTR	1.43	1.73E-01	1.37	1.54E-01	1.90	2.25E-02
sH1N1	FRIH_HUMAN	0.17	6.54E-01	0.50	2.08E-01	1.13	4.48E-03
sH1N1	RDH13_HUMAN	0.70	1.44E-01	0.57	1.68E-01	0.87	1.77E-02
sH1N1	FRIL_HUMAN	0.07	7.12E-01	0.37	8.53E-02	0.70	2.85E-03
sH1N1	CHCH2_HUMAN	-0.07	7.12E-01	-0.20	3.27E-01	-0.53	6.11E-03
sH1N1	CP24A_HUMAN	0.07	3.99E-01	-0.17	5.53E-02	-0.50	2.39E-05
sH1N1	AK1C3_HUMAN	0.50	1.06E-01	0.43	1.03E-01	0.50	2.72E-02
sH1N1	JAK1_HUMAN	0.00	1.00E+00	-0.10	5.03E-01	-0.47	2.85E-03
sH1N1	APOD_BOVIN	-0.03	7.12E-01	-0.33	3.07E-02	-0.47	4.96E-04
sH1N1	CKS2_HUMAN	-0.03	9.25E-01	-0.17	4.97E-01	-0.43	2.90E-02
pdmH1N1	GSDMD_HUMAN	0.67	1.34E-01	0.83	4.79E-02	0.73	6.79E-02
pdmH1N1	ALDOC_PANTR	0.77	2.03E-02	0.77	1.13E-02	0.70	1.33E-02
pdmH1N1	FRIH_HUMAN	0.07	5.38E-01	0.43	1.49E-03	0.73	3.32E-05
pdmH1N1	FRIL_HUMAN	0.20	4.43E-02	0.30	6.23E-03	0.63	3.32E-05
pdmH1N1	AK1C3_HUMAN	0.53	4.95E-02	0.50	4.79E-02	0.47	4.65E-02
pdmH1N1	APOD_BOVIN	-0.07	5.38E-01	-0.33	6.23E-03	-0.50	4.13E-04
pdmH1N1	AGR2_HUMAN	0.17	4.73E-01	0.27	1.88E-01	0.43	3.18E-02
pdmH1N1	DYL1_HUMAN	0.40	4.38E-02	0.37	4.78E-02	0.37	4.13E-02
pdmH1N1	CX7A2_HUMAN	0.37	8.10E-02	0.40	4.79E-02	0.40	4.29E-02
pdmH1N1	ANXA1_CAVCU	0.37	7.01E-02	0.33	6.76E-02	0.40	3.40E-02
H5N1	FRIH_HUMAN	0.17	4.38E-01	0.70	2.96E-03	1.20	1.22E-05
H5N1	FINC_HUMAN	-0.13	6.87E-01	-0.50	1.08E-01	-1.07	5.24E-04
H5N1	PSB4_MOUSE	1.00	1.76E-02	0.83	3.33E-02	0.73	2.50E-02
H5N1	CH60_HUMAN	0.87	8.04E-02	0.97	3.99E-02	0.97	1.70E-02
H5N1	ACOD_HUMAN	-0.07	6.41E-01	-0.33	2.55E-02	-0.97	2.49E-06
H5N1	CLIC1_HUMAN	0.90	8.04E-02	0.90	7.01E-02	0.93	2.51E-02
H5N1	CP24A_HUMAN	0.10	4.86E-01	-0.37	1.62E-02	-0.93	3.08E-06
H5N1	FRIL_HUMAN	0.17	1.55E-01	0.60	5.09E-05	0.90	6.04E-07
H5N1	LAMA5_HUMAN	-0.03	8.52E-01	-0.40	3.87E-02	-0.87	6.99E-05
H5N1	RHOB_HUMAN	-0.03	8.76E-01	-0.33	1.44E-01	-0.83	2.65E-04

Table 3.3 (Continued) – Top-ten dysregulated host proteins

Virus	Protein ID	Time point					
		1h		3h		6h	
		Log_2FC	p-value	Log_2FC	p-value	Log_2FC	p-value
H7N9	FRIL_HUMAN	0.17	3.85E-01	0.63	2.01E-03	1.60	4.01E-07
H7N9	FRIH_HUMAN	0.00	1.00E+00	0.50	2.17E-03	1.43	4.01E-07
H7N9	CLIC1_HUMAN	1.10	2.28E-01	1.03	2.24E-01	1.20	4.23E-02
H7N9	TAP26_HUMAN	0.33	5.85E-01	0.40	4.53E-01	0.87	3.73E-02
H7N9	AF1Q_HUMAN	0.70	1.61E-02	0.57	2.50E-02	0.17	3.61E-01
H7N9	DYL1_HUMAN	0.43	4.08E-03	0.50	6.43E-04	0.60	3.05E-05
H7N9	S38A2_HUMAN	0.00	1.00E+00	-0.20	7.88E-02	-0.60	3.05E-05
H7N9	ACOD_HUMAN	-0.03	7.19E-01	-0.27	7.49E-03	-0.53	2.73E-05
H7N9	CP24A_HUMAN	0.03	7.19E-01	-0.27	5.24E-03	-0.50	2.73E-05
H7N9	LAMC1_HUMAN	0.00	1.00E+00	-0.20	1.68E-01	-0.47	1.05E-03
Mock	CH60_HUMAN	NA	NA	0.53	7.14E-02	0.67	1.81E-02
Mock	DNJC2_HUMAN	NA	NA	0.50	7.14E-02	0.67	1.81E-02
Mock	TAGL2_HUMAN	NA	NA	0.60	7.14E-02	0.60	3.64E-02
Mock	FRIL_HUMAN	NA	NA	0.37	1.11E-01	0.57	1.81E-02
Mock	YBOX1_HUMAN	NA	NA	0.33	1.28E-01	0.57	2.29E-02
Mock	AK1C3_HUMAN	NA	NA	0.53	7.14E-02	0.50	3.64E-02
Mock	GLRX1_HUMAN	NA	NA	0.40	8.30E-02	0.43	3.64E-02
Mock	HMGA2_HUMAN	NA	NA	0.33	1.15E-01	0.40	3.64E-02
Mock	CYB5B_HUMAN	NA	NA	0.37	7.14E-02	0.37	3.64E-02
Mock	B4GT1_HUMAN	NA	NA	0.27	6.87E-02	0.33	1.81E-02

Color coding as follows: red indicates an increase and green a decrease compared to the mock-1h sample. Blue indicates an adjusted p-value under the threshold of 0.05. Log_2FC = Log_2 Fold Change

3.3.5 Global host dysregulation

A major question we wished to answer with this study was whether the HPAI H5N1 strain would induce more changes at a cellular level than low pathogenicity human viruses, and to see how this would compare to the novel H7N9 strain causing the current outbreak in China. To address this, we imported the list of significant proteins into Ingenuity Pathway Studio and performed Core Analysis on each virus at each time point and on the mock-infected cells. Figure 3.6 shows a heat map of the predicted activation and inhibition of all pathways in the IPA database at the 6h p.i. time point. These are organized in broad categories (e.g. cancer, cell death and survival, cell-to-cell signaling, etc.), each comprised of discrete pathways that are either manually curated (e.g. Canonical pathways) or predicted based on published function and relationships between genes. This provides a broad overview of the dysregulation at the cellular level rather than focusing on individual pathways. Because of the stronger coherence of the proteomic responses by 6h p.i., we focused our attention on that later time point. In total, infection with H5N1 virus dysregulated 195 of those pathways compared to 116 for H7N9 infection, 88 for the sH1N1 viruses and 82 for the pH1N1 strain (see Table 3.4).

Table 3.4 – Modulated Pathways at 6h Post Infection

Virus	Decreased		Increased	
	N	Average activation z-score	N	Average activation z-score
sH1N1	62	-0.893	26	0.747
pdmH1N1	31	-0.835	51	1.021
H5N1	116	-0.911	79	0.869
H7N9	64	-1.08	52	0.788
Mock	21	-0.854	30	0.914

* The activation z-score is a measure within IPA that indicates by how much a specific pathway is predicated to be up or down regulated. This is based on the Log2FCold changes of individual proteins within a network and their role in that same network. N=number of pathways affected.

A

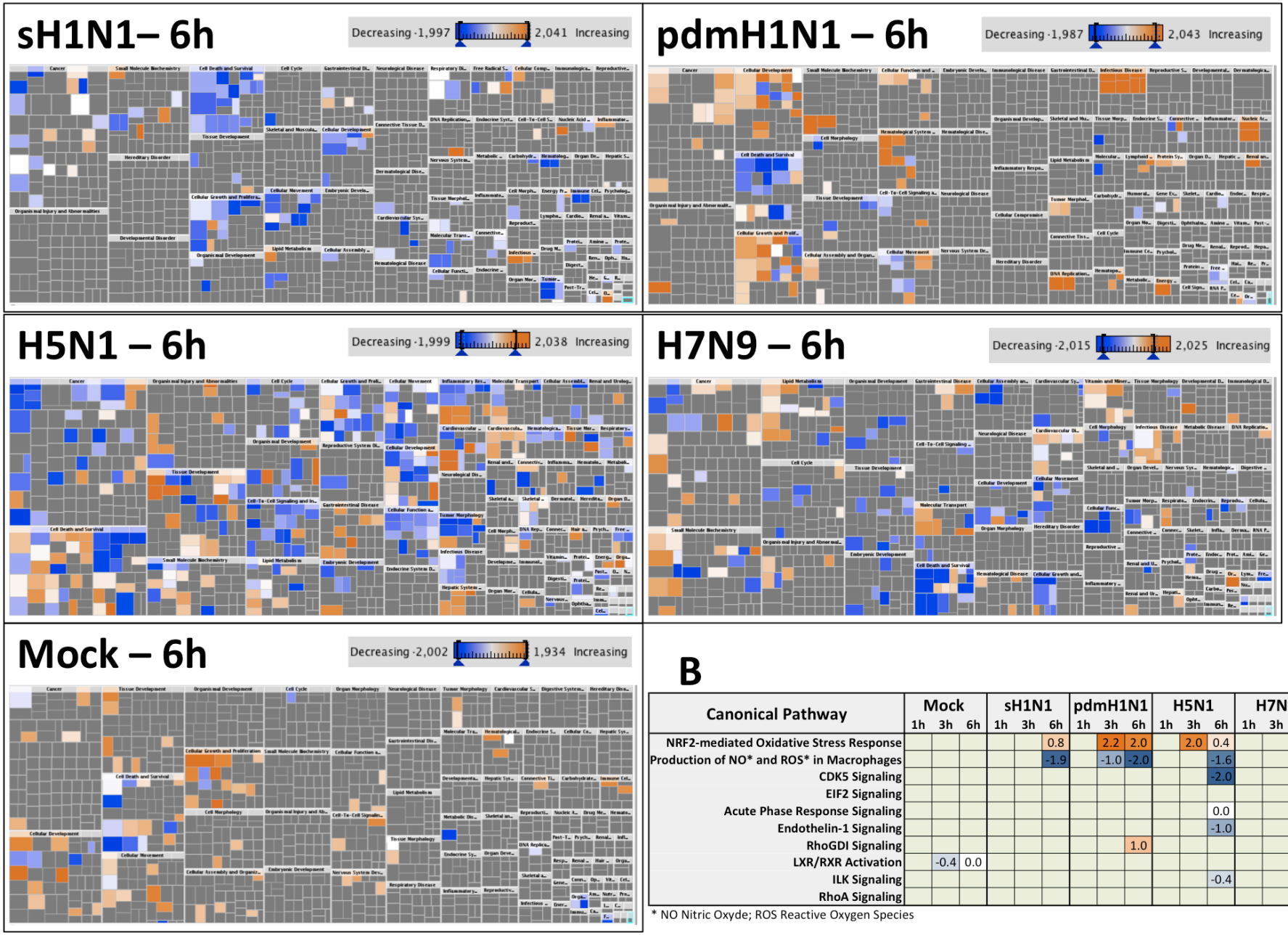

B

Canonical Pathway	Mock			sH1N1			pdmH1N1			H5N1			H7N9		
	1h	3h	6h	1h	3h	6h	1h	3h	6h	1h	3h	6h	1h	3h	6h
NRF2-mediated Oxidative Stress Response						0.8		2.2	2.0		2.0	0.4			1.3
Production of NO* and ROS* in Macrophages						-1.9		-1.0	-2.0			-1.6			
CDK5 Signaling												-2.0			-2.0
EIF2 Signaling															2.4
Acute Phase Response Signaling												0.0			-1.0
Endothelin-1 Signaling												-1.0			
RhoGDI Signaling									1.0						
LXR/RXR Activation		-0.4	0.0												
ILK Signaling												-0.4			
RhoA Signaling															0.4

* NO Nitric Oxyde; ROS Reactive Oxygen Species

C

sH1N1 – 6h

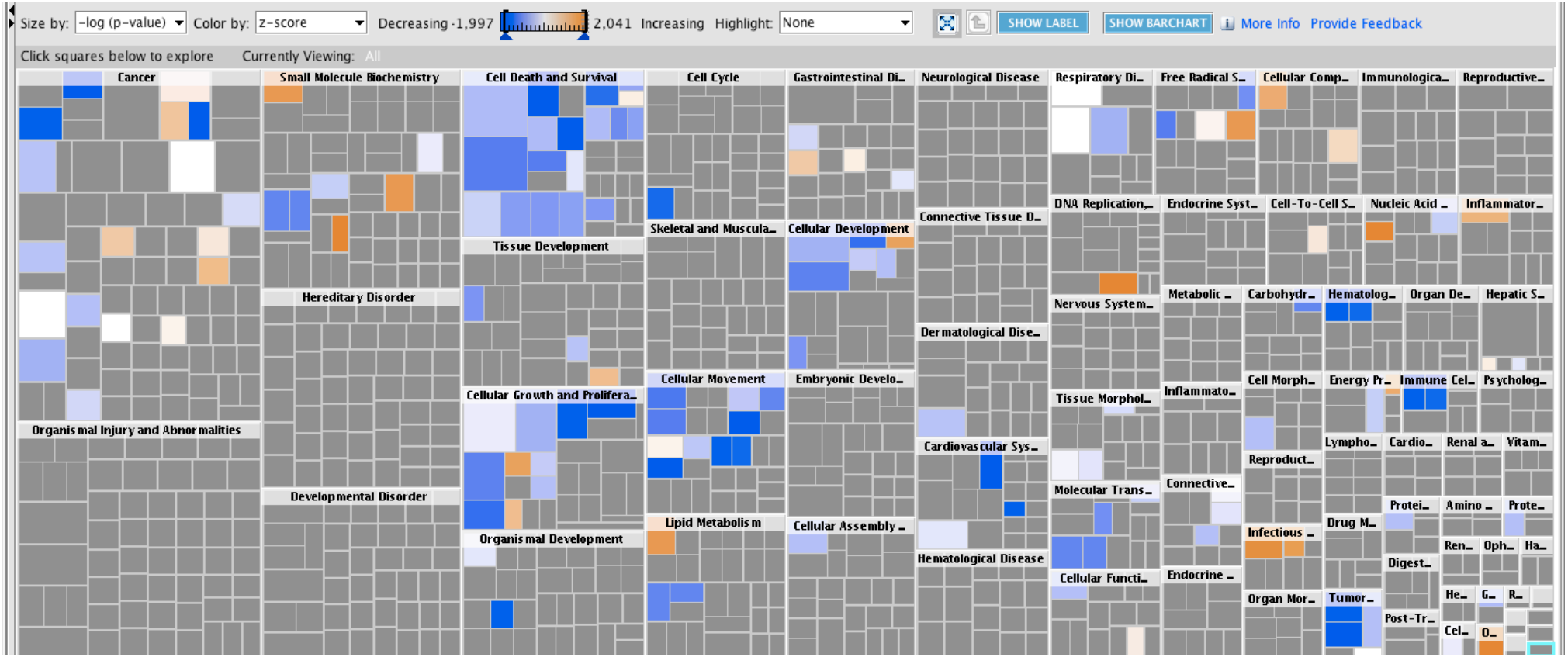
Size by: -log (p-value)
Color by: z-score
Decreasing -1,997
2,041
Increasing
Highlight: None
SHOW LABEL
SHOW BARCHART
More Info
Provide Feedback
Click squares below to explore
Currently Viewing: All
Cancer
Small Molecule Biochemistry
Cell Death and Survival
Cell Cycle
Gastrointestinal Di...
Neurological Disease
Respiratory Di...
Free Radical S...
Cellular Comp...
Immunologica...
Reproductive...
Organismal Injury and Abnormalities
Hereditary Disorder
Tissue Development
Skeletal and Muscula...
Cellular Development
Connective Tissue D...
DNA Replication,...
Endocrine Syst...
Cell-To-Cell S...
Nucleic Acid ...
Inflammator...
Developmental Disorder
Cellular Growth and Prolifera...
Cellular Movement
Embryonic Develo...
Dermatological Dise...
Nervous System...
Metabolic ...
Carbohydr...
Hematolog...
Organ De...
Hepatic S...
Organismal Development
Lipid Metabolism
Cellular Assembly ...
Cardiovascular Sys...
Tissue Morphol...
Inflammato...
Cell Morph...
Energy Pr...
Immune Cel...
Psycholog...
Hematological Disease
Molecular Trans...
Connective...
Reproduct...
Lympho...
Cardio...
Renal a...
Vitam...
Cellular Functi...
Endocrine ...
Infectious ...
Drug M...
Protei...
Amino ...
Prote...
Organ Mor...
Tumor...
Digest...
Ren...
Oph...
Ha...
Post-Tr...
He...
G...
R...
Cel...
O...

pH1N1 – 6h

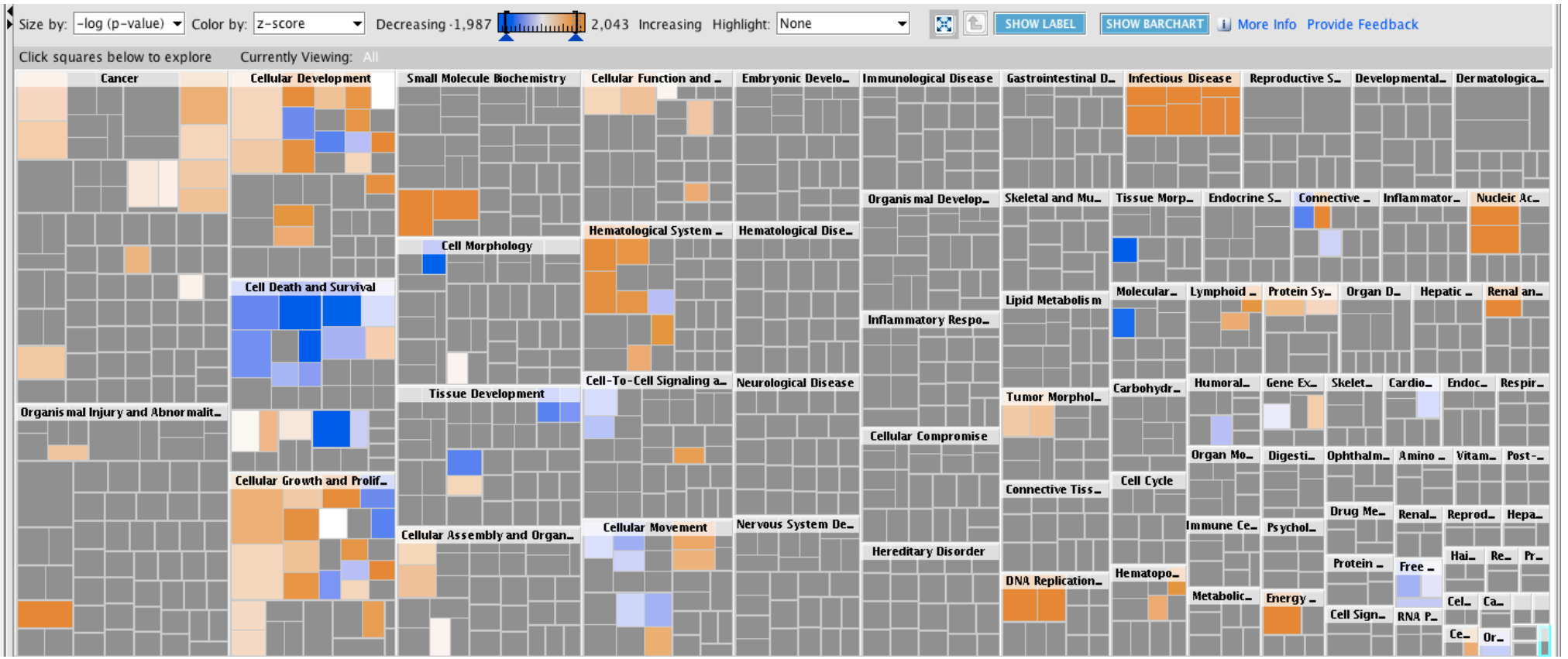
Size by: -log (p-value)
Color by: z-score
Decreasing -1,987
2,043 Increasing
Highlight: None
SHOW LABEL
SHOW BARCHART
More Info
Provide Feedback
Click squares below to explore
Currently Viewing: All
Cancer
Cellular Development
Small Molecule Biochemistry
Cellular Function and ...
Embryonic Develo...
Immunological Disease
Gastrointestinal D...
Infectious Disease
Reproductive S...
Developmental...
Dermatologica...
Organismal Develop...
Skeletal and Mu...
Tissue Morp...
Endocrine S...
Connective ...
Inflammator...
Nucleic Ac...
Hematological System ...
Hematological Dise...
Cell Morphology
Lipid Metabolism
Molecular...
Lymphoid ...
Protein Sy...
Organ D...
Hepatic ...
Renal an...
Inflammatory Respo...
Cell Death and Survival
Carbohydr...
Humoral...
Gene Ex...
Skelet...
Cardio...
Endoc...
Respir...
Organismal Injury and Abnormalit...
Tumor Morphol...
Cellular Compromise
Organ Mo...
Digesti...
Ophthalm...
Amino ...
Vitam...
Post-...
Cellular Growth and Prolif...
Connective Tiss...
Cell Cycle
Drug Me...
Renal...
Reprod...
Hepa...
Tissue Development
Cell-To-Cell Signaling a...
Immune Ce...
Psychol...
Protein ...
Free ...
Hai...
Re...
Pr...
Cellular Movement
Nervous System De...
Hereditary Disorder
DNA Replication...
Hematopo...
Metabolic...
Energy ...
Cell Sign...
RNA P...
Cel...
Ca...
Ce...
Or...
Neurological Disease
Cellular Assembly and Organ...

H5N1 – 6h

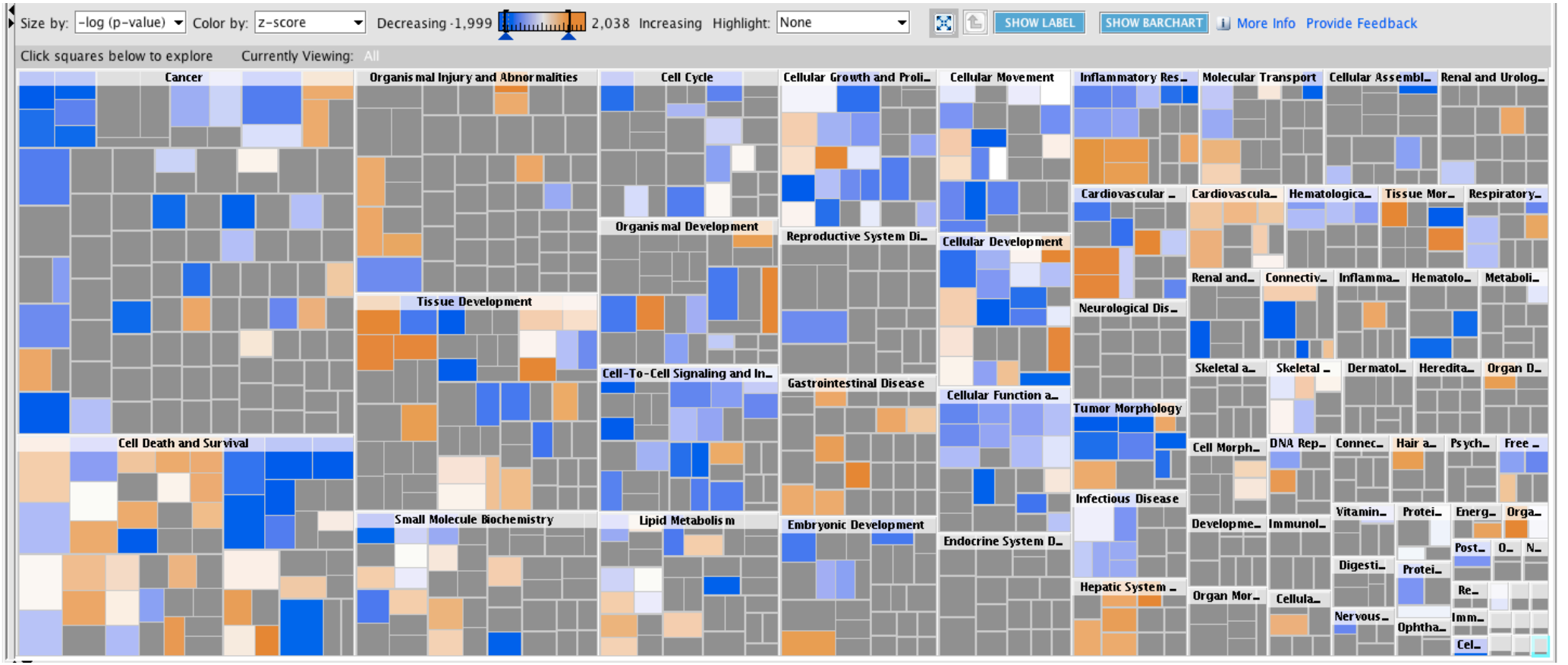
Size by: -log (p-value)
Color by: z-score
Decreasing -1,999
2,038 Increasing
Highlight: None
SHOW LABEL
SHOW BARCHART
More Info
Provide Feedback
Click squares below to explore
Currently Viewing: All
Cancer
Organismal Injury and Abnormalities
Cell Cycle
Cellular Growth and Proli...
Cellular Movement
Inflammatory Res...
Molecular Transport
Cellular Assembl...
Renal and Urolog...
Cardiovascular ...
Cardiovascula...
Hematologica...
Tissue Mor...
Respiratory...
Organismal Development
Reproductive System Di...
Cellular Development
Tissue Development
Renal and...
Connectiv...
Inflamma...
Hematolo...
Metaboli...
Neurological Dis...
Cell Death and Survival
Cell-To-Cell Signaling and In...
Gastrointestinal Disease
Cellular Function a...
Skeletal a...
Skeletal ...
Dermatol...
Heredita...
Organ D...
Tumor Morphology
Cell Morph...
DNA Rep...
Connec...
Hair a...
Psych...
Free ...
Infectious Disease
Vitamin...
Protei...
Energ...
Orga...
Small Molecule Biochemistry
Lipid Metabolism
Embryonic Development
Endocrine System D...
Developme...
Immunol...
Post...
O...
N...
Digesti...
Protei...
Re...
Hepatic System ...
Organ Mor...
Cellula...
Nervous...
Imm...
Ophtha...
Cel...

H7N9 – 6h

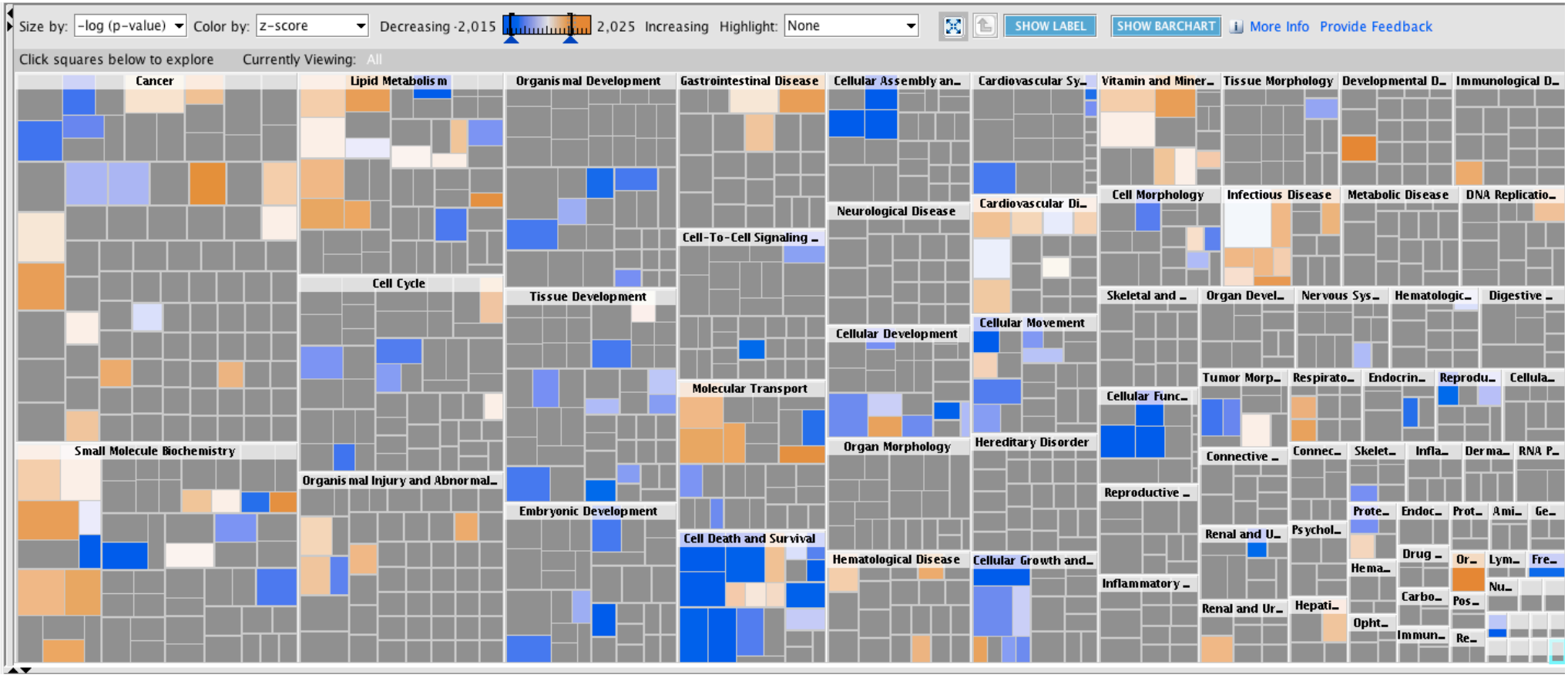
Size by: -log (p-value)
Color by: z-score
Decreasing -2,015
2,025
Increasing
Highlight: None
SHOW LABEL
SHOW BARCHART
More Info
Provide Feedback
Click squares below to explore
Currently Viewing: All
Cancer
Lipid Metabolism
Organismal Development
Gastrointestinal Disease
Cellular Assembly an...
Cardiovascular Sy...
Vitamin and Miner...
Tissue Morphology
Developmental D...
Immunological D...
Cell Morphology
Infectious Disease
Metabolic Disease
DNA Replicatio...
Cell Cycle
Tissue Development
Cell-To-Cell Signaling ...
Neurological Disease
Cardiovascular Di...
Skeletal and ...
Organ Devel...
Nervous Sys...
Hematologic...
Digestive ...
Cellular Movement
Cellular Development
Molecular Transport
Cellular Func...
Tumor Morp...
Respirato...
Endocrin...
Reproduc...
Cellula...
Small Molecule Biochemistry
Organismal Injury and Abnormal...
Embryonic Development
Organ Morphology
Hereditary Disorder
Connective ...
Connec...
Skelet...
Infla...
Derma...
RNA P...
Reproductive ...
Cell Death and Survival
Hematological Disease
Cellular Growth and...
Renal and U...
Psychol...
Prote...
Endoc...
Prot...
Ami...
Ge...
Inflammatory ...
Renal and Ur...
Hepati...
Hema...
Drug ...
Or...
Lym...
Fre...
Carbo...
Pos...
Nu...
Opht...
Immun...
Re...

Mock – 6h

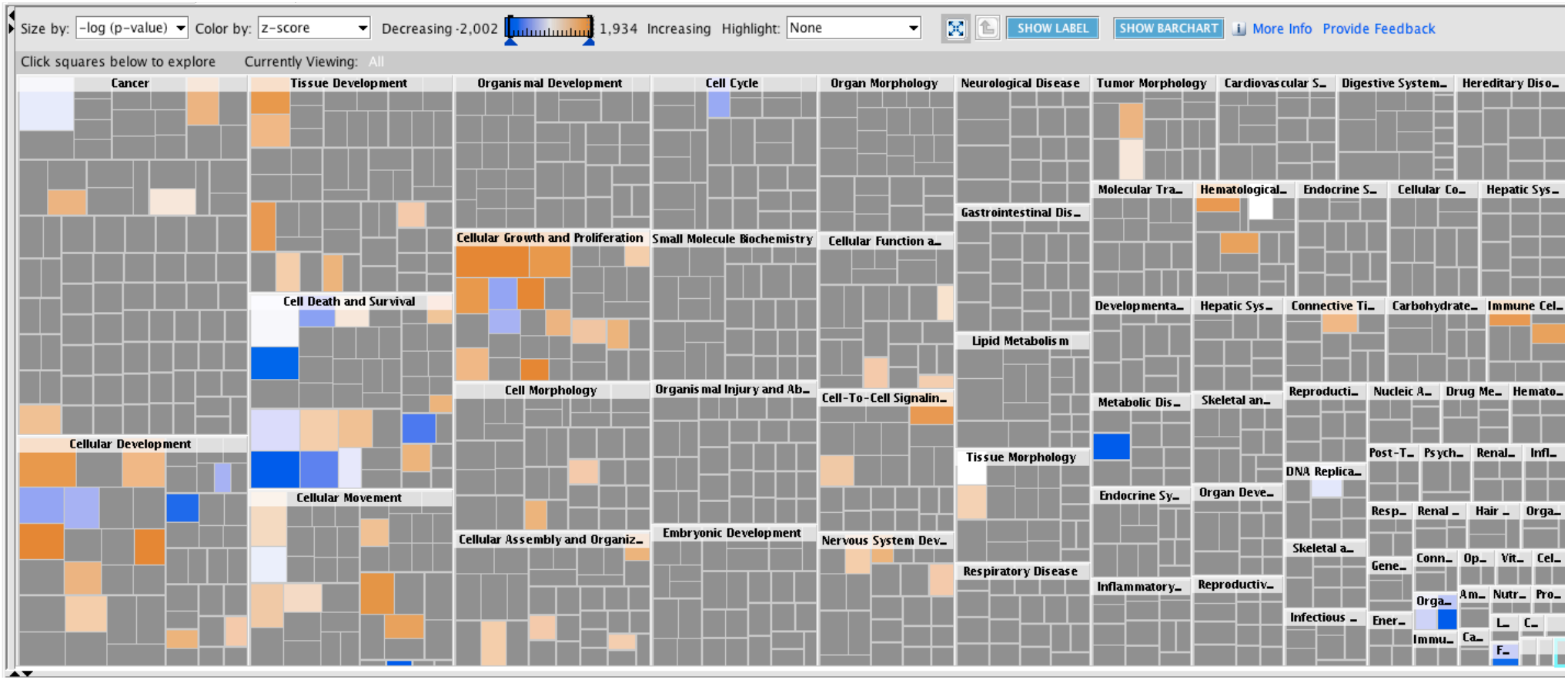

Figure 3.6 - Global Host Dysregulation

A. Global overview of "Disease and Function" heat maps from IPA. Larger rectangles are broad categories of biological functions and diseases; small rectangles represent individual pathways as defined by the IPA database. Size of each rectangle is proportional to the level of significance of the predicted dysregulation (- $\log_{10}$ of p value) and colors are indicative of the predicated activation (orange) or inhibition (blue) of each specific pathway. B. Top 10 canonical pathways of the IPA database predicted to be modulated by infections. C. Zoom-in on the heat maps for each infection at 6h post infection. The activation or inhibition prediction is based on the number of proteins mapped to each pathway as well as their function and up- or down- regulation.

The core and comparison analysis used to generate Figure 3.6 were also performed by restricting biological function to relationships only described in humans (see Figure 3.7). This is a built-in feature of IPA where only studies using human genes are kept for analysis as opposed to using the default data from Mouse, Rat and Human studies. Not surprisingly, this yielded fewer bioinformatically-predicted modulated pathways. At the 6h post infection time point, the Mock infected cells had a total of 21 significantly predicted modulated pathways while the sH1N1, pdmH1N1, H5N1 and H7N9 respectively had 53, 44, 77 and 58 pathways were predicted to be either activated or inhibited. Importantly, regardless of the species used for bioinformatics analysis, the same canonical pathways are predicated to be modulated. The only exception to this is that by restricting the analysis to human-only function mTOR signaling appears modulated in H5N1-infected A549 cells at 6h post infection (figure 3.7B).

Figure 3.7 - Global dysregulation - Human data only

A

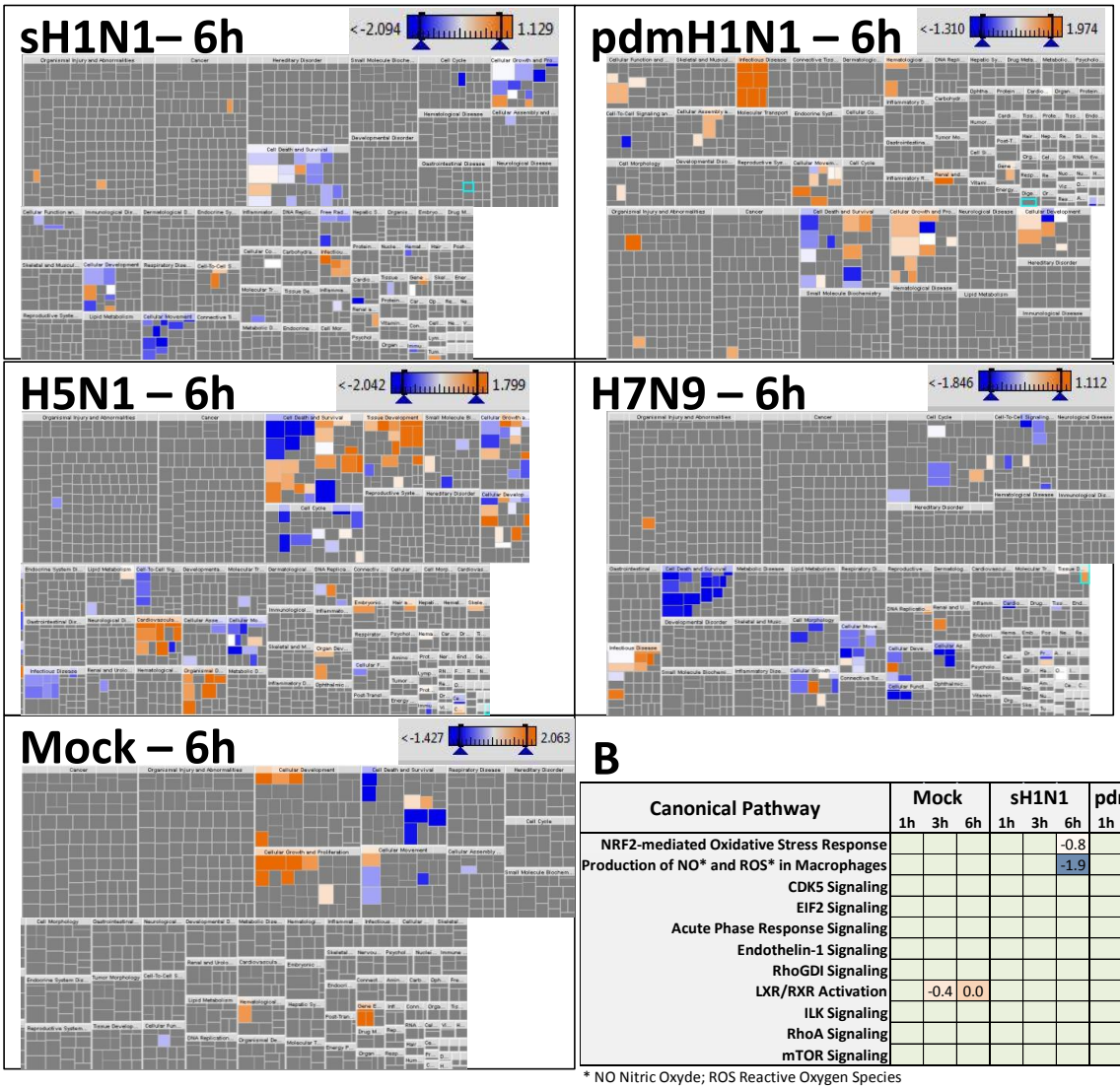

B

Canonical Pathway	Mock			sH1N1			pdmH1N1			H5N1			H7N9		
	1h	3h	6h	1h	3h	6h	1h	3h	6h	1h	3h	6h	1h	3h	6h
NRF2-mediated Oxidative Stress Response						-0.8		-2.2	-2.0		-2.0	-0.4			-1.3
Production of NO* and ROS* in Macrophages						-1.9		-1.0	-2.0			-1.6			
CDK5 Signaling												-2.0			-2.0
EIF2 Signaling															2.4
Acute Phase Response Signaling															-1.0
Endothelin-1 Signaling												-1.0			
RhoGDI Signaling									1.0						
LXR/RXR Activation		-0.4	0.0												
ILK Signaling												-0.4			
RhoA Signaling															0.4
mTOR Signaling												-1.0			

* NO Nitric Oxyde; ROS Reactive Oxygen Species

A. The "Disease and Function" heat maps from IPA when performing a Core analysis restricted to human-only studies. The overall results are the same as in Figure 3.6 in that the H5N1 infection is the one triggering the most dysregulation. B. The NRF2 response also appears to be the most significantly modulated pathway, with other modulated pathways identical to the ones found in Figure 3.6. except for the addition of mTOR signaling inhibition in H5N1 infection.

3.3.6 NRF2 and oxidative stress responses

To probe deeper into the dysregulation caused by infection with these four strains, we used a Comparison analysis to see which, if any, pathways were modulated and whether some were specific to infection by one virus or the other. As shown in Figure 3.6B and 3.7B, the top pathway predicted by IPA to be most affected by infection is the nuclear factor erythroid 2-related factor 2 (NRF2)-mediated oxidative stress response. This was predicted to be activated by all viruses as early as 3h post infection when using Mouse, Rat and Human gene functions and inhibited by all viruses when using Human-only gene functions (Figure 3.7). To clarify the effect of infection on NRF2, we performed western blot on cytoplasmic and nuclear fractions (see figure 3.8) of A549 cells infected at MOIs of 10 with each of the 4 strains studied. These were harvested at 6h post-infection. We did not observe increases in either nuclear or cytoplasmic NRF2 but rather observed a distinct banding pattern for the H5N1 and H7N9-infected cells. This banding pattern is suggestive of the phosphorylated form of NRF2 (top band) and the non-phosphorylated form (bottom band) [161]. It appears that the H5N1 and, to a lesser extent, the H7N9-infected cells have lower amounts of putatively-phosphorylated NRF2 in their nucleus. The strong induction of one down-stream anti-oxidant mediator (Ferritin, FRIH) was independently confirmed by Western Blot for all infected samples (Figure 3.8E). Other proteins involved in oxidative stress response identified as being significantly modulated by infection include CATA, FRIH, FRIL, GSTO1, NQO1, PPIB and PRDX1 (sH1N1); MRP1, CBR1, FRIH, FRIL and GSTP1 (pdmH1N1); CBR1, FRIH, FRIL, GSH1, HMOX1, PRDX6 and SCRB1 (H5N1) and FRIH, FRIL, GSH1, GSHR, NQO1 and SCRCB1 (H7N9). See table 3.5 for a summary of those proteins.

Figure 3.8 - NRF2 oxidative stress response

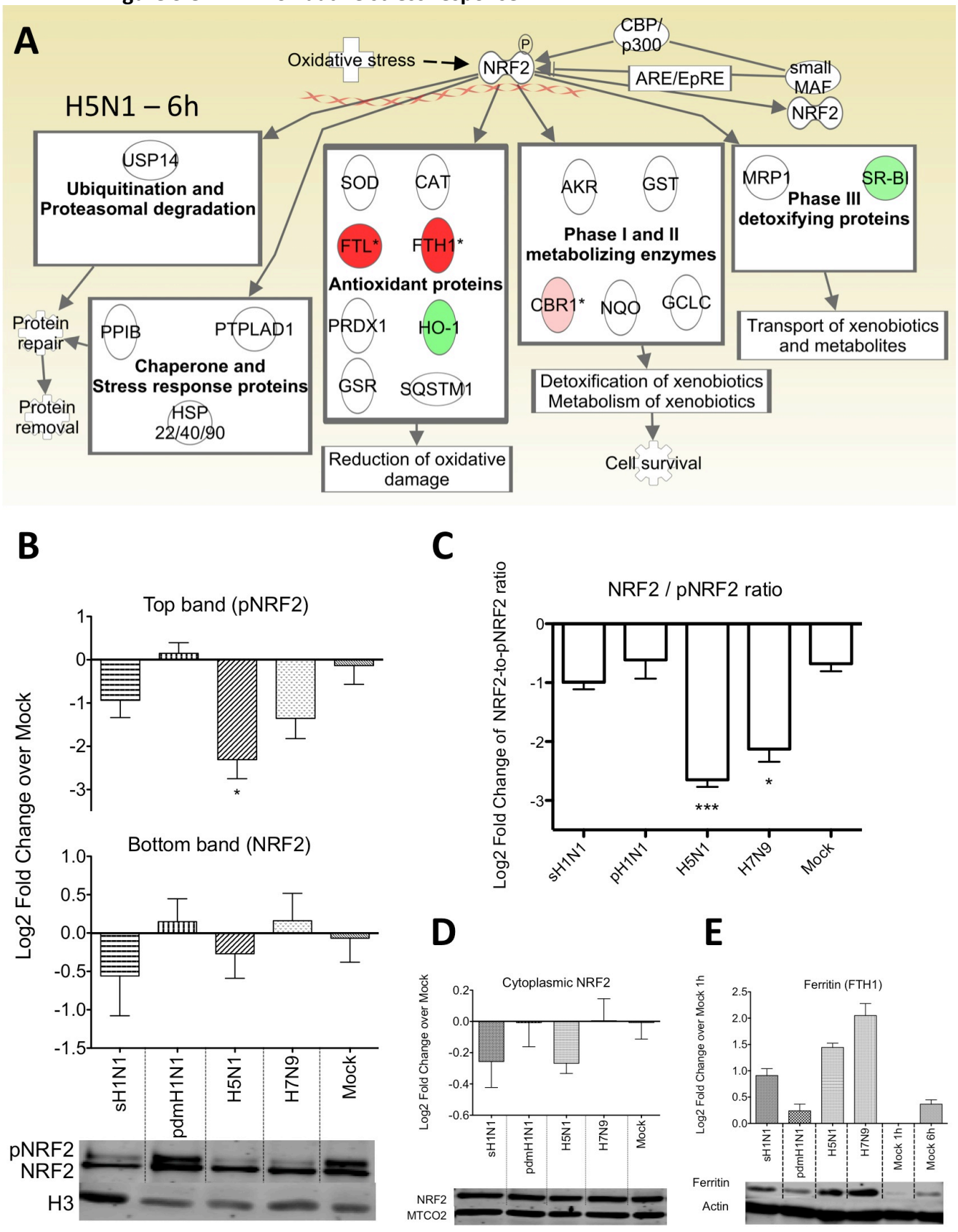

NRF2-mediated oxidative stress response. A. Simplified version of the NRF2 pathway defined in IPA showing the proteins found in the proteomic screen for the H5N1-infected cells at 6h post infection as well as their multiple biological functions. Green indicates down-regulation and red indicates up-regulation compared to the same Mock 1h sample. All proteins indicated in the figure have been found to be significantly modulated in at least one of the infected samples (see table 3.5). B. Western blot and densitometry analysis of NRF2 in Nuclear fractions of A549 cells infected with each strain for 6h. The double-banding pattern is consistent with previously-described phosphorylation of nuclear NRF2 [39] with the top band being the putatively-phosphorylated form. Each band was normalized to H3 histone and the Log2 Fold change over the mock is shown. The intensity of the top band for the H5N1 infected cells is significantly lower than that of the mock. C. The Log2 fold-change of the ratio of the top to the bottom band is shown for each condition D. Cytoplasmic NRF2 does not appear to change during infection. Each band was normalized to MTCO2 and the Log2 Fold change over the mock is shown. For all NRF2 samples, n=3 except for sH1N1 (n=2), paired one-tail student-test were done for statistics. E. Western blot confirmation of the activation of Ferritin at 6h post infection. Triplicate samples were normalized to actin and their log2 fold change was measured over the Mock 1h sample.

The down regulation of one more protein potentially involved in hypoxic stress, CHCHD2, was also independently confirmed by Western Blot (Figure 3.9) and will be further discussed in Chapter 5.

Figure 3.9 - CHCHD2 validation

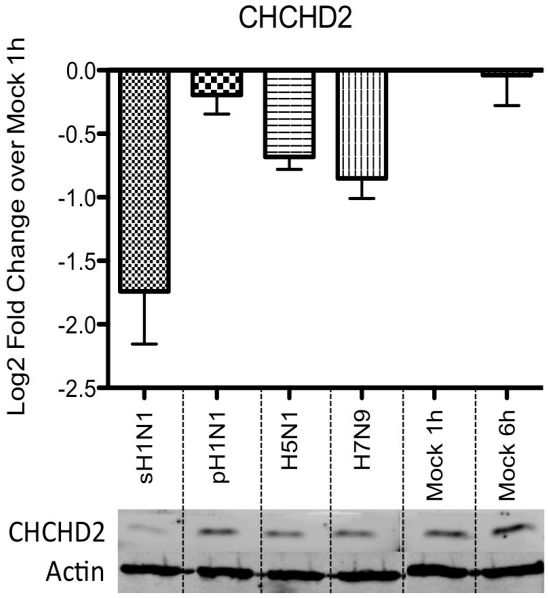

Western blot confirmation of the downregulation of CHCHD2 at 6h post infection by the sH1N1 strain. Triplicate samples were normalized to actin and their $\log_2$ fold change was normalized to the Mock 1h sample. In all infected samples, CHCHD2 was down-regulated, with the strongest effect observed in sH1N1 infected cells, corroborating the iTRAQ data (see table 3.3).

Table 3.5 – Summary of proteins involved in oxidative stress

Protein ID	Protein name	Log2 Fold-Change											
		sH1N1			pH1N1			H5N1			H7N9		
		1	3	6	1	3	6	1	3	6	1	3	6
CATA	Catalase	ns	ns	-0.2	ns	ns	ns	ns	ns	ns	ns	ns	ns
CBR1	Carbonyl reductase 1	ns	ns	ns	ns	0.2	0.2	0.2	ns	ns	ns	ns	ns
FRIH	Ferritin - Heavey chain	ns	ns	1.1	ns	0.4	0.7	ns	0.7	1.2	ns	0.5	1.4
FRIL	Ferritin - Light chain	ns	ns	0.7	0.2	0.3	0.6	ns	0.6	0.9	ns	0.6	1.6
GSH1	Glutamate-Cysteine Ligase, Catalytic Subunit	ns	ns	ns	ns	ns	ns	ns	0.2	ns	ns	0.3	0.2
GSHR	Glutathione reductase	ns	ns	ns	ns	ns	ns	ns	ns	ns	ns	ns	0.2
GSTO1	Glutathione S-Transferase Omega 1	ns	ns	0.2	ns	ns	ns	ns	ns	ns	ns	ns	0.1
GSTP1	Glutathione S-transferase pi 1	ns	ns	ns	ns	ns	0.2	ns	ns	ns	ns	ns	ns
HMOX1	Heme oxygenase (decycling) 1	ns	ns	ns	ns	ns	ns	ns	ns	-0.3	ns	ns	ns
MRP1	Multidrug Resistance Associated Protein 1	ns	ns	ns	ns	0.2	ns	ns	ns	ns	ns	ns	ns
NQO1	NAD(P)H dehydrogenase, quinone 1	0.2	0.2	0.2	ns	ns	ns	ns	ns	ns	ns	ns	0.2
PPIB	Peptidylprolyl isomerase B (cyclophilin B)	ns	ns	0.1	ns	ns	ns	ns	ns	ns	ns	ns	ns
PRDX1	Peroxiredoxin 1	ns	ns	0.2	ns	ns	ns	ns	ns	ns	ns	ns	ns
PRDX6	Peroxiredoxin 6	ns	ns	ns	ns	ns	ns	0.3	0.3	0.3	ns	ns	ns
SCRB1	Scavenger receptor class B member 1	ns	ns	ns	ns	ns	ns	ns	ns	-0.3	ns	ns	-0.2

ns : non-significant

3.3.7 Fibronectin inhibition in H5N1 and H7N9 infection

In a recent study, Leung *et al.* identified fibronectin (FN1) as a specific entry factor for IAV that have tropism for α(2,6)-linked sialic acid surface glycoproteins [162]. They convincingly demonstrated this by whole HA swapping between IAV A/WSN H1N1 (α(2,6)-tropic) and A/Indonesia/05/2005 (H5N1) (α(2,3)-tropic) and by inserting single point mutations in the HA of each of these strains to change their sialic acid tropism. In our proteomic screen, fibronectin was significantly down-regulated by infection with the H5N1 and H7N9 strains, both α(2,3)-tropic viruses and was not affected in the cells infected by the two H1N1 (and α(2,6)-tropic) strains. This was also independently confirmed by immunoblot analysis (Figure 3.10).

Figure 3.10 - Fibronectin validation

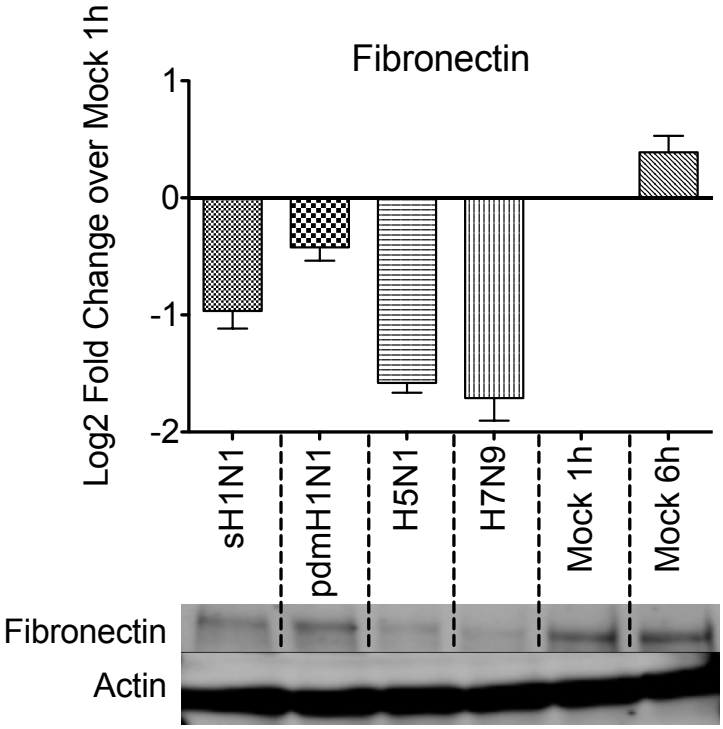

Western Blot confirmation of the inhibition of fibronectin at 6h post infection. Triplicate samples were normalized to actin and their $\log_2$ fold change was normalized to the Mock 1h sample. In all infected samples, fibronectin was down-regulated, with the strongest effect observed in the H5N1 and H7N9 infected cells.

To understand whether there were major differences in fibronectin regulation during infection, we probed our datasets for both direct (i.e. either direct protein-protein interactions or regulatory effect) and indirect (i.e. an effect mediated by an intermediate molecule) interaction partners using a simple and unbiased method. A novel network visualization termed FLEUR (Focused Layout of Entities with Unbiased Relations) was generated by sequentially probing all the 6h p.i. datasets for all the predicted direct and indirect interacting partners of fibronectin defined by IPA (see Figure 3.11). This generates unbiased results as, unlike in other analytic approaches, all the proteins in a dataset are included in the analysis. We started with the 6h Mock set that yielded 13 proteins including 8 unique proteins. The sH1N1, pH1N1, H5N1 and H7N9 respectively yielded 34, 26, 37 and 42 total proteins with 16, 20, 23 and 29 unique proteins respectively (figure 3.12).

Figure 3.11 - FLEUR network of fibronectin

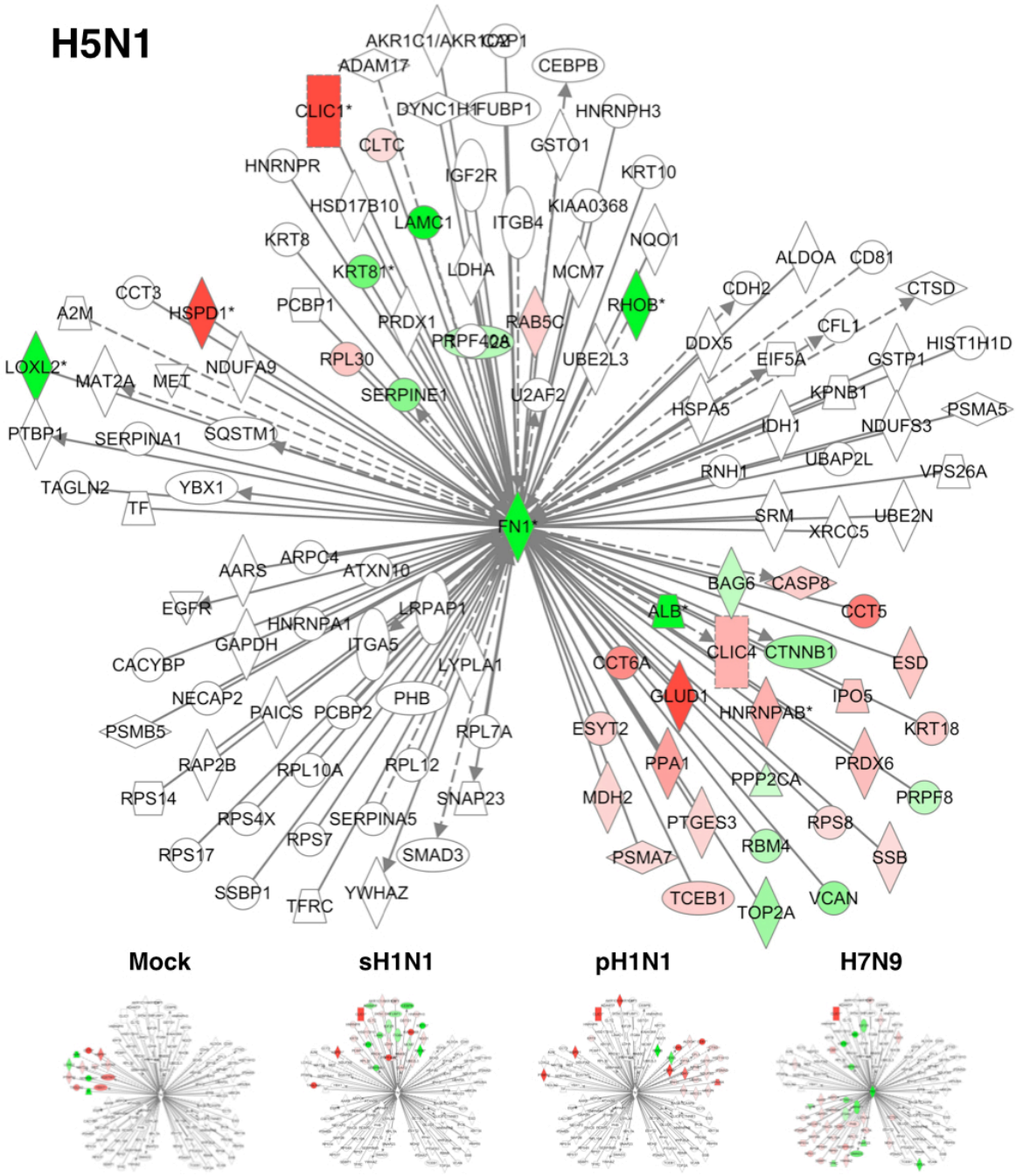

FLEUR (Focused Layout of Entities with Unbiased Relations) interaction network generated by sequentially overlaying proteins with fibronectin (FN1) interactions in each datasets at 6h post infection. Direct interactions are shown by solid lines and indirect interactions by dashed lines. Green indicates down-regulation and red indicates up-regulation compared to the same Mock 1h sample. Each small network are identical copies of the larger one, overlaid with the protein expression data from cells infected with each specified virus.

Figure 3.12 shows a 5-way Venn diagram detailing the overlap of proteins for each infection. The majority of proteins are unique to each infection with the H7N9 and the H5N1 strain having the most proteins interacting with fibronectin.

Figure 3.12 - Overlapping proteins

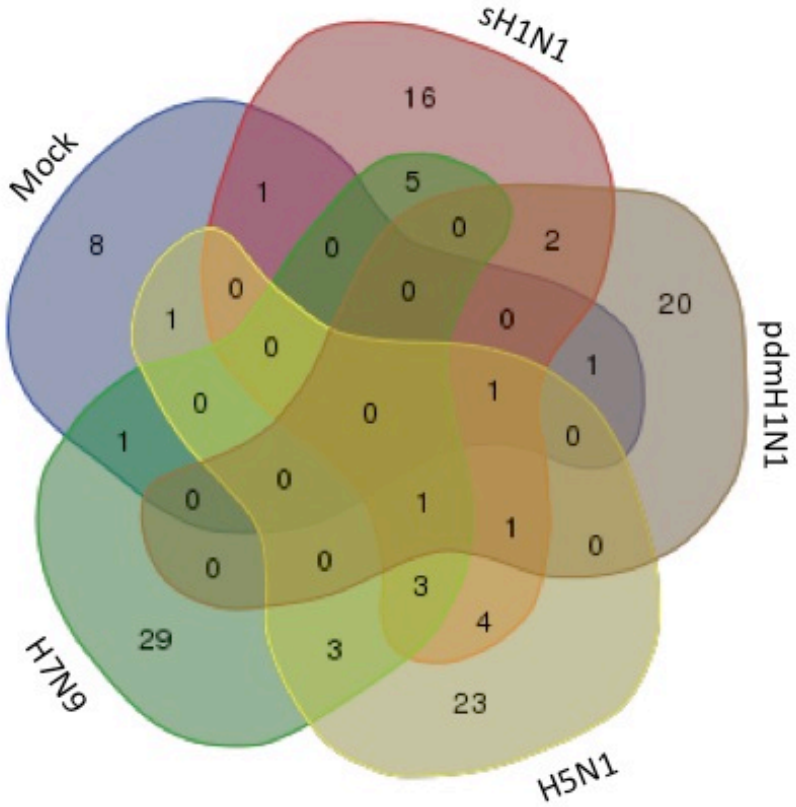

Five-way non-proportional Venn diagram showing the numbers of unique and common proteins interacting with fibronectin in and between each dataset.

3.4 Summary

The results presented in this Chapter shed light on the host response in A549 cells during infection by four strains of influenza A virus of varying pathogenicity. We infected A549 cells cultured under stringent growth conditions with high MOIs of viruses from clean stocks and confirmed infection using both Western Blotting, mass spectrometry and extensive growth kinetics studies (see next Chapter).

Overall, we quantitated over 7,700 proteins in 5 groups of three biological replicates for each infection condition. Each of those triplicates consisted of cells infected with one of four strains harvested at 1, 3 and 6h post infection well as a group of mock-infected samples at those same time points. Further, each triplicate contained the Mock-1h samples which enabled us to directly compare all strains at all time points. Overall, over 7,000 proteins were quantified. Within each triplicate, over 3,600 proteins overlapped the three replicates and the total overlap of the experiment was of over 2,900 proteins when looking at all strains, replicates and time points. Our multiplexing scheme enabled us to directly compare all the strains at all time points while having mock samples at all time points.

The most important finding of this study was that, on a global scale, infection with the H5N1 strain induced the most profound changes to the host proteome as measured by the number of modulated pathways predicted by IPA. This was despite the fact that it had fewer significantly modulated proteins compared to the H7N9-infected cells. The discussion of Chapter five will focus on two major axis: oxidative stress and fibronectin. However, all our data will also be available online as supplemental information to a currently under-review publication and we

hope that others will be able to use it to pursue bioinformatics analysis on other proteins and pathways on which they have expertise.

As mentioned, we identified a potential regulatory mechanism of fibronectin expression during infection by human and avian viruses which could have significance both as a drug target for human strains as well as a marker of cross-species adaptation (see Discussion in Chapter 5). Importantly our shotgun proteomic and extensive bioinformatics analysis led us to discover that infection with the H5N1 strain, and, to a lesser extent with the H7N9 strain potentially inhibits the phosphorylation and/or nuclear translocation of NRF2, a major regulator of cellular response to oxidative stress. Ferritin, a major anti-oxidant protein, as well as CHCHD2 (a protein involved in hypoxic response) have also been validated by immunoblot analysis. The role of oxidative stress in infection will be further discussed in Chapter 5.

Chapter Four – Growth properties of low pathogenicity human and low and highly pathogenic avian influenza viruses

4.1 Introduction and rationale

The work presented in this Chapter was originally a side-project of the main Proteomic experiments of Chapter 3. As we realized that viral kinetic studies would be an excellent complement to understanding the host response, we (re)-established a collaboration with the Beauchemin Lab at Ryerson University. The input needed for successful modeling of infections consists of extensive but simple measures of infectious particles and RNA copy numbers over time as well as carefully controlled infection conditions. We achieved a high level of control of infections in Chapter 3 with stringent culture conditions of A549 cells and extensive titrations of concentrated stocks.

Although most biologist cringe at the mention of mathematical modeling and would readily consider it more akin to witchcraft than Science, one needs to remember that we use models for many important biological phenomena. The best example is the 1953 study by Watson and Crick where they modeled the structure of DNA based on experimental results [163]. This model is still in use today and still accurately predicts the DNA properties. A particular appeal of current study was the opportunity to interact with Physicists and Computer Scientist. Inter-disciplinary collaboration can bring forward the best of both fields. The stringent, calculating minds of Physicists and the practical and pragmatic vision of biologists can unite to strive to better explain complex phenomenon, binging forward conclusions that neither field could have discovered on their own.

Like any model where we explain a biological phenomenon, models of infection are based on a series of basic assumptions describing basic viral replication. Virions infect cells. Cells produce virions. In the case of lytic infections like the ones caused by influenza viruses, infected cells eventually die and virions eventually lose infectivity. Viruses replicating faster or to higher titres must then modulate one of those steps to achieve their overall observed viral replication. The goal of mathematical modeling is to find the series of equations that are sufficiently robust to accurately mimic experimentally-obtained data.

All the modeling and mathematical work was done by Prof. Catherine Beauchemin at Ryerson University in Toronto. All the virology experiments where done by Philippe Simon with the assistance of Marc-Antoine de la Vega and Emelissa Mendoza at the National Microbiology Laboratory in Winnipeg.

The work presented in this Chapter is a separate manuscript currently in the final stages of being submitted for peer-reviewed publication.

4.2 Hypothesis and objectives

The main hypothesis of this work is that influenza strains of higher pathogenicity will have enhanced replication kinetics compared to strains of low pathogenicity. We further hypothesize that there might be differences in specific parameters of replication that could explain an overall increased or decreased replication capacity.

The objectives of this study can be defined as follows:

1. Confirm infection in A549 cells
2. Determine the sets of experiments needed to obtain the high-quality data needed to build the model
    a. Reliably measure growth kinetics of each strain in terms of infectious particles and copy numbers
3. Replicate the *in vitro* yield experiments using computer simulation to validate the model

4.3 Results

We evaluated and compared the infection kinetics of two human virus strains (sH1N1 and pH1N1) causing mild disease in humans to two avian virus strains (H5N1 and H7N9) causing severe human infections. For this purpose, two distinct infection assays were performed which, together, provide complementary information on different aspects of the replication kinetics of these strains. The single-cycle (SC) assay is an infection at high MOI (3 PFU/cell) where all cells are infected approximately simultaneously. The viral load produced over time allows one to directly observe the average timing for initiation of virus release (the duration of the eclipse phase), and the kinetics of virus production ramp-up, within a single, newly infected cell. The multiple-cycle (MC) assay is an infection at low MOI (0.01 PFU/cell) where a small population of initially infected cells provide the viral progeny necessary to trigger a second cycle of infection. This causes second and third cycles allowing one to observe the average period and amplitude of successive infection cycles. A cell-free, mock-yield (MY) assay was also performed to evaluate the stability of virus infectivity over time at 37°C.

4.3.3 Traditional growth kinetics of avian influenza strains

Overall, the most striking differences are observed in the MC infections for the peak titers. The H5N1 and H7N9 reached higher maximum average titres (H5N1 = 3.67 x10^8 $TCID_{50}$/ml; H7N9 = 2.89 x 10^8 $TCID_{50}$/ml; sH1N1 = 2.52 x 10^7 $TCID_{50}$/ml; pH1N1 = 4.48 x 10^7 $TCID_{50}$/ml). These maximum titres were reached between 42 and 53 hours post infection for the H5N1 and H7N9 strains and at 66 hours post infection for the sH1N1 and pH1N1 strains. This suggests that the H5N1 and H7N9 strains undergo successive infection cycles more rapidly than the sH1N1 and pH1N1 strains and/or infect a greater number of cells within each cycle. In the SC infection

assay, intensive virus production and release also appears to begin earlier for the H5N1 and H7N9 strains, beginning around 3h–4h post-infection compared to 5h–6h for the sH1N1 and pH1N1 strains, suggesting a longer delay for virus production and release for the two human strains, consistent with longer elapsed time between successive infection cycles with these strains (Figure 4.1).

Figure 4.1 - Traditional growth kinetics

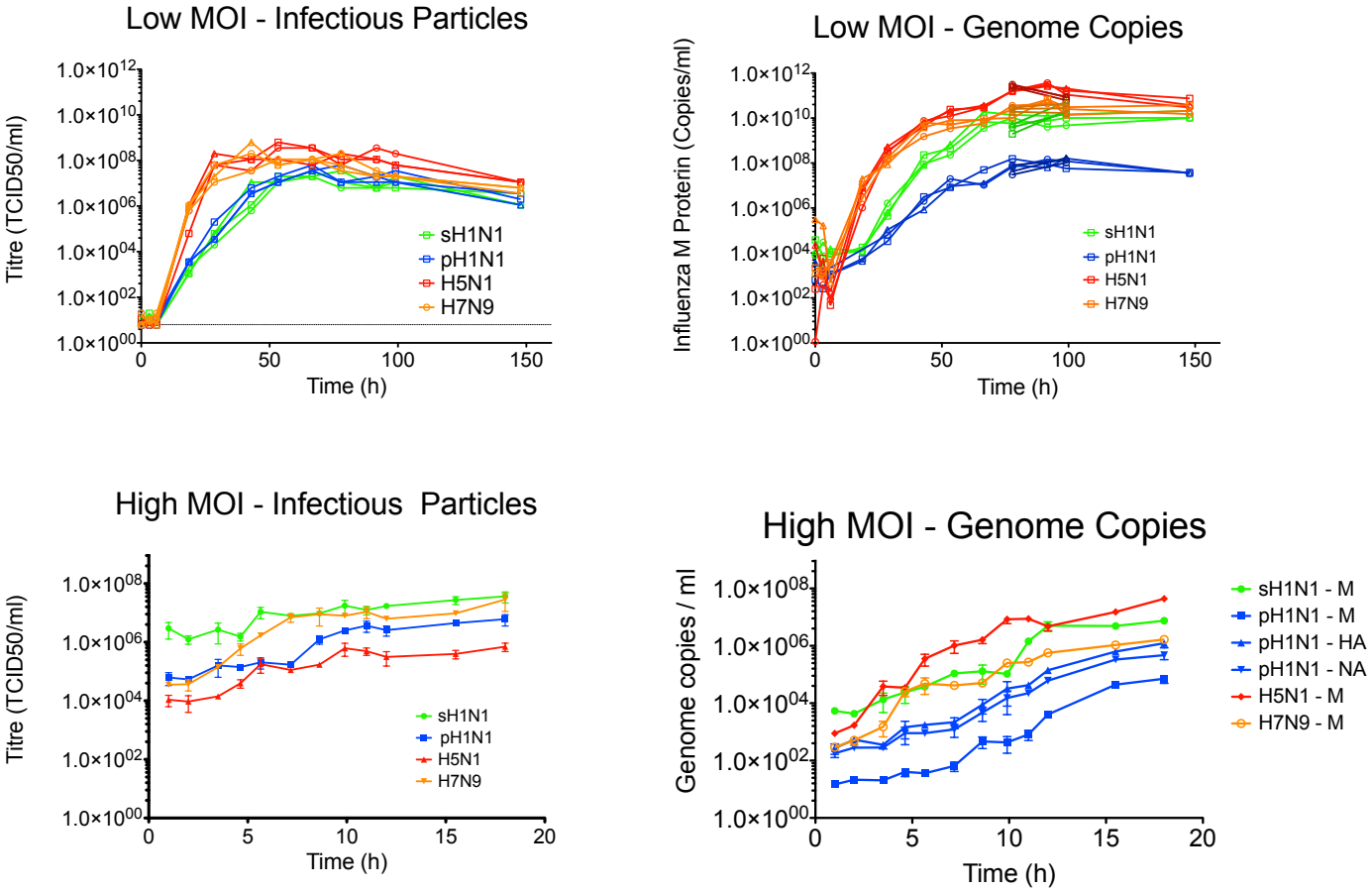

Low MOI (0.01 PFU/cell) and High MOI (3 PFU/cell) kinetics were measured in triplicate for each strain over 5 days (low MOI) and 24 h (high MOI). The readout was $TCID_{50}$ (measuring infectious particles) as well as genome copies per ml (a surrogate to particle counts). Overall, in the low MOI assay the H5N1 and H7N9 strains exhibited faster growth and reached higher peak titers then the two H1N1 strains.

4.3.3 Modeling the growth kinetics

To gain a quantitative understanding of these differences, the experimental data were analyzed using our mathematical model, and a Markov chain Monte Carlo (MCMC) method was used to determine the parameters characterizing the replication efficiency of each of the four strains. Figure 4.2 shows 900 simulated infections, for each strain, for 900 different parameter sets, each drawn from our distribution of 600,000 sets per strain, obtained through our MCMC process and overlaid with experimental data (dots). Those 900 iterations correspond to combinations of parameters that yield the best *in silico* fit to the experimental data and thus those from which the values of the variables can be extracted with good confidence. These simulated viral infections illustrate how the uncertainty in a strain's replication parameters, due to experimental variability, translates into deviations in the shape of the infection time course predicted by the mathematical model. The individual strain's replication parameters are reported in Table 4.1. Figure 4.3 presents the probability distributions for the value of key parameters characterizing different aspects of the viral replication efficiency for each strain.

Table 4.1 - Parameter characterizing the replication of each strain and p-values

Parameter*	sH1N1	pdmH1N1	H5N1	H7N9
Degradation, $c_{\mathrm{TCID}_{50}}$ (1/h)	0.0573 [0.03, 0.098]	0.0414 [0.017, 0.079]	0.0657 [0.038, 0.1]	0.0596 [0.032, 0.098]
Eclipse phase, τ_E (h)	7.04 [5.6, 9.7]	9.15 [6.9, 11]	6.27 [5.5, 7.1]	6.05 [5.4, 6.7]
Infecting time, t_{inf} (min)	76.1 [49, 100]	43.3 [27, 65]	20.4 [14, 28]	15.2 [10, 22]
Prod. rate (RNA/cell/h)	$10^{3.03}$ [2.7,3.6]	10^{2} [1.6,2.7]	$10^{3.8}$ [3.6,4]	$10^{2.85}$ [2.6,3.1]
Infection rate (cells/h)	$10^{1.34}$ [1,1.8]	$10^{1.97}$ [1.5,2.6]	$10^{2.42}$ [2.1,2.8]	$10^{2.72}$ [2.3,3.1]

Parameter	sH1N1:pH1N1	sH1N1:H5N1	sH1N1:H7N9	pH1N1:H5N1	pH1N1:H7N9	H5N1:H7N9
Degradation, $c_{\mathrm{TCID}_{50}}$ (1/h)	0.233	0.364	0.466	0.140	0.208	0.397
Eclipse phase, τ_E (h)	0.104	0.201	0.122	**0.010**	**0.004**	0.339
Infecting time, t_{inf} (min)	**0.029**	**< 0.001**	**< 0.001**	**0.007**	**< 0.001**	0.139
Prod. rate (RNA/cell/h)	**0.005**	**0.009**	0.169	**< 0.001**	**0.012**	**< 0.001**
Infection rate (cells/h)	**0.033**	**< 0.001**	**< 0.001**	0.088	**0.018**	0.135

* The mode and 95% credible region (analogous to the 95% confidence interval) for each parameter distribution are shown. The bottom table indicates differences of statistical significance (p-values) between each pair of strain. Bold values are $p < 0.05$.

Figure 4.2 - Experimental data and modeling fit

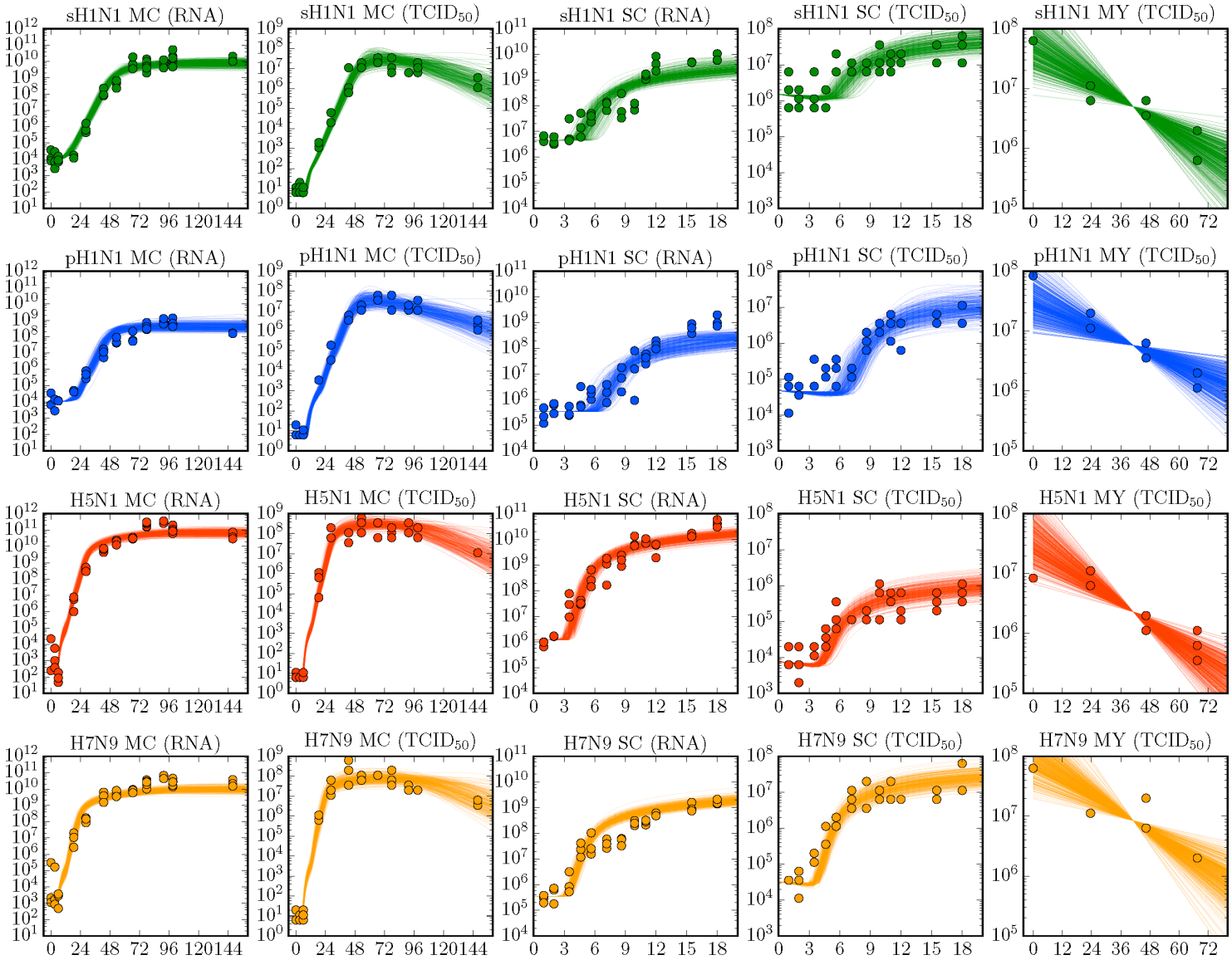

Comparison of infection kinetics and agreement with the mathematical model. The experimental data for the low-MOI, multiple-cycle (MC), high-MOI, single-cycle (SC) infection assay and the mock-yield (MY) assay are represented as circles while the lines represent independent iterations of our model-generated results. Each line represent an independent *in silico* simulation of the model (n=900). At each time point, supernatant samples were harvested in triplicate, titrated by $TCID_{50}$, and viral RNA was quantified by qRT-PCR. Color coding as follows: Seasonal H1N1 (sH1N1, green); 2009 pandemic H1N1 (pH1N1, blue); H5N1 (red) and H7N9 (orange). These data were used to extract the probability distribution for the parameters characterizing the virus replication efficacy of each strain (Figure 4.3, Table 4.1).

4.3.3 Quantitation of viral life cycle parameters

For all strains, the rate at which virions lose infectivity in the medium at 37°C is similar. The eclipse phase – the time elapsed from the successful infection of a cell by a virion to the release of the first virion produced by that cell – is insignificantly shorter (by 1h–1.5h) for the H5N1 and H7N9 strains compared to that of the sH1N1 strain, but significantly shorter (by 3h) compared to that of the human pH1N1 strain. After the newly infected cell begins releasing virions, the time elapsed before its virion progeny infects its first cell, defined as the infecting time, is again significantly shorter for the H5N1 (15 min) and H7N9 (20 min) strains compared to the H1N1 strains (43 min for pH1N1, 76 min for sH1N1). In addition, the virion production rate per infected cell for the H5N1 strain was significantly larger than that of the three other strains, with H5N1-infected cells producing and releasing nearly 100 times more virions per hour than cells infected with pH1N1, and around 10 times more than cells infected with either the sH1N1 or H7N9 strain. Cells infected with the H7N9 or sH1N1 strain produced virions at comparable rates. Interestingly, we find that the viral output from the H5N1 and H7N9 strains caused a comparable number of infections per hour, despite the significantly higher virion production rate of the H5N1 strain compared to the H7N9 strain. This may suggests that a larger proportion of the H7N9 virions produced are infectious compared to the H5N1 virions. Ultimately, the shorter eclipse phase and infecting time, and the higher rate of infections per hour observed for the infections with the H5N1 and H7N9 strains all contribute to their significantly more rapid (by ~1 day) infection progression (the up-slope of the viral titer curves) and higher peak viral loads, compared to that seen for infections with the two H1N1 strains.

Figure 4.3 - Replication parameters value distributions

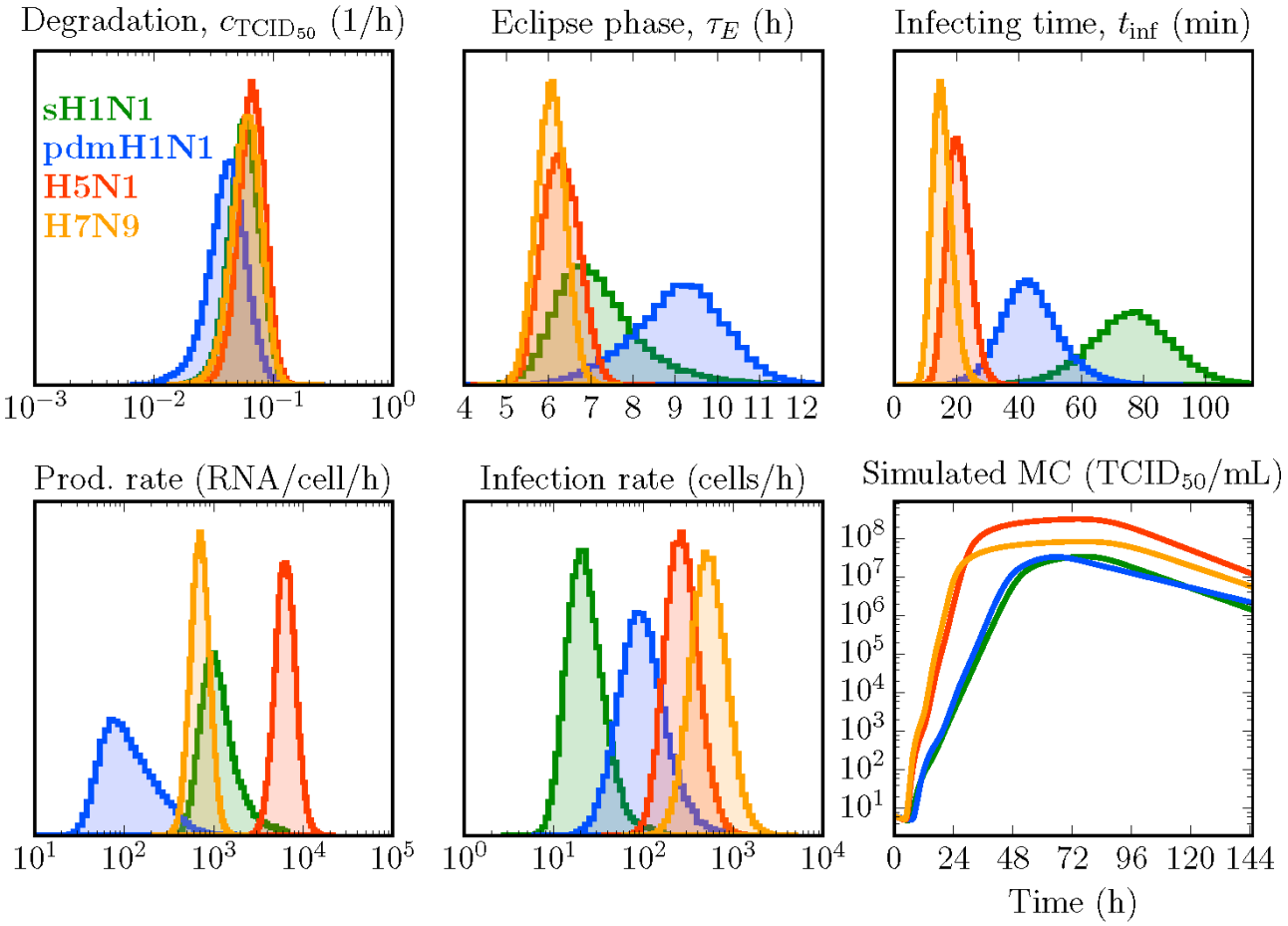

Probability distribution of key parameters for each of the four strains. The degradation rate is a measure of the stability of the virions. The eclipse phase is the time elapsed between the successful infection of a cell and the release of its first virion. The infecting time is the time between the release of the first virion from the newly infected cell and the infection of a cell by this progeny virion. Once virus production and release is well underway in the infected cell, virions will be produced at a certain rate (Prod. rate measured in RNA/cell/h). This rate of production of virion progeny will result in a number of infections per hour (Infection rate in cells/h). The simulated multiple-cycle (MC) assay (bottom-right panel) was produced by using the best-fit parameters obtained with our MCMC method and illustrates how these parameters, together, yield the experimentally-observed viral growth rate (see Figure 4.1).

4.4 Summary

In this study, we confirmed that all four strains productively infected A549 cells and also used mathematical modeling to assess whether there were differences in the various steps of the infection cycle. Traditional growth kinetics showed that the H5N1 and H7N9 replicate to higher peak titers (in the 10^8 PFU/ml range vs 10^6-10^7 PFU/ml for the sH1N1 and pH1N1 strain) and reach those titers approximately 24h before the two H1N1 strains. These results where integrated in a mathematical model of infection that allowed us to de-construct and quantify each steps of the *in vitro* viral replication. As such, we found that the faster and higher growth kinetics of the H5N1 and H7N9 strains in A549 can be explained by significantly enhanced infection of cells and by an increased production rate for the H5N1 strain. We also found that the poor replication observed for the pH1N1 strain generally exhibited poor replication with longer eclipse phase as well as lower production rates compared to all other strains. These findings are summarized in figure 4.4.

Figure 4.4 - Comparative viral dynamics

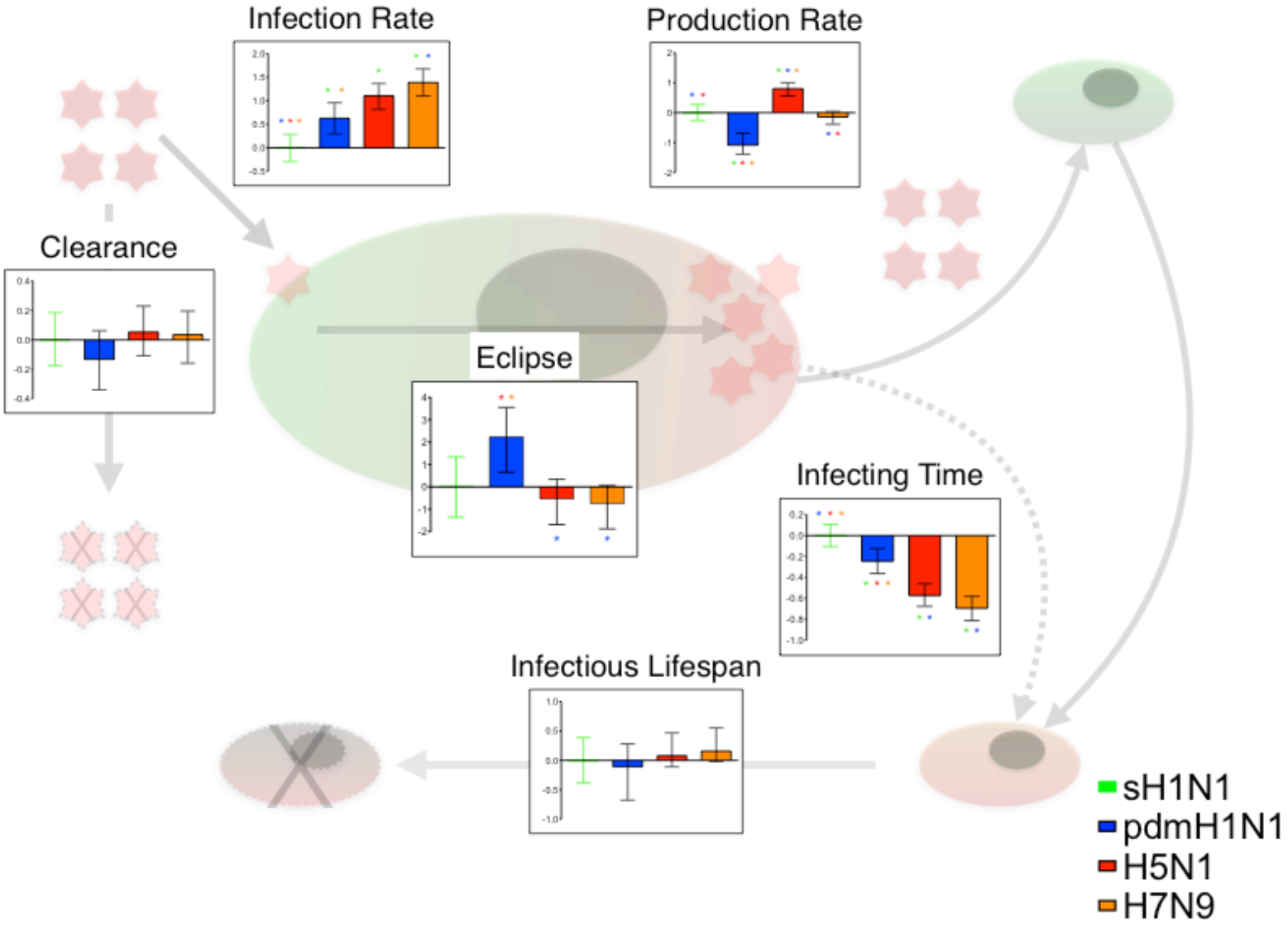

Summary of replication parameters. A simplified representation of the parameters as defined by the model is shown as a unit-less Log_{10} ratio of each parameter to the sH1N1 strain. For the Eclipse parameter, it is a subtraction to the sH1N1 eclipse phase length with units in hours. Colored asterisks indicate significant differences between strains.

Chapter Five – Discussion

5.1 Host response to low pathogenicity human and low and highly pathogenic avian influenza viruses

5.1.1 Infection confirmation and viral protein expression

We used NS1 as a marker of viral replication as this viral protein is not carried in the virion and is only expressed upon novel infection [148]. Our results indicate that viral replication starts as early as 3h post infection for the sH1N1, H7N9 and H5N1 strains. This is also confirmed by our iTRAQ results (Table 3.1). The ratio of viral proteins was measured against the Mock-infected sample at 1h post-infection. As the Mock 1h sample does not contain any viral proteins, the ratios are based on the background intensities of the precursor iTRAQ ions [164]. While the Log_2 fold changes of the sH1N1, pH1N1 and H7N9 viral proteins at 6h are very high only the H5N1-infected cells exhibited statistically-significant increases at 1h post-infection while only the H5N1 and the H7N9 infected cells had significant increases at 3h post infection. This study was designed to measure host protein abundances, not specifically the expression of viral proteins. The purpose of Table 3.1 is to show that viral replication occurs. Because of the compression issues inherent to iTRAQ [164], the actual change in protein expression will be reflected as a much smaller value in the proteomic dataset. The most important outcome to be observed is the directionality of the change in expression (i.e. up or down) as opposed to their absolute values. To systematically study the quantitative increase of viral proteins over time using our iTRAQ approach, the mock cell lysate at 1h could be spiked with artificial viral peptides or proteins in order to provide a more reliable denominator yet this falls outside of the

scope or our study. Nonetheless, our results are in agreement with several other studies that have used A549 cells in the context of influenza infection (Eg. [153], [165], [166]).

5.1.2 H5N1 global dysregulation

Infection with the HPAI strain H5N1 constantly caused more dysregulation to the cell proteome then any of the three other strains. This is most obvious by examination of the IPA results (Figure 3.6) in conjunction with the total number of significantly dysregulated proteins. More than any specific pathway, this indicates that infection with a highly pathogenic avian influenza strain of H5N1 subtype induces more profound changes at the cellular level. While the H7N9 virus infection modulated expression of more proteins (206 vs 154 for the H5N1 strain - see Table 3.2), it failed to modulate as many canonical pathways in IPA (see Table 3.3). So, by simply looking at numbers the H7N9 strain may appear to cause the most dysregulation. Yet based on their biological functions, fewer proteins significantly modulated by the H5N1 infection caused broader dysregulation to the host. This high degree of dysregulation caused by H5N1 virus infection is consistent with a previous global proteomic screen [130] where strong dysregulation was found as early as 1h post infection in primary macrophages infected with either H5N1 or H1N1 strains. In our study, we found the most changes occurring at the 6h post-infection time point. Differences are probably due to different cell types and IAV strains tested. However, the overall message from both studies is the same; infection with H5N1 induced the most changes to the cellular proteome. From a mechanistic perspective, this supports the idea that the important pathology seen at the organismal level during infection by these viruses is caused both by differences in tissue tropism, host response and by unique intracellular modulation.

5.1.3 Oxidative stress response

A few studies have shown that oxidative stress during IAV infection is an important factor in apoptosis and also has physiological relevance in infected mice [167]–[169]. Specifically, compared to wild-types, mice deficient for NRF2 showed increases of oxidative and inflammatory genes when infected with influenza [167]. NRF2 has been described as an important regulator, central in the production of anti-oxidant molecules during inflammation, oxidative and electrophilic stresses to cells [170]. Our bioinformatics results indicate that NRF2 is the most important pathway modulated upon infection, yet it was unclear how. To investigate this finding, we infected A549 cells at MOI of 10 with our four strains, harvested lysates at 6h post infection and fractionated them into their cytosolic and nuclear components. Western blot analysis and densitometry was performed to measure the amount of NRF2 present in each fraction. We found a double banding pattern observed in previous studies that has been identified as the phosphorylated form (top band) and non-phosphorylated form (bottom band) [161] of NRF2. This pattern was observed only in the nuclear fractions, consistent with our knowledge on NRF2 which needs to be phosphorylated to be imported into the nucleus and perform its transcriptional role [161], [171]. Furthermore, the H5N1-infected cells exhibited a statistically-significant lower amount of the top putatively phosphorylated NRF2 band (pNRF2). The H7N9-infected cells also had a trend for lower pNRF2. The ratio of pNRF2 to NRF2 was statistically significantly lower for both H5N1 and H7N9-infected cells compared to the mock. Based on the function of NRF2, this would potentially indicate that H5N1 and, to a lesser extent, H7N9 are capable of inhibiting this important element of the oxidative stress response.

To our knowledge, this is the first study to describe a potential role of NRF2 in infection with highly pathogenic avian influenza viruses. This warrants further work to better understand whether strains of different pathogenicity can specifically modulate the NRF2 response to their advantage and how an increase in oxidative stress in the cell would benefit a virus during infection. Conversely, it could also be a good indicator of the more severe symptoms exhibited by infection with the H7N9 and H5N1 strains: whether they actively inhibit oxidative stress responses or whether that inhibition is a by-product of a more aggressive modulation of the host response to sustain higher viral replication, the end-state for the host would result in increased damage to the cells and potentially more severe symptoms. A particular hallmark of H5N1 infection is the induction of a cytokine storm. It is not unreasonable to imagine a situation where infection combined with poor cellular response to oxidative stress would lead to inflammation and subsequent triggering of a deadly cytokine storm.

Two proteins involved in oxidative stress response and identified in our top-ten list of most significantly dysregulated proteins (See Table 3.3) have also been confirmed by immunoblot analysis. In all our analyses and no matter which statistical approach we used, the protein Ferritin (FRIH, FRIL) was identified as being strongly up-regulated in cells infected by all the IAV strains we used. This large, 450 kDa protein, composed of 24 subunits of both heavy (FRIH) and light (FRIL) monomers (in mammals) is considered a major iron storage protein. Serum ferritin levels are routinely tested in hospital as part of normal blood work and high values can be indicative of an ongoing inflammatory process [172], [173]. Not surprisingly, high ferritin levels have been observed in H5N1-infected patients [174]. This could be due both to a normal

pathophysiological host response to an inflammatory process such as infection and could also be aggravated by the inhibition of the protective NRF2 oxidative stress response.

Our study uncovered several other significant proteins involved in the NRF2 oxidative stress in infected A549 cells. The full list and associated modulation is available in Table 3.5. Amongst those genes, we observed a moderate increase of two proteins of the Glutathione S Transferase family (GST) in sH1N1 and H7N9-infected cells (GSTO1) as well as a moderate increase of GSTP1 in pH1N1-infected cells. Interestingly, no GST were found to be significantly modulated upon H5N1 infection. This is somewhat in contrast with a previous study on gene expression of inflammatory genes by Zhang et al. [175]. In that study, they observed that the expression of GST was "almost eliminated" in the kidney of chicken infected with a H5N1 HPAI strain. Although we did not observe this, GST is under the control of NRF2 and NRF2-null mice exhibit lower constitutive and inducible levels of GST transcripts [176]. While we did not observe a significant decrease of GST in our H5N1-infected A549 cells, our results on NRF2 potential dephosphorylation in those same cells could explain the low levels of GST observed by Zhang et al. Glutathione transferases, as their name indicate, are enzymes able to conjugate reduced glutathione moieties to foreign toxins and proteins in cells, serving an important role in detoxification and response to oxidative stress [177], [178]. Interestingly, a recent study has shown that proteins of the peroxiredoxin family can be glutathionylated and secreted from macrophages stimulated by lipopolysaccharides (LPS), a powerful inducer of oxidative stress. In that proteomic study, Checconni et al. [179] have also identified Peroxiredoxin 1 and 2 (PRDX1, PRDX2) as being secreted by A549 cells infected with the lab-adapted H1N1 PR8 strain. From their study, it is unclear whether PRDX1 and 2 are glutathionylated, yet we have also observed

a statistical increase in PRDX1 amounts in the sH1N1-infected A549 cells at 6h post infection. In H5N1-infected cells, we observed a significant increase in PRDX6, another member of the Peroxiredoxin family. We did not test whether those proteins were glutathionylated, yet this would be something of interest, especially in the context of NRF2 inhibition in H5N1 and H7N9-infected cells.

One protein involved in oxidative/hypoxic stress and identified in Table 3.3 yet not apparently under the control of NRF2 is CHCHD2 (Coiled-Helix-Coiled-Helix Domain Containing 2). Its inhibition during infection was validated by Western Blot analysis (see Figure 3.9). Although to our knowledge no studies have linked it to influenza infection, it has been described as binding COX4I2, a cytochrome c oxidase (COX) of the respiratory chain, and to activate its transcription both under hypoxic and normal conditions [180]. This is of particular interest as, while COXes can be ubiquitously expressed in the human body, COX4I2 is predominantly found in the lungs [181]. We have observed and confirmed a significant down-regulation of CHCHD2 in sH1N1-infected A549 cells while pH1N1 had levels compared to the mock-infected cells. For H5N1 and H7N9-infected cells, the levels appeared intermediate, between the Mock and those of sH1N1, yet only in the sH1N1 was the difference statistically significant based on our iTRAQ proteomic results. It is unclear how, from a viral perspective, infection would be more efficient by repressing COX4I2 and thereby limiting cellular aerobic metabolism. Perhaps other yet unknown roles of CHCHD2 will be discovered in future studies. When looking at the NRF2 and CHCHD2 results discussed above and that the second most important canonical pathway identified by IPA is the production of nitric oxide and reactive oxygen species in macrophages, it appears quite evident that oxidative stress (and its

modulation) plays a significant role in infection at a basic cellular level and potentially contribute to the pathogenesis at the organismal level.

A limitation of our proteomic screen is that it measures abundance of proteins. This has the potential of missing important host responses mediated by other mechanisms. The best example would be either phosphorylation cascades or nuclear translocations. In both cases, these pathways could be highly inhibited or activated yet the overall protein abundance in the cells would remain unchanged. As such, those would be un-detected by our current approach. Another issue is that we may miss proteins severely inhibited by infection (or constitutively expressed at very low levels) while having a bias towards those overexpressed during infection. In the first case, those would be detected in the Mock-infected samples but may be missed in the infected samples. In the second, while those proteins would be detected in infected samples they would not have a good reference spectra in the mocks.

5.1.4 Fibronectin

The importance of fibronectin in influenza virus infection was demonstrated in a prior study by Leung *et al.* [162]. It was identified as a key entry factor specifically required for viruses with a tropism for glycoproteins with α(2,6)-linked sialic acid (SA) moieties. In our study, we used two independent methods, iTRAQ and Western Blot, to confirm that fibronectin expression was significantly reduced in H5N1- and H7N9-infected A549 cells compared to the low pathogenicity α(2,6)-tropic H1N1 strains. The study of Leung *et al.* did not attempt to explain the regulation behind fibronectin expression. Our results demonstrate that this important protein is most strongly down regulated in cells infected by HPAI H5N1 and H7N9 strains and that infection by

all strains induces major changes in other proteins involved in fibronectin regulation. Infection with all viruses caused several fibronectin-interacting proteins to be modulated. This is interesting in that, according to our current understanding of the role of fibronectin in IAV infection, this protein would not be necessary for H5N1, may play a minor role in infection with H7N9 strains, but would be important for infection with H1N1 strains. The sialic acid tropism of the A/Anhui/1/2013 (H7N9) strain we used has been described as being mixed, enabling binding to both α(2,3) and α(2,6)-linked moieties [76], yet fibronectin was seen as being strongly down-regulated in H7N9-infected cells. One must keep in mind that human infections by that strain are relatively rare events and that its primary replication occurs in poultry. As such, although it could infect cells carrying both α(2,3) and α(2,6) SA its natural reservoir in birds would have α(2,3) receptors. This would limit the importance of fibronectin for its replication and could explain why, despite having a mixed tropism, it still inhibits it.

Fibronectin (FN1) is a large, ~260 kDa glycoprotein with multiple different binding domains [182] that forms di-sulfide-linked dimers in plasma and multimers at the cell surface and in the extracellular matrix (Figure 5.1). It has been recognized as a crucial component of the extracellular matrix (ECM) where its multiple binding-domains anchor together a variety of extracellular molecules including collagen, fibrin, heparin, DNA and actin. An excellent recent review details the importance of the different domains for ECM arrangement [183]. It also proposes a model where extracellular FN1 dimers are recruited by transmembrane integrins which then cluster at the cellular membrane, driving the amalgamation of intracytosolic proteins and further FN1 recruitment in the extracellular space. Once enough FN1 proteins are recruited, they form insoluble links, creating a stable ECM scaffold (Figure 5.2).

Figure 5.1 - Fibronectin

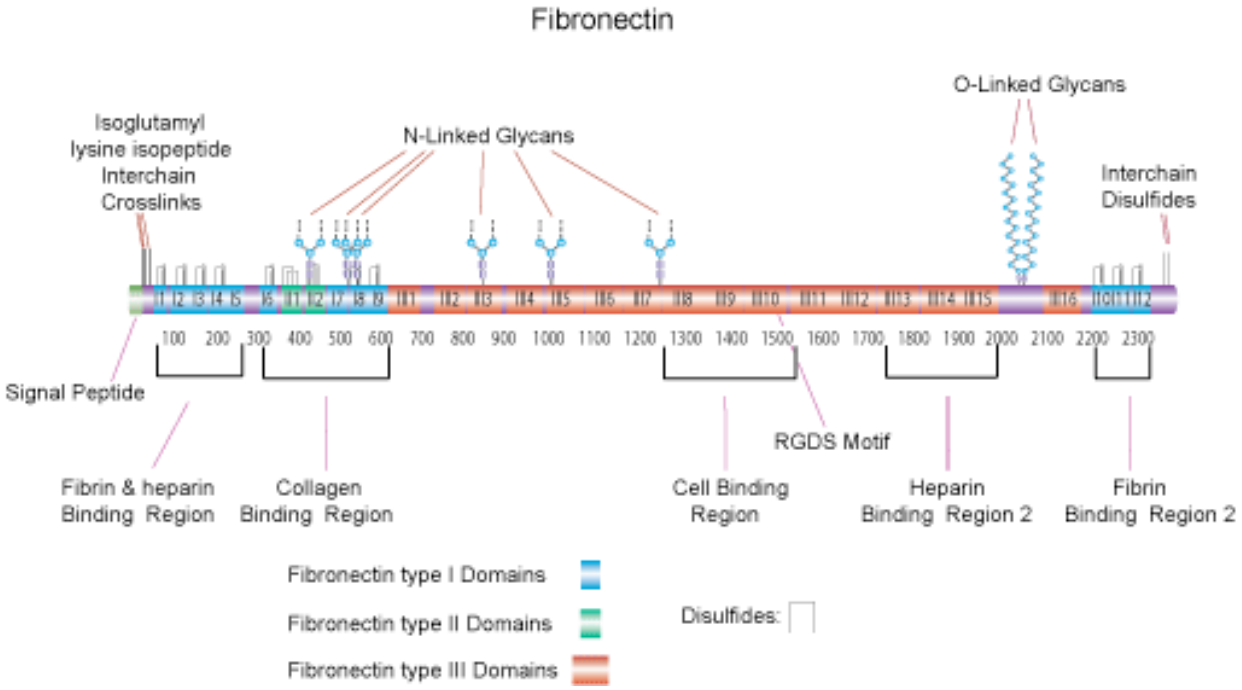

Schematic representation of a Fibronectin monomer. Image reproduced with permission from SigmaAldrich.

It is tempting to hypothesize that avian, α(2,3)-tropic strains such as the H5N1 and H7N9 viruses naturally do not need fibronectin as an entry factor and so do not suffer from its inhibition. Consequently, when avian viruses cross the species barrier to infect humans (and change their tropism to α(2,6)), they may need to develop a regulatory mechanism that would stop the inhibition of fibronectin. The resulting maintenance of fibronectin expression – and potentially better cohesion of the ECM – on the cell surface would then facilitate infection and provide emerging strains with a stronger foothold in their new host. Leung *et al.* have argued that α(2,6)-tropic virions do not bind directly to FN1 but rather are internalized in as part of a FN1-dependent mechanism [162]. The turnover of FN1 in the ECM has been described as being mediated by caveolin-1 endocytosis [184] and to process dynamically [185]. It is not inconceivable that virions could bind to other molecules of the ECM and thus be internalized

during ECM turnover. Conversely, avian strains with preferences of α(2,3)-SA and not requiring FN1 for entry would have an advantage in reducing the amount of fibronectin on the surface of the cells. This would enhance infection by making the cell more accessible to virions.

Figure 5.2 - Fibronectin multimerization in extracellular matrix formation

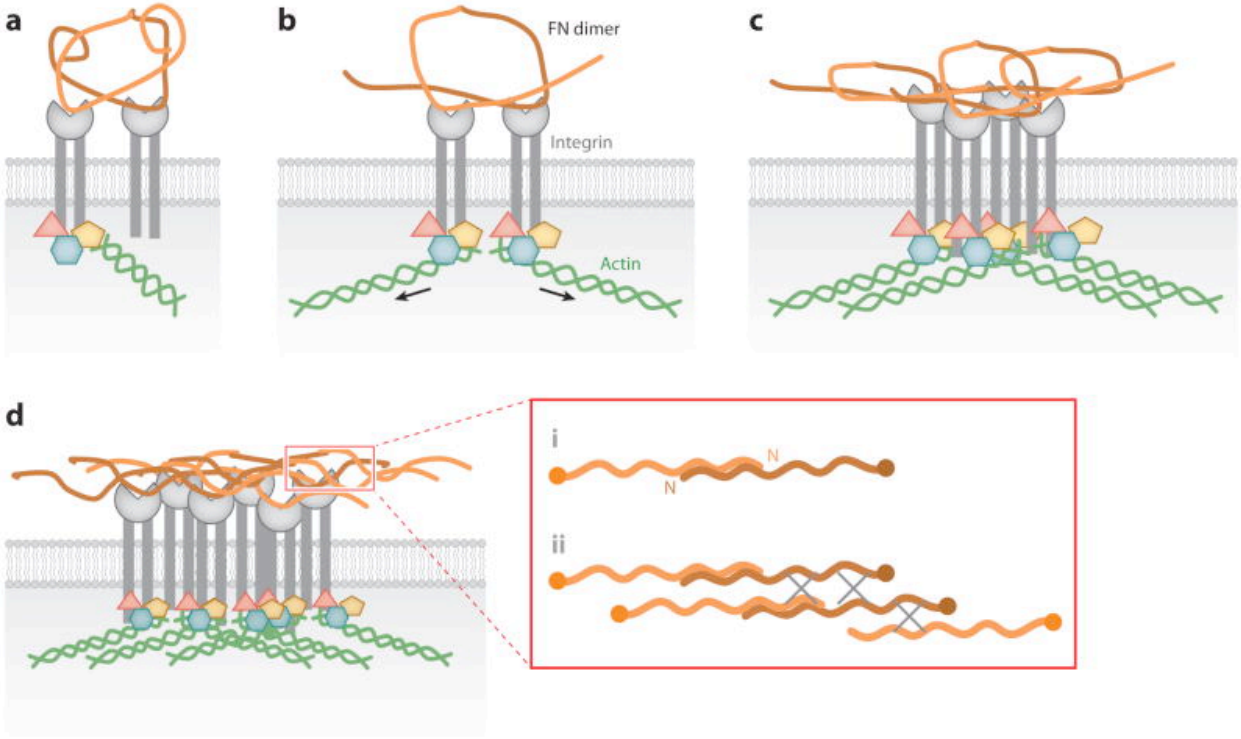

A proposed model of the role of Fibronectin (FN1) in the assembly of extracellular matrix. A. FN1 dimers are recruited to the cell surface by integrins B. and C. Additional integrins congregate to the membrane which makes the cell contract. This contraction induce changes in FN1 conformation and leads to rearrangement (D) and the formation of insoluble fibrillar matrix. Figure from [183].

Based on our proteomic results and further bioinformatics analysis of the FLEUR network presented in figure 3.11 it is possible to further uncover a potential Fibronectin-regulating mechanism during infection. The proteins present in the FLEUR network represent proteins interacting both directly and indirectly with fibronectin in many possible ways (protein-protein interactions, activation, inhibition, transcription, phosphorylation, expression, localization, etc,

etc). By filtering only those proteins that act on fibronectin for inhibition, localization, expression and activation we obtained a much shorter list of only 6 proteins significantly modulated during infection at the 6h time point. This is presented in figure 5.3. The interaction of each of those six proteins with fibronectin is summarized in table 5.1 and briefly discussed below.

Figure 5.3 - Fibronectin regulation

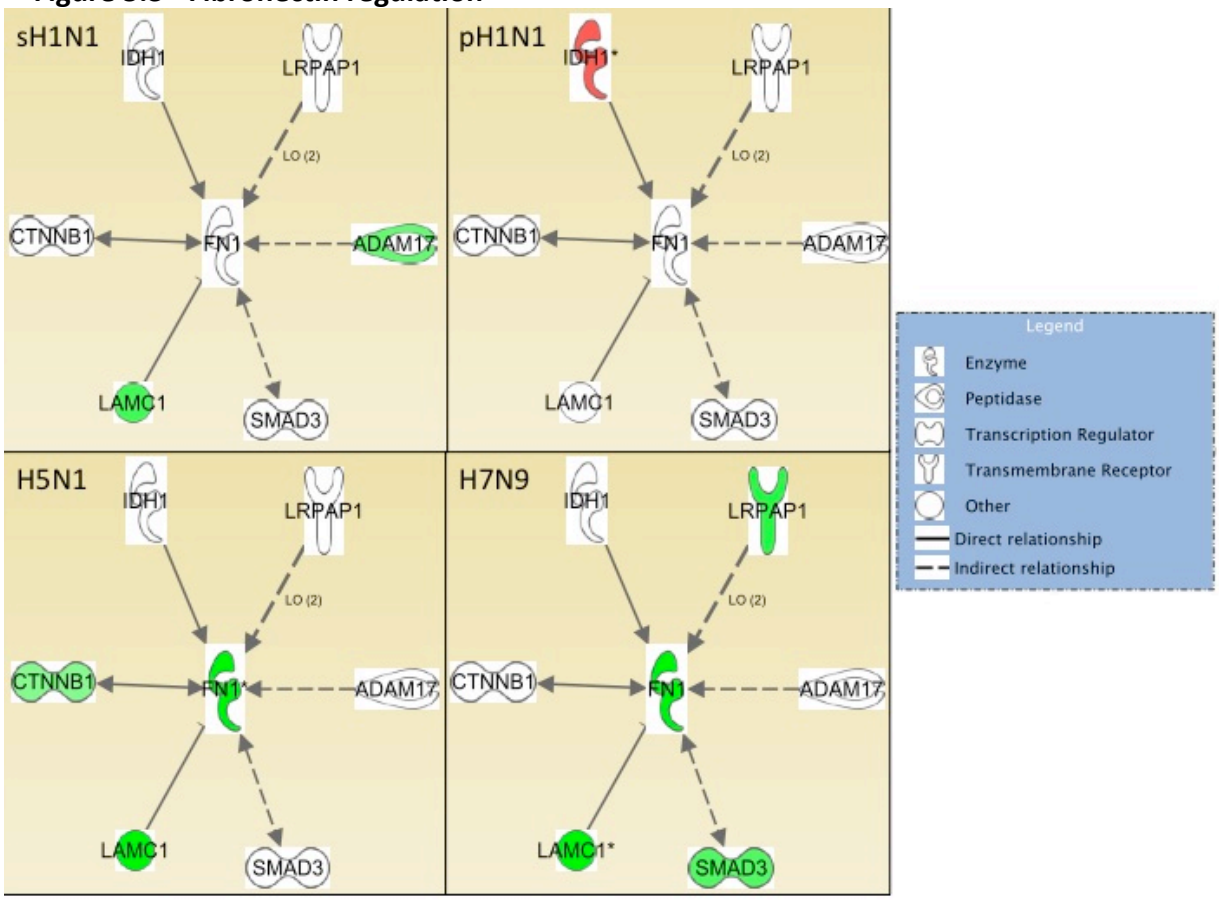

Significantly-modulated host proteins that either activate, inhibit, enhance expression or play a role in the localization of fibronectin are represented for each of the 6h post infection datasets. Red indicates up-regulation while green indicate down-regulation. A pointed arrow indicates activation while a bar indicates inhibition.

Table 5.1 - Proteins involved in the regulation of fibronectin

Gene ID	Protein Name	Interaction with Fibronectin (Fn1) *(recovered and adapted from the IPA database)*	Reference
LRPAP1	Low density lipoprotein Receptor-related Protein Associated Protein 1	LRPAP1 protein increases accumulation of mouse Fibronectin protein LRPAP1 protein increases localization of human Fibronectin protein to culture supernatant	[186] [187]
ADAM17	A Disintegrin And Metallopeptidase domain 17	Interference of mouse Tace [Adam17] mRNA by siRNA decreases expression of mouse Fibronectin mRNA	[188]
SMAD3	SMAD family member 3	Interference of human SMAD3 mRNA by siRNA prevents production of human Fn1 mRNA	[191]
LAMC1	Laminin-111	Mouse Laminin-111 [Laminin] complex(es) decreases expression of mouse Fn1 protein	[195]
CTNNB1	Beta-catenin	Human Beta-Catenin [CTNNB1] protein increases expression of human Fibronectin protein	[197]
IDH1	Isocitrate Dehydrogenase 1	Mutant human IDH1 protein (p.R132H) increases expression of Fn1 mRNA	[200]

LRPAP1

Two studies [186], [187] have described the role of LRPAP1 in the context of Fibronectin regulation, LRPAP1, sometimes referred simply as Receptor-associate protein or RAP, is a potent ligand of the Low Density Lipoprotein-Receptor-Related Protein (LRP). LRP has been shown to bind Fibronectin and inhibit its accumulation at the cell surface. LRPAP1 can outcompete FN1 binding on LRP, thereby increasing FN1 amounts at the cell surface and into the supernatant. To our knowledge, ours is the first study to measure LRPAP1 levels during influenza (or any viral) infections.

ADAM17

In a study of fibrosis in the context of heart hypertrophy and hypertension, Wang et al [188] found that siRNA targeted to ADAM17 - also known as Tumor necrosis factor alpha converting enzyme (TACE) – could inhibit the synthesis of fibronectin mRNA. In their experiments, they induced cardiac hypertrophy and fibrosis by treating rats with angiotensin II and then measured mRNA transcripts of fibrosis-related genes including FN1. They found that silencing ADAM17 inhibited the synthesis of FN1 mRNA both with and without angiotensin treatment, indicating that ADAM17 potentially regulates FN1 gene expression. The only studies linking ADAM17 and influenza [189], [190] indicate that it plays a role in processing TNF-a in CD8+ T cells and contributes to increased lung injury during infection.

SMAD3

Smads are part of the transforming growth factor beta-2 (TGF-B2) signaling pathway. The link between SMAD3 and FN1 has been studied in the context of ocular pathologies in a human lens cell line. In their study, Li et al [191] found that silencing SMAD3 inhibited the production of fibronectin. Interestingly, in a recent study another group found that during HPAI H5N1 infection SMAD3 was activated and increased TGF-B1 production, ultimately improving survival rates of infected mice [192]. More closely related to FN1 and its important role in the ECM, a study by Jolly et al [193] found that TGF-B activity increased cell death and lung damage and collagen deposition in PR8-infected mice and that this response was attenuated in SMAD3 knock-out mice. Finally, in a lung fibrosis model in mice, Ashley et al. [194] showed that H1N1-infected animals were able to clear the infection whereas animals infected by a herpes virus

were not. They linked phosphorylated SMAD3 to increased lung fibrosis.

LAMC1

In a study on embryonic development in mice, Fujiwara et al [195] found that embryoid bodies (EB) of LAMC1-/- mice had more deposition of FN1 at their basal membranes compared to those of LAMC1+/- EBs, suggesting that, in the absence of LAMC1, fibronectin will accumulate at the basal membrane and therefore that LAMC1 has an inhibitory effect on FN1. This is apparently important in the field of development, yet not studies have, thus far, linked LAMC1 and Fibronectin in the context of influenza infection although a systems biology study on Newcastle disease virus (NDV - a paramyxovirus) has identified it as being differently expressed at the mRNA level in NDV-infected chicken [196].

CTNNB1

Beta-catenin (CTNNB1) has been identified as able to restore fibronectin expression and de novo synthesis even when up-stream mediator in the beta-catenin/LEF-1 signaling pathway (a pathway responsible for FN1 gene expression) are absent or blocked [197]. Beta-catenin has been shown to be an anti-viral mediator, able to inhibit viral replication by triggering the expression of interferon-stimulated genes (ISGs). At the same time, influenza viruses are able to block its action by modulating the RIG-I/NFkB signaling cascade [198]. That study was done in A549 cells and compared the PR8 strain with a LPAI H7N7 strain. No major differences were found between those two viruses. Similarly, a study using PR8 and infection in umbilical cord vein and focusing on vascular permeability found a significant decrease of beta-catenin during

infection that correlated with increased vascular permeability [199]. It is unclear how/if this could be linked to fibronectin, but lower beta-catenin (which we have observed in H5N1-infected cells) may also mean less fibronectin which would contribute to the disruption of the ECM and may play a role in vascular permeability.

IDH1

Isocitrate dehydrogenases play an important role in cancer biology, with mutations in those genes potentially leading to cancer phenotypes. In their study, Grassian et al [200] identified mutations in the IDH1 gene that could increase the expression of fibronectin although the WT gene by itself did not. This would potentially be an interesting human genetic marker to study in the context of influenza infections yet we have not found any literature connecting IDH1 and influenza.

In all cases no clear regulatory mechanism has been described linking fibronectin expression, those regulatory proteins identified in our study and infection with low and high virulence strains of influenza. From a pandemic preparedness perspective, the discovery of a specific FN1-modulation mechanism would have immense importance. Not only could it be harnessed to develop novel therapies to combat human strains; it could also potentially be used as a marker to monitor avian-to-human adaptation of novel strains and give advance warning about their potential for causing pandemics.

5.2 Growth properties of low pathogenicity human and low and highly pathogenic avian influenza viruses

Wild waterfowls are considered to be the main reservoir for IAV, harboring all of the 16 HA and 9 NA subtypes [10][11]. Comparatively, humans can be considered accidental hosts of IAV as only a handful of subtypes have been able to gain a foothold and establish themselves in the population. Seasonal human strains of H1N1, H3N2 and H2N2 subtypes have circulated since the pandemic of 1918 [63]. Only a few HPAI strains (subtypes H5N1, H7N7 and H7N3) and LPAI strains (subtypes H9N2, H7N2, H7N3, H7N7, H10N7 and H7N9) have thus far crossed the species barrier and infected humans [11]. Importantly, most human infections avian strains causes only a mild if undetectable disease similar to seasonal influenza and human infection by avian strains cannot be transmitted efficient, if at all, so that humans are dead end hosts for these avian viruses. However, HPAI H5N1 and the recent LPAI H7N9 strains cause diseases with very high mortality rate and acute symptoms [11]. There is concern that continued infections in humans could lead to a novel pandemic strain, whether by further adaptation or reassortment with viruses that are competent for human-to-human transmission. Many factors need to be taken into account to explain the different degree of virulence of influenza strains. Host immunity and genetics, routes and doses of infection, viral tropism, replicative capacities of strains all combine to create either a mild or a lethal infection. *In vitro* studies offer an isolated system where strain-specific differences in virus replication kinetics and associated, intracellular host processes can be studied independently of host factors such as immunity, genetics, infection route and doses.

By using a simple mathematical model of *in vitro* infection, we have been able to highlight key differences in the replication parameters of mild seasonal and pandemic H1N1 strains compared to H5N1 and H7N9 avian strains that cause significant mortality in humans. Compared to the sH1N1 strain, the pH1N1 had a significantly longer eclipse phase while compared to the pH1N1 strain the H5N1 and H7N9 strains had significantly shorter eclipse phases. In earlier work, we found that the length of the eclipse phase was a good indicator of the efficiency of virus release and/or the efficiency of the neuraminidase activity of the strain [139], [143]. Our results could indicate that, in A549 infections, the virion progeny of the sH1N1, H5N1 and H7N9 strains are released more easily from the producing cell than that of the pH1N1 strain, potentially pointing to higher neuraminidase activity and/or lower hemagglutinin receptor affinity. Another important aspect of infection is that the H5N1 and the H7N9 strains had significantly shorter infecting times then the two other strains. This is a measure of how long it takes for virions from infected cells to cause infection in new, non-infected cells. It is a good indicator of the overall capacity of a strain to cause infection. This enhanced infection capacity by the H5N1 and the H7N9 strains can be further attributed to a different mechanism for each virus. The H5N1 exhibited a higher production rate, that is, per infection it produced more infectious progeny faster than the three other strains. Conversely, the H7N9 strain exhibited enhanced infection rates compared to the sH1N1 and pH1N1 strains, meaning that it had a greater ability to infect new cells. When looking at the experimental growth kinetics of figure 4.1, one clearly sees that the H5N1 and H7N9 seem to have a replicative advantage over the H1N1 strains. However, the more detailed differences in replication parameters are impossible to understand without further detailing the replication

cycle. Using a mathematical model is an excellent way to achieve this, especially for later events that cannot be dissociated from the first steps of infection.

Overall, our study indicates that the higher growth kinetics of the H5N1 and H7N9 strains, respectively a HPAI and a LPAI strain, differ in specific definable parameters of their replicative ability compared not only to the 2009 and seasonal H1N1 human viruses, but also between each other. Based on our model of infection, the H7N9 virus would more readily infect cells while the H5N1 strain would generate more progeny. A549 cells have been shown to express both α(2,3) and α(2,6)-linked sialic acids on their surface glycoproteins [201] so the explanation to this disparity is probably more complex than a simple question of affinity based on differential receptor binding properties between the viruses. The Anhui/1/13 H7N9 strain has a mixed affinity for α(2,3) and α(2,6)- linked sialic acid (SA) [76] while the Indonesia/5/05 H5N1 strain has a more restrictive affinity for the α(2,3) SA species yet both readily infect A549 cells. Our finding that the eclipse phase of the pH1N1 strain was longer correlates well with the independent finding that it expresses its Non-Structural 1 (NS1) protein the latest (at 6h post-infection instead of 3h) compared to the three other strains (see Chapter 3). This protein is not carried by the virions and is expressed early during infection [148], [202]. Interestingly, the proteomic study of Chapter 3 measuring the host response of the same four virus strains in A549 cells showed that on a global level the H5N1 strain induced the most profound changes to the cellular proteome and affected the greatest number of metabolic pathways. Both the sH1N1 and pH1N1 strains induced comparatively fewer changes in the host.

By combining basic virology with mathematical modeling, we have shown that the higher replication kinetics of high and medium pathogenicity H5N1 and H7N9 strains likely derives from two different mechanisms. The HPAI H5N1 strain showed an increased production rate while the H7N9 strain showed an increased infection rate. Of the two low pathogenic H1N1 strains, the pH1N1 strain had a longer eclipse phase while cells infected by the sH1N1 had a longer infecting time. Further study will provide understanding of the significance of these distinctions between viruses and their ability to cause a range of disease manifestations.

Chapter Six – Conclusion and Future Works

6.1 Conclusion

The work presented in this Thesis focused on studying the replication of strains of influenza of varying pathogenicity. It approached the problem by looking both at the intracellular host responses as well as by extensively characterizing differences in the growth kinetics of four strains. The strains studied in this work cause a continuum of diseases in human, from mild infections by the seasonal H1N1 and 2009 Pandemic H1N1 strains to severe infections with 20% lethality rates with the H7N9 LPAI strain and finally a representative strain of the H5N1 HPAI subtype causing up to 60% lethality in localized outbreaks since 1997. We used an immortalized human lung adenocarcinoma (A549) cell line as a simple and robust model of infection, offering a good compromise between technical feasibility and biological relevance. The use of *in vitro* models of infection has its limitations, yet it provides an environment where most of the complex variables affecting infection in an organism are either absent or controlled.

From a functional host response perspective, we have shown that infection by the H5N1 subtype induced the most changes to the host early during infection. To our knowledge, this is the first comparative proteomic study to systematically analyze and contrast the host response to low pathogenic H1N1, highly pathogenic H5N1 and to the novel H7N9 IAV strains. We used a simple and elegant labeling strategy that enabled us to directly compare 15 experimental conditions, including time-matched controls. Our results showed that infection by a highly pathogenic avian influenza H5N1 strain induced the most profound changes at the proteomic level in A549 human lung cells. While we must be careful to not over-interpret *in vitro* data

obtained by infection of an immortalized cell line, our results are in general agreement with other studies that have shown that strains of higher pathogenicity have the potential to significantly modulate the host response at a very basic cellular level [130][131]. Compared to *in vivo* infection, using a tightly controlled *in vitro* infection model allowed us to study the most fundamental effect of viral replication on cells without the confounding factors found in organism such as the complex interplay between infection, immunity and inflammation. This is the first report to identify the NRF2 pathway as being differentially modulated during infection by H5N1 and H7N9 strains compared to human mild H1N1 strains. Our results highlight that infection by highly pathogenic strains has the potential to modulated this important regulatory mechanism and could lead to increased organismal injuries sustained by uncontrolled oxidative stress. While previous studies focused on laboratory-adapted strains (such as PR8) and low pathogenicity H1N1 strains, we have expanded this research to highly virulent and pathogenic strains of influenza. We have also showed that infection by the H5N1 and H7N9 strains downregulated fibronectin, a protein described as being vital for infection with α(2,6)-tropic strains of IAV. Our results highlight that infection with each strain modulated different subsets of host proteins interacting with fibronectin, which suggests that FN1 inhibition by the H5N1 and H7N9 strains may offer an advantage in replication as those primarily avian strains would not need that protein for entry [162].

As mentioned previously, a limitation of systems biology studies is that the large amount of data generated can be daunting to interpret. Aside from the global dysregulation of H5N1-infected cells, we have focused our attention on two aspects we found to be of particular interest: fibronectin, mostly because of the complementarity and high relevance with the Leung

et al [162] as well as NRF2 and oxidative stress as these were the most significant pathways found by bioinformatics analysis. Combined with a peer-reviewed publication, our data will be uploaded to an open-source database and we hope that other groups with different interests and expertise will be able to mine it and uncover interesting findings worthy of further validation and research.

The modeling study enabled us to understand why the H7N9 and H5N1 strains had more efficient replication kinetics then the two H1N1 strains. As an interesting avenue for further thought and experimental exploration these data pose the question: Are these strain causing more dysregulation in the host because the replicate more efficiently or are they able to more efficiently deregulate the host machinery in order to achieve higher growth kinetics? Our results show that while the H5N1 and H7N9 had overall similar peak titres and replication rates, the H7N9 strain had an advantage in infection while the H5N1 strain had an advantage in production. At the same time, the pH1N1 strain had a longer eclipse phase and infected cells had low production rates. Overall, the modeling aspect enabled us to extend the reach and output of simple virological experiments and complements the host-response study in showing that the H5N1 and H7N9 possess intrinsically higher replication capacity than the two H1N1 strains.

To conclude, our results point to the concept that the more aggressive disease observed in patients infected with an H7N9 or H5N1 strain of influenza correlates well with enhanced *in vitro* replication kinetics as well as more profound host-responses fundamental cellular level.

6.2 Major findings

1. Infection with an H5N1 strain, although triggering fewer proteins to be significantly modulated than the H7N9 strain, induces the greatest changes to the host in terms of the functionality of the modulated proteins and their effect on a greater number of biological pathways as predicted by bioinformatics analysis.

2. The H5N1 and H7N9 viruses significantly reduce the amount of fibronectin present in A549 cells while this inhibitions seem lifted or partially lifted in cells infected by seasonal and 2009 pandemic H1N1 strains.

3. The H5N1 and H7N9 viruses both have more efficient replication kinetics in A549 cells although this is driven by different aspects of their respective replication cycles, with the H7N9 virus showing an advantage in infection while the H5N1 virus has an advantage in production.

4. The 2009 pandemic H1N1 virus strain induces few changes to the host proteome and while it has similar overall growth kinetics as a seasonal H1N1 isolate it suffers from a longer eclipse phase and lower infection capacity.

5. Infection by the H5N1 – and to a lesser extent by the H7N9 strain – has an effect on the nuclear accumulation of NRF2 and potentially affect its phosphorylation in the nucleus.

6.3 Future directions

The work presented in this thesis paves the way to several different research avenues. The four first ideas stem directly from the results of the research presented in this Thesis while the last two are more ambitious personal curiosities developed during my PhD.

1. Systems Biology. Massive advances have been made in next-gen sequencing in the last 5-10 years. This technology could be harnessed to complement the current proteomic screen and study the whole transcriptome of cells infected by arrays of strains causing a continuum of illness. Similarly, focused approaches such as Luminex technology could be used to detail the oxidative stress responses in infected cells, providing additional validation and confirmation of this important aspect of infection.

   As stated previously, a limitation of current proteomic studies is that only relatively abundant proteins can be measured by mass spectrometry. This results in total proteome coverage of about 30% with some bias against low abundance proteins. Transcriptomic studies can circumvent this limitation by amplifying virtually all the mRNA found in cells. A next step into the systems biology studies of the strains used in this thesis would be to infect A549 cells at the same MOI and harvest at the same time points and send the extracted mRNA for next gen sequencing. Extensive bioinformatics analysis would then be needed to correlate the changes found at the protein level with those at the transcript level. Because of the inherent deeper coverage of such an approach, several new genes of interest could be discovered and our overall finding of

deeper host response modulation during H5N1 infection could be further confirmed and studied.

2. FIbronectin inhibition and regulation as a mechanism of human adaptation. Ocriplasmin (sold as Jetrea) is a recombinant protease, approved by the FDA in 2012 as a drug that degrades fibronectin. It is primarily used to treat vitreomacular adhesion [203], [204] via intravitreal injections. As fibronectin appears to be important for infection with human strains of influenza, ocriplasmin should be rapidly tested *in vitro* and in animal models (mice or ferret) to see if it can afford protection against infection. The route of admission will need to be carefully evaluated, as the current intravitreal administration is poorly compatible with the infection route of influenza. However, one could envision using a nebulizer-type device to deliver the drug to the respiratory tract. This is route of admission is already used with Zanamivir (sold as Relenza). It would further have the potential benefit of reducing the amount of fibronectin present in the upper airways, thereby reducing the capacity of human IAVs to infect those cells.

From an evolutionary and cross-species adaptation perspective, a hypothesis generated by our results is that IAV, which are primarily hosted in aquatic birds do not require fibronectin for infection whereas those comparatively few strains that can infect humans do. A large-scale study comparing fibronectin requirements for different human and avian strains of various subtypes – including human H1N1 and H3N2 as well as avian H5N1, H7N9 and H7N7 – could help understand whether this could be used as a marker

for adaptation. Specifically, one could design an experiment where purely avian, mixed avian/human and purely human strains would be propagated in cells either expression or silenced for fibronectin. In cells silenced for fibronectin, one would expect the viruses of mixed tropism to exhibit intermediate growth capacities compared to the human strains (no replication) and avian strains (unaffected replication). Another approach to this question would be to artificially adapt several different HPAI strains isolated at passage zero in birds by serially passaging them in cells overexpression α(2,6) sialic acids [205]. Each passage could be aliquoted and subjected to next-generation sequencing as well as assessing the *in vitro* growth in cells expression or silenced for fibronectin. Beyond the very well described α(2,6)/α(2,3) modulating mutations in HA, this could reveal novel viral genes involved in host adaptation.

Combating and curing diseases is the ultimate goal of biomedical research and repurposing an approved drug to target host factors important to viral infection would be a highly practical and applied research avenue. From an epidemiology perspective, a better understanding of potential mechanisms driving fibronectin inhibition or expression by infection could provide public health agencies with important markers of cross-species adaptation of avian strains.

3. Involvement of NRF2 in influenza infections. Another obvious research avenue stemming from the results presented in this thesis revolves around the role of NRF2 during infection. The doublet consistently observed in nuclear fractions of infected cells

is highly similar to the doublet described as being the phosphorylated and non-phosphorylated forms of NRF2 and is consistent with our current knowledge of NRF2. An initial step would be to enrich and deplete phosphoproteins and probe the nuclear and cytoplasmic fractions with phospho-specific primary antibodies. Further steps would be to understand where this inhibition of the phosphor-NRF2 occurs. Is phosphorylation blocked in the cytoplasm – which would limit its nuclear import? Is it imported in the nucleus and then dephosphorylate? Is it simply not activated and actively inhibited in the early phases of infection? For all these steps, is there a specific viral protein responsible for this effect?

Understanding why and how the apparent dephosphorylation occurs in H5N1 and H7N9-infected cells could be a key finding to better understand the pathogenicity of those strains in human infections. Indeed, current research has identified NRF2 as a central player in oxidative stress response. Could strains causing severe disease in humans (such as the H5N1 and H7N9 studied here) have a mechanism to abrogate the host defenses to oxidative stress? An aberrant immune and inflammatory response has been linked to the increased severity of disease during infection by H5N1 strains. Increased cellular damage caused by un-checked oxidative stress (due to NRF2 inhibition) may play a significant role in triggering this response and could be targeted for new therapeutics avenues. Specifically, which viral protein(s) is responsible and can it be blocked, thereby restoring a measure of survivability to the host?

4. Modeling of infection in knock-down cell lines. A key question surrounding every high-throughput screening method is “is this gene important in the replication of the virus” and “which part of the cycle does it affect”. These questions can be addressed by gene knock-down experiments. After generating a stable knock-down cell line, all that would be needed to implement the mathematical model used in this thesis is several hours of repetitive but simple laboratory work using well-established tools and techniques such as TCID50 measurement and quantitative PCR. This in turn could provide important information as to which steps of the viral life cycle is impacted by interesting genes, potentially solving the conundrum presented in the conclusion of this thesis. Specifically, what comes first: host response modulation or higher replicative capacities?

   This approach could be used to better understand at which step of the viral replication is a gene of interest acting. In this work, we have compared the growth of several strains in a single cell line. The corresponding experiment can be made with any number of cell lines and strains. A series of stable knock down cells for genes of interest could be generated and all the cells infected at low and high MOIs with a single (or multiple, depending on how many summer students are available) IAV strains. The growth kinetic experiments described in this thesis could then be repeated and the role of each genes in the viral life cycle could then be pin-pointed to discreet steps of infection. Compared to other approaches, this builds on techniques already extensively used in our laboratory and would not require any new expertise while delivering exciting new data and further strengthening our inter-disciplinary collaboration.

5. Host protein incorporation in influenza virions. As mentioned in the introduction of this Thesis, viruses have the ability to incorporate host proteins in a seemingly specific way and with the retention of some of their biological activities. A few studies have detailed this for influenza viruses, but all used either mild seasonal isolates or highly lab adapted strains. Both the Shaw [20] and LeBouder [22] studies used the lab-adapted WSN H1N1 strain. Berri et al. also used the WSN strain as well as another lab-adapted strain (PR8) and a human H3N2 isolate [21]. Hutchinston et al. [23] used PR8 (both WT and several recombinant viruses), WSN and an influenza B strain. These are all either highly adapted laboratory or low pathogenicity strains and to our knowledge no one has used highly virulent strains such as those studied here. Therefore, a major question still remaining to be solved is: Are there differences in host protein incorporation between low and high virulence strains of IAV? Both the LeBouer and Berri study have shown the role of Annexin in promoting infection, either by inhibiting interferon response or by converting plasminogen to plasmin. But again, this has not been studied in the context of highly pathogenic viruses.

   A major challenge of those projects is obtaining extremely pure virus preparations. The four studies mentioned above used ultracentrifugation on sucrose gradients, which, while a good start, could potentially be improved by using FPLC chromatographic separation [206] of the sucrose gradient-purified virions. Either using this ultrapure viral preparation or relying on the well-established sucrose gradient approach, modern mass

spectrometry-based proteomics can readily identify and quantitate virtually all proteins present in the virions. Similar to what has been done in this thesis, stocks of various strains representing a continuum of pathogenicity could be cultured, concentrated and extensively purified prior to being digested and labeled with iTRAQ. This quantitative host-protein incorporation study would then not only provide information on the identity, but also relative abundance of host proteins incorporated in those different strains. Understanding whether strains of low and high pathogenicity contain the same complement of host proteins (both in terms of identity and abundance) or whether this is yet another important difference that could be linked to the pathogenesis would be a fascinating research program. The FPLC separation technique developed to achieve ultrapure stocks could also be used towards aim 6.

6. Is influenza a multipartite virus? Fascinating and poorly accepted research suggests that influenza viruses could in fact be a multipartite virus [19]. That is, co-infection of cells by virions with incomplete complements of the 8 genome segments could cause productive infections because the virions could supplement each other for the missing gene segments. The phenomenon of multipartite viruses is for now only described in plant viruses (e.g. [207]), yet devising a research program to study the composition of influenza (sub)virions using the tools of the 21st century would be highly interesting from a fundamental virology perspective. Specifically, linking physical virions, infectious particles and genomic and proteomic content in such a way that individual viruses are represented (as opposed to averaged in mixed population) could potentially

revolutionize our understanding of viruses. Like in the previous “future work” item, a major challenge would be to extensively purify sufficient quantities influenza (sub)virions to then evaluate their protein composition (by mass spectrometry) as well as their genomic content (by next generation sequencing and/or quantitative PCR). Although this is a daunting task, I see two potential (an potentially complementary) approaches to the purification issue.

First, using preparative ultracentrifugation, with very long run times (12-24h) at very high speeds (around 100,000 x g) combined with a continuous gradient where fractions would be harvested sequentially, thereby allowing (sub)virion differing by only a few Siemens to be separated. This could also be combined with FPLC separation [206] where chromatographic fractions would be eluted in non-denaturing buffer conditions and harvested sequentially. This would generate a number of fractions representing particles of increasing density (ultracentrifugation) or chromatographic migration speed (FPLC). Each of those fractions could then be probed for infectivity (plaque assay, TCID50), genomic content (next-gen sequencing), proteomic content (iTRAQ and LC-MS/MS) and morphology (Electron microscopy). Concurrently, this could also be addressed by reverse genetics. Complementation experiments where transfection of each individual segments could be studied to see which combinations are required to re-create a lytic infection, potentially using VLP intermediates.

If the multipartite hypothesis is correct, then one would expect to find a continuum of particles containing incomplete genomes and differential sets of both viral and host proteins (see previous aim). Furthermore, combinations of those highly purified sub particles could be used to understand what are the ideal ratios to generate typical infections in relevant animal models (ferrets) and *in vitro*. A common theme of interest is whether key differences exist between strains of low and high pathogenicity and this approach would readily unveil such differences as radically alter our fundamental understanding of virus biology.

Chapter Seven – References

[1] C. Morgan, K. C. Hsu, R. A. Rifkind, A. W. Knox, and H. M. Rose, "The Application of Ferritin-Conjugated Antibody to Electron Microscopic Studies of Influenza Virus in Infeccted cells: 1. the Cellular Surface.," *J. Exp. Med.*, vol. 114, no. 5, pp. 825–832, 1961.

[2] M. L. Shaw and P. Palese, "Orthomyxoviridae," in *Fields Virology*, 6th ed., D. M. Knipe and P. M. Howley, Eds. Philadelphia: Lippincott Williams & Wilkins, 2013, pp. 1151–1185.

[3] D. Baltimore, "Expression of animal virus genomes.," *Bacteriol. Rev.*, vol. 35, no. 3, pp. 235–41, 1971.

[4] P. M. Wright, G. Neumann, and Y. Kawaoka, "Orthomyxoviruses," in *Fields Virology*, 6th ed., D. M. Knipe and P. M. Howley, Eds. Philadelphia: Lippincott Williams & Wilkins, 2013, pp. 1186–1243.

[5] Center for Disease Control and Prevention, "Types of Influenza Viruses," 2014. [Online]. Available: http://www.cdc.gov/flu/about/viruses/types.htm. [Accessed: 25-Jan-2015].

[6] P. C. Roberts, R. A. Lamb, and R. W. Compans, "The M1 and M2 proteins of influenza A virus are important determinants in filamentous particle formation.," *Virology*, vol. 240, no. 1, pp. 127–137, 1998.

[7] V. M. MOSLEY and R. W. G. WYCKOFF, "Electron Micrography of the Virus of Influenza," *Nature*, vol. 157, no. 3983. pp. 263–263, 1946.

[8] D. P. Nayak, R. A. Balogun, H. Yamada, Z. H. Zhou, and S. Barman, "Influenza virus morphogenesis and budding," *Virus Research*, vol. 143, no. 2. pp. 147–161, 2009.

[9] Y. Wu, Y. Wu, B. Tefsen, Y. Shi, and G. F. Gao, "Bat-derived influenza-like viruses H17N10 and H18N11," *Trends in Microbiology*, vol. 22, no. 4. pp. 183–191, 2014.

[10] S.-W. Yoon, R. J. Webby, and R. G. Webster, "Evolution and ecology of influenza A viruses.," *Curr. Top. Microbiol. Immunol.*, vol. 385, pp. 359–75, 2014.

[11] Y. Poovorawan, S. Pyungporn, S. Prachayangprecha, and J. Makkoch, "Global alert to avian influenza virus infection: from H5N1 to H7N9.," *Pathog. Glob. Health*, vol. 107, no. 5, pp. 217–23, 2013.

[12] K. Das, J. M. Aramini, L. C. Ma, R. Krug, and E. Arnold, "Structures of influenza A proteins and insights into antiviral drug targets.," *Nat Struc Mol Biol*, vol. 17, pp. 530–538, 2010.

[13] P. Gómez-Puertas, C. Albo, E. Pérez-Pastrana, A. Vivo, and A. Portela, "Influenza virus matrix protein is the major driving force in virus budding.," *J. Virol.*, vol. 74, no. 24, pp. 11538–11547, 2000.

[14] R. A. Lamb and P. W. Choppin, “Synthesis of influenza virus protein in infected cells : Translation of viral polypepties, including three P polypeptides, from RAN produced by primary transcription.,” *Virology*, vol. 74, pp. 504–519, 1976.

[15] S. C. Inglis, R. A. Lamb, A. R. Carroll, and B. W. J. Mahy, “Polypeptides specified by the influenza virus genome. I. Evidence for eight distinct gene products specified by fowl plaque virus. ,” *Virology*, no. 74, pp. 489–503, 1976.

[16] K. Apostolov and T. H. Flewett, “Internal structure of influenza virus,” *Virology*, vol. 26, pp. 506–508, 1965.

[17] K. G. Murti, W. J. Bean, and R. G. Webster, “Helical ribonucleoproteins of influenza virus: An electron microscope analysis.,” *Virology*, vol. 104, pp. 224–229, 1980.

[18] N.-A. M. Molinari, I. R. Ortega-Sanchez, M. L. Messonnier, W. W. Thompson, P. M. Wortley, E. Weintraub, and C. B. Bridges, “The annual impact of seasonal influenza in the US: measuring disease burden and costs,” *Vaccine*, vol. 25, no. 27. pp. 5086–5096, 2007.

[19] C. B. Brooke, W. L. Ince, J. Wrammert, R. Ahmed, P. C. Wilson, J. R. Bennink, and J. W. Yewdell, “Most influenza a virions fail to express at least one essential viral protein.,” *J. Virol.*, vol. 87, no. 6, pp. 3155–62, 2013.

[20] M. L. Shaw, K. L. Stone, C. M. Colangelo, E. E. Gulcicek, and P. Palese, “Cellular proteins in influenza virus particles.,” *PLoS Pathog.*, vol. 4, no. 6, p. e1000085, 2008.

[21] F. Berri, G. Haffar, V. B. Lê, A. Sadewasser, K. Paki, B. Lina, T. Wolff, and B. Riteau, “Annexin V incorporated into influenza virus particles inhibits gamma interferon signaling and promotes viral replication.,” *J. Virol.*, vol. 88, no. 19, pp. 11215–28, 2014.

[22] F. LeBouder, E. Morello, G. F. Rimmelzwaan, F. Bosse, C. Péchoux, B. Delmas, and B. Riteau, “Annexin II incorporated into influenza virus particles supports virus replication by converting plasminogen into plasmin.,” *J. Virol.*, vol. 82, no. 14, pp. 6820–6828, 2008.

[23] E. C. Hutchinson, P. D. Charles, S. S. Hester, B. Thomas, D. Trudgian, M. Martínez-Alonso, and E. Fodor, “Conserved and host-specific features of influenza virion architecture.,” *Nat. Commun.*, vol. 5, no. May, p. 4816, 2014.

[24] C. Stegen, Y. Yakova, D. Henaff, J. Nadjar, J. Duron, and R. Lippé, “Analysis of Virion-Incorporated Host Proteins Required for Herpes Simplex Virus Type 1 Infection through a RNA Interference Screen.,” *PLoS One*, vol. 8, no. 1, p. e53276, 2013.

[25] R. Lippé, “Deciphering novel host-herpesvirus interactions by virion proteomics.,” *Front. Microbiol.*, vol. 3, no. May, p. 181, 2012.

[26] S. Loret, G. Guay, and R. Lippé, “Comprehensive characterization of extracellular herpes simplex virus type 1 virions.,” *J. Virol.*, vol. 82, no. 17, pp. 8605–18, 2008.

[27] R. Cantin, S. Méthot, and M. J. Tremblay, “Plunder and stowaways: incorporation of cellular proteins by enveloped viruses.,” *J. Virol.*, vol. 79, no. 11, pp. 6577–87, 2005.

[28] T. Amet, M. Ghabril, N. Chalasani, D. Byrd, N. Hu, A. Grantham, Z. Liu, X. Qin, J. J. He, and Q. Yu, “CD59 incorporation protects hepatitis C virus against complement-mediated destruction.,” *Hepatology*, vol. 55, no. 2, pp. 354–63, 2012.

[29] Center for Disease Control and Prevention, “Images of Influenza Virus,” 2014. [Online]. Available: http://www.cdc.gov/flu/images/h1n1/3d_influenza_transparent_key_pieslice_180.gif. [Accessed: 25-Apr-2015].

[30] D. Kobasa, A. Takada, K. Shinya, M. Hatta, P. Halfmann, S. Theriault, H. Suzuki, H. Nishimura, K. Mitamura, N. Sugaya, T. Usui, T. Murata, Y. Maeda, S. Watanabe, M. Suresh, T. Suzuki, Y. Suzuki, H. Feldmann, and Y. Kawaoka, “Enhanced virulence of influenza A viruses with the haemagglutinin of the 1918 pandemic virus.,” *Nature*, vol. 431, no. 7009, pp. 703–707, 2004.

[31] R. Wagner, M. Matrosovich, and H. D. Klenk, “Functional balance between haemagglutinin and neuraminidase in influenza virus infections,” *Reviews in Medical Virology*, vol. 12, no. 3. pp. 159–166, 2002.

[32] I. A. Wilson, J. J. Skehel, and D. C. Wiley, “Structure of the haemagglutinin membrane glycoprotein of influenza virus at 3 A resolution.,” *Nature*, vol. 289, no. 5796, pp. 366–373, 1981.

[33] X. Xu, X. Zhu, R. A. Dwek, J. Stevens, and I. A. Wilson, “Structural characterization of the 1918 influenza virus H1N1 neuraminidase.,” *J. Virol.*, vol. 82, no. 21, pp. 10493–10501, 2008.

[34] D. A. Steinhauer, “Role of hemagglutinin cleavage for the pathogenicity of influenza virus,” *Virology*, vol. 258, no. 1. pp. 1–20, 1999.

[35] D. C. Wiley and J. J. Skehel, “Crystallization and x-ray diffraction studies on the haemagglutinin glycoprotein from the membrane of influenza virus.,” *J Mol Biol*, vol. 112, pp. 343–347, 1977.

[36] J. Chen, K. H. Lee, D. A. Steinhauer, D. J. Stevens, J. J. Skehel, and D. C. Wiley, “Structure of the hemagglutinin precursor cleavage site, a determinant of influenza pathogenicity and the origin of the labile conformation,” *CELL-CAMBRIDGE MA-*, vol. 95. pp. 409–416, 1998.

[37] E. Böttcher-Friebertshäuser, W. Garten, M. Matrosovich, and H. D. Klenk, “The Hemagglutinin: A Determinant of Pathogenicity,” in *Current topics in microbiology and immunology*, vol. 351, no. July, 2014, pp. 3–34.

[38] W. Garten and E. Friebertshäuser, “Proteases of the respiratory tract activating influenza viruses: Identification, characterization and cellular compartmentalization,” 2011. [Online]. Available: https://www.uni-marburg.de/sfb593/projects/projectb2/index_html/view?language_sync=1. [Accessed: 25-Apr-2015].

[39] S. B. Sato, K. Kawasaki, and S.-I. Ohnishi, “Heamolytic activity of influenza virus hemagglutinin glycoproteins activated in mildly acidic environments,” *Proc Natl Acad Sci USA*, vol. 80, pp. 3153–3157, 1983.

[40] J. White, K. Matlin, and A. Helenius, “Cell fusion by Semliki Forest, influenza, and vesicular stomatitis virus.,” *J Cell Biol*, vol. 89, pp. 674–679, 1981.

[41] T. O. Edinger, M. O. Pohl, and S. Stertz, “Entry of influenza A virus: Host factors and antiviral targets,” *Journal of General Virology*, vol. 95, no. PART 2. pp. 263–277, 2014.

[42] K. Shinya, M. Ebina, S. Yamada, M. Ono, N. Kasai, and Y. Kawaoka, “Avian flu: influenza virus receptors in the human airway.,” *Nature*, vol. 440, no. 7083, pp. 435–436, 2006.

[43] J. N. S. S. Couceiro, J. C. Paulson, and L. G. Baum, “Influenza virus strains selectively recognize sialyloligosaccharides on human respiratory epithelium; the role of the host cell in selection of hemagglutinin receptor specificity,” *Virus Res.*, vol. 29, no. 2, pp. 155–165, 1993.

[44] K. S. Matlin, H. Reggio, A. Helenius, and K. Simons, “Infectious entry pathway of influenza virus in a canine kidney cell line,” *J. Cell Biol.*, vol. 91, no. 3 I, pp. 601–613, 1981.

[45] S. B. Sieczkarski and G. R. Whittaker, “Influenza virus can enter and infect cells in the absence of clathrin-mediated endocytosis.,” *J. Virol.*, vol. 76, no. 20, pp. 10455–10464, 2002.

[46] E. de Vries, D. M. Tscherne, M. J. Wienholts, V. Cobos-Jiménez, F. Scholte, A. García-Sastre, P. J. M. Rottier, and C. A. M. de Haan, “Dissection of the influenza a virus endocytic routes reveals macropinocytosis as an alternative entry pathway,” *PLoS Pathog.*, vol. 7, no. 3, p. e1001329, 2011.

[47] J. A. Gruenke, R. T. Armstrong, W. W. Newcomb, J. C. Brown, and J. M. White, “New insights into the spring-loaded conformational change of influenza virus hemagglutinin,” *J Virol*, vol. 76, no. 9, pp. 4456–4466, 2002.

[48] R. E. O’Neill, R. Jaskunas, G. Blobel, P. Palese, and J. Moroianu, “Nuclear import of influenza virus RNA can be mediated by viral nucleoprotein and transport factors required for protein import,” *J. Biol. Chem.*, vol. 270, no. 39, pp. 22701–22704, 1995.

[49] J. F. Cros and P. Palese, “Trafficking of viral genomic RNA into and out of the nucleus: Influenza, Thogoto and Borna disease viruses,” *Virus Research*, vol. 95, no. 1–2. pp. 3–12, 2003.

[50] G. Neumann, G. G. Brownlee, E. Fodor, and Y. Kawaoka, “Orthomyxovirus replication, transcription, and polyadenylation.,” *Curr. Top. Microbiol. Immunol.*, vol. 283, pp. 121–143, 2004.

[51] R. Sanjuán, M. R. Nebot, N. Chirico, L. M. Mansky, and R. Belshaw, “Viral mutation rates.,” *J. Virol.*, vol. 84, no. 19, pp. 9733–9748, 2010.

[52] J. Steel and A. Lowen, “Influenza A Virus Reassortment,” *Curr. Top. Microbiol. Immunol.*, vol. 351, no. July, pp. 139–157, 2014.

[53] R. A. Medina and A. García-Sastre, “Influenza A viruses: new research developments.,” *Nat. Rev. Microbiol.*, vol. 9, no. 8, pp. 590–603, 2011.

[54] S. Broor, A. Krishnan, D. S. Roy, S. Dhakad, S. Kaushik, M. A. Mir, Y. Singh, A. Moen, M. Chadha, A. C. Mishra, and R. B. Lal, “Dynamic patterns of circulating seasonal and pandemic A(H1N1)pdm09 influenza viruses from 2007-2010 in and around Delhi, India,” *PLoS One*, vol. 7, no. 1, 2012.

[55] C. C. Blyth, A. Kelso, K. A. McPhie, V. M. Ratnamohan, M. Catton, J. D. Druce, D. W. Smith, S. H. Williams, Q. S. Huang, L. Lopez, B. D. Schoub, M. Venter, and D. E. Dwyer, “The impact of the pandemic influenza a(H1N1) 2009 virus on seasonal influenza a viruses in the southern hemisphere, 2009,” *Eurosurveillance*, vol. 15, no. 31, 2010.

[56] A. Nicoll, “A new decade, a new seasonal influenza: The Council of the European Union Recommendation on seasonal influenza vaccination,” *Eurosurveillance*, vol. 15, no. 1, pp. 1–2, 2010.

[57] K. G. Nicholson, J. M. Wood, and M. Zambon, “Influenza,” in *Lancet*, 2003, vol. 362, no. 9397, pp. 1733–1745.

[58] W. W. Thompson, M. R. Moore, E. Weintraub, P.-Y. Cheng, X. Jin, C. B. Bridges, J. S. Bresee, and D. K. Shay, “Estimating influenza-associated deaths in the United States.,” *Am. J. Public Health*, vol. 99 Suppl 2, pp. S225–30, 2009.

[59] C. W. Potter, “A history of influenza,” *Journal of applied microbiology*, vol. 91, no. 4. pp. 572–579, 2001.

[60] M. R. Hilleman, “Realities and enigmas of human viral influenza: pathogenesis, epidemiology and control,” *Vaccine*, vol. 20, no. 25–26. pp. 3068–3087, 2002.

[61] J. K. Taubenberger and D. M. Morens, “Influenza: the once and future pandemic,” *Public health reports (Washington, DC : 1974)*, vol. 125 Suppl . pp. 16–26, 2010.

[62] F. S. Dawood, A. D. Iuliano, C. Reed, M. I. Meltzer, D. K. Shay, P. Y. Cheng, D. Bandaranayake, R. F. Breiman, W. A. Brooks, P. Buchy, D. R. Feikin, K. B. Fowler, A. Gordon, N. T. Hien, P. Horby, Q. S. Huang, M. A. Katz, A. Krishnan, R. Lal, J. M. Montgomery, K. Mølbak, R. Pebody, A. M. Presanis, H. Razuri, A. Steens, Y. O. Tinoco, J. Wallinga, H. Yu, S. Vong, J. Bresee, and M. A. Widdowson, “Estimated global mortality associated with the first 12 months of 2009 pandemic influenza A H1N1 virus circulation: A modelling study,” *Lancet Infect. Dis.*, vol. 12, no. 9, pp. 687–695, 2012.

[63] D. M. Morens, J. K. Taubenberger, and A. S. Fauci, “The persistent legacy of the 1918 influenza virus.,” *N. Engl. J. Med.*, vol. 361, no. 3, pp. 225–9, 2009.

[64] S. Tong, X. Zhu, Y. Li, M. Shi, J. Zhang, M. Bourgeois, H. Yang, X. Chen, S. Recuenco, J. Gomez, L. M. Chen, A. Johnson, Y. Tao, C. Dreyfus, W. Yu, R. McBride, P. J. Carney, A. T. Gilbert, J. Chang, Z. Guo, C. T. Davis, J. C. Paulson, J. Stevens, C. E. Rupprecht, E. C. Holmes, I. A. Wilson, and R. O. Donis, “New World Bats Harbor Diverse Influenza A Viruses,” *PLoS Pathog.*, vol. 9, no. 10, 2013.

[65] World Organisation for Animal Health, “Avian influenza,” *OIE Terr. Man.*, vol. 28, no. 1, pp. 9–13, 2009.

[66] Food and Agriculture Organization of the United Nations, “Epidemiology of Avian Influenza,” 2015. [Online]. Available: http://www.fao.org/avianflu/en/clinical.html. [Accessed: 30-May-2015].

[67] M. Du Ry van Beest Holle, A. Meijer, M. Koopmans, and C. M. de Jager, “Human-to-human transmission of avian influenza A/H7N7, The Netherlands, 2003.,” *Euro Surveill. Bull. Eur. sur les Mal. Transm. = Eur. Commun. Dis. Bull.*, vol. 10, no. 12, pp. 264–268, 2005.

[68] S. A. Tweed, D. M. Skowronski, S. T. David, A. Larder, M. Petric, W. Lees, Y. Li, J. Katz, M. Krajden, R. Tellier, C. Halpert, M. Hirst, C. Astell, D. Lawrence, and A. Mak, “Human illness from avian influenza H7N3, British Columbia,” *Emerg. Infect. Dis.*, vol. 10, no. 12, pp. 2196–2199, 2004.

[69] Center for Disease Control and Prevention, “Highly Pathogenic Avian Influenza A (H5N1) in People | Avian Influenza (Flu),” 2014. [Online]. Available: http://www.cdc.gov/flu/avianflu/h5n1-people.htm. [Accessed: 26-Jan-2015].

[70] Center for Disease Control and Prevention, *Isolation of avian influenza A(H5N1) viruses from humans--Hong Kong, May-December 1997.*, vol. 46, no. 50. 1997, pp. 1204–1207.

[71] World Health Organization, “Cumulative number of confirmed human cases for avian influenza A(H5N1) reported to WHO, 2003-2015,” 2015. [Online]. Available: http://www.who.int/influenza/human_animal_interface/EN_GIP_20150106CumulativeNumberH5N1cases_corrected.pdf?ua=1.

[72] Canadian Broadcasting Corporation, “H5N1 bird flu death confirmed in Alberta, 1st in North America - Politics - CBC News,” 2014. [Online]. Available: http://www.cbc.ca/news/politics/h5n1-bird-flu-death-confirmed-in-alberta-1st-in-north-america-1.2489160. [Accessed: 24-Feb-2015].

[73] FluTrackers, “China - Hong Kong closely monitors 4 additional human cases of H7N9 in Mainland - 2 new cases in Guangdong - January 23, 2015,” 2015.

[74] World Health Organization, “WHO | Human infection with avian influenza A(H7N9) virus – Canada.” [Online]. Available: http://www.who.int/csr/don/01-february-2015-avian-influenza/en/. [Accessed: 05-Feb-2015].

[75] D. M. Morens, J. K. Taubenberger, and A. S. Fauci, “H7N9 avian influenza A virus and the perpetual challenge of potential human pandemicity,” *MBio*, vol. 4, no. 4, pp. 3–6, 2013.

[76] T. Watanabe, M. Kiso, S. Fukuyama, N. Nakajima, M. Imai, S. Yamada, S. Murakami, S. Yamayoshi, K. Iwatsuki-Horimoto, Y. Sakoda, E. Takashita, R. McBride, T. Noda, M. Hatta, H. Imai, D. Zhao, N. Kishida, M. Shirakura, R. P. de Vries, S. Shichinohe, M. Okamatsu, T. Tamura, Y. Tomita, N. Fujimoto, K. Goto, H. Katsura, E. Kawakami, I. Ishikawa, S. Watanabe, M. Ito, Y. Sakai-Tagawa, Y. Sugita, R. Uraki, R. Yamaji, A. J. Eisfeld, G. Zhong, S. Fan, J. Ping, E. a Maher, A. Hanson, Y. Uchida, T. Saito, M. Ozawa, G. Neumann, H. Kida, T. Odagiri, J. C. Paulson, H. Hasegawa, M. Tashiro, and

Y. Kawaoka, “Characterization of H7N9 influenza A viruses isolated from humans.,” *Nature*, vol. 501, no. 7468, pp. 551–5, 2013.

[77] World Health Organization, “2003_2013_AvianInfluenza,” 2014. [Online]. Available: http://gamapserver.who.int/mapLibrary/Files/Maps/2003_2013_AvianInfluenza_GlobalMap_24Jan14.png.

[78] “New England Journal of Medicine H7N9 Map,” 2015. [Online]. Available: http://www.healthmap.org/h7n9/. [Accessed: 25-Apr-2015].

[79] N. J. Cox and K. Subbarao, “Influenza,” *Lancet*, vol. 354, no. 9186, pp. 1277–1282, 1999.

[80] R. H. Alford, J. A. Kasel, P. J. Gerone, and V. Knight, “Human influenza resulting from aerosol inhalation.,” *Proc. Soc. Exp. Biol. Med.*, vol. 122, no. 3, pp. 800–804, 1966.

[81] R. Eccles, “Understanding the symptoms of the common cold and influenza,” *Lancet Infectious Diseases*, vol. 5, no. 11. pp. 718–725, 2005.

[82] K. K. W. To, I. F. N. Hung, I. W. S. Li, K.-L. Lee, C.-K. Koo, W.-W. Yan, R. Liu, K.-Y. Ho, K.-H. Chu, C.-L. Watt, W.-K. Luk, K.-Y. Lai, F.-L. Chow, T. Mok, T. Buckley, J. F. W. Chan, S. S. Y. Wong, B. Zheng, H. Chen, C. C. Y. Lau, H. Tse, V. C. C. Cheng, K.-H. Chan, and K.-Y. Yuen, “Delayed clearance of viral load and marked cytokine activation in severe cases of pandemic H1N1 2009 influenza virus infection.,” *Clin. Infect. Dis.*, vol. 50, no. 6, pp. 850–859, 2010.

[83] S. Esposito, C. Daleno, F. Baldanti, A. Scala, G. Campanini, F. Taroni, E. Fossali, C. Pelucchi, and N. Principi, “Viral shedding in children infected by pandemic A/H1N1/2009 influenza virus.,” *Virol. J.*, vol. 8, p. 349, 2011.

[84] R. W. Rüttimann, P. E. Bonvehí, D. Vilar-Compte, R. E. Isturiz, J. a Labarca, and E. I. Vidal, “Influenza among the elderly in the Americas: a consensus statement.,” *Rev. Panam. Salud Publica*, vol. 33, no. 6, pp. 446–52, 2013.

[85] M. McMillan, K. Porritt, D. Kralik, L. Costi, and H. Marshall, “Influenza vaccination during pregnancy: A systematic review of fetal death, spontaneous abortion, and congenital malformation safety outcomes.,” *Vaccine*. 2015.

[86] L. S. L. Kersun, A. F. A. Reilly, S. S. E. Coffin, and K. K. E. Sullivan, “Protecting pediatric oncology patients from influenza,” *Oncologist*, vol. 18, no. 2, pp. 204–11, 2013.

[87] M. H. Almond, D. F. McAuley, M. P. Wise, and M. J. D. Griffiths, “Influenza-related pneumonia,” *Clin. Med. J. R. Coll. Physicians London*, vol. 12, no. 1, pp. 67–70, 2012.

[88] C. M. MARTIN, C. M. KUNIN, L. S. GOTTLIEB, M. W. BARNES, C. LIU, and M. FINLAND, “Asian influenza A in Boston, 1957-1958. I. Observations in thirty-two influenza-associated fatal cases.,” *AMA. Arch. Intern. Med.*, vol. 103, no. 4, pp. 515–531, 1959.

[89] J. A. McCullers, “The co-pathogenesis of influenza viruses with bacteria in the lung.,” *Nat. Rev. Microbiol.*, vol. 12, no. 4, pp. 252–62, 2014.

[90] L. ROBERTSON, J. P. CALEY, and J. MOORE, “Importance of Staphylococcus aureus in pneumonia in the 1957 epidemic of influenza A.,” *Lancet*, vol. 2, no. 7040, pp. 233–6, 1958.

[91] J. F. Brundage and G. D. Shanks, “Deaths from bacterial pneumonia during 1918-19 influenza pandemic,” *Emerging Infectious Diseases*, vol. 14, no. 8. pp. 1193–1199, 2008.

[92] S. Sethi, “Bacterial pneumonia. Managing a deadly complication of influenza in older adults with comorbid disease.,” *Geriatrics*, vol. 57, no. 3, pp. 56–61, 2002.

[93] E. D. KILBOURNE, “Studies on influenza in the pandemic of 1957-1958. III. Isolation of influenza A (Asian strain) viruses from influenza patients with pulmonary complications; details of virus isolation and characterization of isolates, with quantitative comparison of isol,” *J. Clin. Invest.*, vol. 38, no. 1 Part 2, pp. 266–274, 1959.

[94] E. S. Hurwitz, D. B. Nelson, C. Davis, D. Morens, and L. B. Schonberger, “National surveillance for Reye syndrome: a five-year review.,” *Pediatrics*, vol. 70, no. 6, pp. 895–900, Dec. 1982.

[95] M. B. Rothberg and S. D. Haessler, “Complications of seasonal and pandemic influenza.,” *Crit. Care Med.*, vol. 38, no. 4 Suppl, pp. e91–e97, 2010.

[96] T. Vickers, “Influenza A virus subtype H5N1,” 2015. [Online]. Available: http://en.wikipedia.org/wiki/Influenza_A_virus_subtype_H5N1#/media/File:H1N1_versus_H5N1_pathology.png. [Accessed: 26-Apr-2015].

[97] C. Korteweg and J. Gu, “Pathology, molecular biology, and pathogenesis of avian influenza A (H5N1) infection in humans.,” *Am. J. Pathol.*, vol. 172, no. 5, pp. 1155–70, 2008.

[98] J. S. M. Peiris, W. C. Yu, C. W. Leung, C. Y. Cheung, W. F. Ng, J. M. Nicholls, T. K. Ng, K. H. Chan, S. T. Lai, W. L. Lim, K. Y. Yuen, and Y. Guan, “Re-emergence of fatal human influenza A subtype H5N1 disease,” *Lancet*, vol. 363, no. 9409, pp. 617–619, 2004.

[99] M. D. de Jong, C. P. Simmons, T. T. Thanh, V. M. Hien, G. J. D. Smith, T. N. B. Chau, D. M. Hoang, N. V. V. Chau, T. H. Khanh, V. C. Dong, P. T. Qui, B. Van Cam, D. Q. Ha, Y. Guan, J. S. M. Peiris, N. T. Chinh, T. T. Hien, and J. Farrar, “Fatal outcome of human influenza A (H5N1) is associated with high viral load and hypercytokinemia.,” *Nat. Med.*, vol. 12, no. 10, pp. 1203–7, 2006.

[100] M. Uiprasertkul, P. Puthavathana, K. Sangsiriwut, P. Pooruk, K. Srisook, M. Peiris, J. M. Nicholls, K. Chokephaibulkit, N. Vanprapar, and P. Auewarakul, “Influenza A H5N1 replication sites in humans.,” *Emerg. Infect. Dis.*, vol. 11, no. 7, pp. 1036–41, 2005.

[101] J. Gu, Z. Xie, Z. Gao, J. Liu, C. Korteweg, J. Ye, L. T. Lau, J. Lu, Z. Gao, B. Zhang, M. A. McNutt, M. Lu, V. M. Anderson, E. Gong, A. C. H. Yu, and W. I. Lipkin, “H5N1 infection of the respiratory tract and beyond: a molecular pathology study.,” *Lancet*, vol. 370, no. 9593, pp. 1137–45, 2007.

[102] M. D. de Jong, V. C. Bach, T. Q. Phan, M. H. Vo, T. T. Tran, B. H. Nguyen, M. Beld, T. P. Le, H. K. Truong, V. V. C. Nguyen, T. H. Tran, Q. H. Do, and J. Farrar, "Fatal avian influenza A (H5N1) in a child presenting with diarrhea followed by coma.," *N. Engl. J. Med.*, vol. 352, no. 7, pp. 686–91, 2005.

[103] J. S. M. Peiris, M. D. De Jong, and Y. Guan, "Avian Influenza Virus (H5N1): a Threat to Human Health," *Clinical Microbiology Reviews*, vol. 20, no. 2. pp. 243–267, 2007.

[104] M. D. Van Kerkhove, E. Mumford, A. W. Mounts, J. Bresee, S. Ly, C. B. Bridges, and J. Otte, "Highly pathogenic avian influenza (H5N1): pathways of exposure at the animal-human interface, a systematic review.," *PLoS One*, vol. 6, no. 1, p. e14582, 2011.

[105] S. Nasreen, S. U. Khan, S. P. Luby, E. S. Gurley, J. Abedin, R. U. Zaman, B. M. Sohel, M. Rahman, K. Hancock, M. Z. Levine, V. Veguilla, D. Wang, C. Holiday, E. Gillis, K. Sturm-Ramirez, J. S. Bresee, M. Rahman, T. M. Uyeki, J. M. Katz, and E. Azziz-Baumgartner, "Highly Pathogenic Avian Influenza A(H5N1) Virus Infection among Workers at Live Bird Markets, Bangladesh, 2009-2010.," *Emerg. Infect. Dis.*, vol. 21, no. 4, pp. 629–37, 2015.

[106] S. Vong, B. Coghlan, S. Mardy, D. Holl, H. Seng, S. Ly, M. J. Miller, P. Buchy, Y. Froehlich, J. B. Dufourcq, T. M. Uyeki, W. Lim, and T. Sok, "Low frequency of poultry-to-human H5NI virus transmission, southern Cambodia, 2005.," *Emerg. Infect. Dis.*, vol. 12, no. 10, pp. 1542–7, 2006.

[107] T. C. Dung, P. N. Dinh, V. S. Nam, L. M. Tan, N. L. K. Hang, L. T. Thanh, and L. Q. Mai, "Seroprevalence survey of avian influenza A(H5N1) among live poultry market workers in northern Viet Nam, 2011.," *West. Pacific Surveill. response J. WPSAR*, vol. 5, no. 4, pp. 21–6, 2014

[108] S. P. Gygi, Y. Rochon, B. R. Franza, and R. Aebersold, "Correlation between protein and mRNA abundance in yeast.," *Mol. Cell. Biol.*, vol. 19, no. 3, pp. 1720–1730, 1999.

[109] K. Coombs, "Quantitative proteomics of complex mixtures.," *Expert Rev. Proteomics*, vol. 8, no. 5, pp. 659–77, 2011.

[110] X. Han, A. Aslanian, and J. R. Yates, "Mass spectrometry for proteomics," *Current Opinion in Chemical Biology*, vol. 12, no. 5. pp. 483–490, 2008.

[111] J. J. Thomson, *Rays of Positive Electricity and their application to chemical analysis.*, 1st ed. London: Longmans, Green and Co., 1913.

[112] M. Karas and F. Hillenkamp, "Laser desorption ionization of proteins with molecular masses exceeding 10,000 daltons.," *Anal. Chem.*, vol. 60, no. 20, pp. 2299–301, 1988.

[113] J. B. Fenn, M. Mann, C. K. Meng, S. F. Wong, and C. M. Whitehouse, "Electrospray ionization for mass spectrometry of large biomolecules.," *Science*, vol. 246, no. 4926, pp. 64–71, 1989.

[114] J. Clark, "THE MASS SPECTROMETER," 2015. [Online]. Available: http://www.chemguide.co.uk/analysis/masspec/howitworks.html#top. [Accessed: 25-Apr-2015].

[115] Lamond, “MS/MS Modes,” 2010. [Online]. Available: http://www.lamondlab.com/MSResource/images/lcms/ChroSpectra.jpg. [Accessed: 25-Apr-2015].

[116] J. S. Minden, “DIGE: past and future.,” *Methods Mol. Biol.*, vol. 854, pp. 3–8, 2012.

[117] M. Unlü, M. E. Morgan, and J. S. Minden, “Difference gel electrophoresis: a single gel method for detecting changes in protein extracts.,” *Electrophoresis*, vol. 18, no. 11, pp. 2071–2077, 1997.

[118] D. R. Stein, X. Hu, S. J. McCorrister, G. R. Westmacott, F. A. Plummer, T. B. Ball, and M. S. Carpenter, “High pH reversed-phase chromatography as a superior fractionation scheme compared to off-gel isoelectric focusing for complex proteome analysis.,” *Proteomics*, vol. 13, no. 20, pp. 2956–66, 2013.

[119] R. C. Dwivedi, V. Spicer, M. Harder, M. Antonovici, W. Ens, K. G. Standing, J. a Wilkins, and O. V Krokhin, “Practical implementation of 2D HPLC scheme with accurate peptide retention prediction in both dimensions for high-throughput bottom-up proteomics.,” *Anal. Chem.*, vol. 80, no. 18, pp. 7036–42, 2008.

[120] S. Wiese, K. A. Reidegeld, H. E. Meyer, and B. Warscheid, “Protein labeling by iTRAQ: a new tool for quantitative mass spectrometry in proteome research,” *Proteomics*, vol. 7, no. 3. pp. 340–350, 2007.

[121] S. P. Gygi, B. Rist, S. A. Gerber, F. Turecek, M. H. Gelb, and R. Aebersold, “Quantitative analysis of complex protein mixtures using isotope-coded affinity tags.,” *Nat. Biotechnol.*, vol. 17, no. 10, pp. 994–999, 1999.

[122] Applied Biosystems, “Applied Biosystems iTRAQ™ Reagents,” 2004. [Online]. Available: http://www3.appliedbiosystems.com/cms/groups/psm_marketing/documents/generaldocuments/cms_041463.pdf. [Accessed: 25-Apr-2015].

[123] R. Y. Tweedie-Cullen and M. Livingstone-Zatchej, “Quantitative analysis of protein expression using iTRAQ and mass spectrometry,” *Protocol Exchange*. 2008.

[124] C. Dapat, R. Saito, H. Suzuki, and T. Horigome, “Quantitative phosphoproteomic analysis of host responses in human lung epithelial (A549) cells during influenza virus infection,” *Virus Res.*, vol. 179, no. 1, pp. 53–63, 2014.

[125] X. Wu, H. Wang, L. Bai, Y. Yu, Z. Sun, Y. Yan, and J. Zhou, “Mitochondrial proteomic analysis of human host cells infected with H3N2 swine influenza virus,” *J. Proteomics*, vol. 91, pp. 136–150, 2013.

[126] X. Wu, S. Wang, Y. Yu, J. Zhang, Z. Sun, Y. Yan, and J. Zhou, “Subcellular proteomic analysis of human host cells infected with H3N2 swine influenza virus,” *Proteomics*, vol. 13, no. 22, pp. 3309–3326, 2013.

[127] C. Liu, A. Zhang, J. Guo, J. Yang, H. Zhou, H. Chen, and M. Jin, “Identification of human host proteins contributing to H5N1 influenza virus propagation by membrane proteomics,” *J. Proteome Res.*, vol. 11, no. 11, pp. 5396–5405, 2012.

[128] K. Coombs, A. Berard, W. Xu, O. Krokhin, X. Meng, J. P. Cortens, D. Kobasa, J. Wilkins, and E. G. Brown, “Quantitative proteomic analyses of influenza virus-infected cultured human lung cells.,” *J. Virol.*, vol. 84, no. 20, pp. 10888–906, 2010.

[129] V. D. Menachery, A. J. Eisfeld, A. Schäfer, L. Josset, A. C. Sims, S. Proll, S. Fan, C. Li, G. Neumann, S. C. Tilton, J. Chang, L. E. Gralinski, C. Long, R. Green, C. M. Williams, J. Weiss, M. M. Matzke, B.-J. Webb-Robertson, A. A. Schepmoes, A. K. Shukla, T. O. Metz, R. D. Smith, K. M. Waters, M. G. Katze, Y. Kawaoka, and R. S. Baric, “Pathogenic influenza viruses and coronaviruses utilize similar and contrasting approaches to control interferon-stimulated gene responses.,” *MBio*, vol. 5, no. 3, pp. e01174–14, 2014.

[130] C. Y. Cheung, E. Y. Chan, A. Krasnoselsky, D. Purdy, A. T. Navare, J. T. Bryan, C. K. L. Leung, K. P. Y. Hui, J. S. M. Peiris, and M. G. Katze, “H5N1 Virus Causes Significant Perturbations in Host Proteome Very Early in Influenza Virus-Infected Primary Human Monocyte-Derived Macrophages.,” *J. Infect. Dis.*, vol. 206, pp. 640–645, 2012.

[131] V. Wahl-Jensen, S. Kurz, F. Feldmann, L. K. Buehler, J. Kindrachuk, V. DeFilippis, J. da Silva Correia, K. Früh, J. H. Kuhn, D. R. Burton, and H. Feldmann, “Ebola virion attachment and entry into human macrophages profoundly effects early cellular gene expression.,” *PLoS Negl. Trop. Dis.*, vol. 5, no. 10, p. e1359, 2011.

[132] A. S. Perelson, “Modelling viral and immune system dynamics.,” *Nat. Rev. Immunol.*, vol. 2, no. 1, pp. 28–36, 2002.

[133] A. Chatterjee, J. Guedj, and A. S. Perelson, “Mathematical modelling of HCV infection: What can it teach us in the era of direct-acting antiviral agents?,” *Antivir. Ther.*, vol. 17, no. 6 PART B, pp. 1171–1182, 2012.

[134] A. S. Perelson, A. U. Neumann, M. Markowitz, J. M. Leonard, and D. D. Ho, “HIV-1 dynamics in vivo: virion clearance rate, infected cell life-span, and viral generation time.,” *Science*, vol. 271, no. 5255, pp. 1582–1586, 1996.

[135] J. M. Coffin, “HIV population dynamics in vivo: implications for genetic variation, pathogenesis, and therapy.,” *Science*, vol. 267, no. 5197, pp. 483–489, 1995.

[136] J. Mittler, P. Essunger, G. J. Yuen, N. Clendeninn, M. Markowitz, and A. S. Perelson, “Short-term measures of relative efficacy predict longer-term reductions in human immunodeficiency virus type 1 RNA levels following nelfinavir monotherapy,” *Antimicrob. Agents Chemother.*, vol. 45, no. 5, pp. 1438–1443, 2001.

[137] B. U. Mueller, S. L. Zeichner, V. A. Kuznetsov, M. Heath-Chiozzi, P. A. Pizzo, and D. S. Dimitrov, “Individual prognoses of long-term responses to antiretroviral treatment based on virological,

immunological and pharmacological parameters measured during the first week under therapy.," 1998.

[138] A. U. Neumann, N. P. Lam, H. Dahari, D. R. Gretch, T. E. Wiley, T. J. Layden, and A. S. Perelson, "Hepatitis C viral dynamics in vivo and the antiviral efficacy of interferon-alpha therapy.," *Science*, vol. 2, no. 282(5386), pp. 103-7, 1998

[139] B. P. Holder, P. Simon, L. E. Liao, Y. Abed, X. Bouhy, C. A. A. Beauchemin, and G. Boivin, "Assessing the In Vitro Fitness of an Oseltamivir-Resistant Seasonal A/H1N1 Influenza Strain Using a Mathematical Model.," *PLoS One*, vol. 6, no. 3, p. e14767, 2011.

[140] A. Moscona, "Global transmission of oseltamivir-resistant influenza," *The New England journal of medicine*, vol. 360, no. 10. pp. 953–956, 2009.

[141] V. Correia, H. R. de Andrade, L. A. Santos, A. Lackenby, and M. Zambon, "Antiviral drug profile of seasonal influenza viruses circulating in Portugal from 2004/2005 to 2008/2009 winter seasons," *Antiviral research*. 2010.

[142] A. Lackenby, C. I. Thompson, and J. Democratis, "The potential impact of neuraminidase inhibitor resistant influenza," *Current Opinion in Infectious Diseases*, vol. 21, no. 6. pp. 626–638, 2008.

[143] L. T. Pinilla, B. P. Holder, Y. Abed, G. Boivin, and C. a a Beauchemin, "The H275Y neuraminidase mutation of the pandemic A/H1N1 virus lengthens the eclipse phase and reduces viral output of infected cells, potentially compromising fitness in ferrets.," *J. Virol.*, 2012.

[144] J. K. Baillie and P. Digard, "Influenza - Time to Target the Host?," *N. Engl. J. Med.*, vol. 369, no. 2, pp. 191–193, 2013.

[145] I. N. Kandun, H. Wibisono, E. R. Sedyaningsih, Yusharmen, W. Hadisoedarsuno, W. Purba, H. Santoso, C. Septiawati, E. Tresnaningsih, B. Heriyanto, D. Yuwono, S. Harun, S. Soeroso, S. Giriputra, P. J. Blair, A. Jeremijenko, H. Kosasih, S. D. Putnam, G. Samaan, M. Silitonga, K. H. Chan, L. L. M. Poon, W. Lim, A. Klimov, S. Lindstrom, Y. Guan, R. Donis, J. Katz, N. Cox, M. Peiris, and T. M. Uyeki, "Three Indonesian clusters of H5N1 virus infection in 2005.," *N. Engl. J. Med.*, vol. 355, no. 21, pp. 2186–2194, 2006.

[146] M. Matrosovich, T. Matrosovich, W. Garten, and H.-D. Klenk, "New low-viscosity overlay medium for viral plaque assays," *Virol. J.*, vol. 3, p. 63, 2006.

[147] M. Carpenter, "SDS for protein lysate preparation - Personal Communication." Winnipeg, 2010.

[148] M. N. Rahim, M. Selman, P. J. Sauder, N. E. Forbes, W. Stecho, W. Xu, M. Lebar, E. G. Brown, and K. M. Coombs, "Generation and characterization of a new panel of broadly reactive anti-NS1 mAbs for detection of influenza A virus.," *J. Gen. Virol.*, vol. 94, no. Pt 3, pp. 593–605, 2013.

[149] J. R. Wiśniewski, A. Zougman, N. Nagaraj, and M. Mann, "Universal sample preparation method for proteome analysis.," *Nat. Methods*, vol. 6, no. 5, pp. 359–62, 2009.

[150] AB Sciex, “iTRAQ (R) Reagents - 4plex Application Kit - Protein Protocol.” AB Sciex, p. Foster City CA, 2010.

[151] B. C. Searle, “Scaffold: a bioinformatic tool for validating MS/MS-based proteomic studies.,” *Proteomics*, vol. 10, no. 6, pp. 1265–9, 010.

[152] A. L. Kroeker, P. Ezzati, K. M. Coombs, and A. J. Halayko, “Influenza A infection of primary human airway epithelial cells up-regulates proteins related to purine metabolism and ubiquitin-related signaling,” *J. Proteome Res.*, vol. 12, no. 7, pp. 3139–3151, 2013.

[153] A. L. Kroeker, P. Ezzati, A. J. Halayko, and K. M. Coombs, “Response of primary human airway epithelial cells to influenza infection: A quantitative proteomic study,” *J. Proteome Res.*, vol. 11, no. 8, pp. 4132–4146, 2012.

[154] C. Chen, K. Grennan, J. Badner, D. Zhang, E. Gershon, L. Jin, and C. Liu, “Removing batch effects in analysis of expression microarray data: an evaluation of six batch adjustment methods.,” *PLoS One*, vol. 6, no. 2, p. e17238, 2011.

[155] W. E. Johnson, C. Li, and A. Rabinovic, “Adjusting batch effects in microarray expression data using empirical Bayes methods,” *Biostatistics*, vol. 8, no. 1, pp. 118–127, 2007.

[156] Y. Benjamini and Y. Hochberg, “Controlling the false discovery rate: a practical and powerful approach to multiple testing,” *J R Stat. Soc B*, vol. 57, no. 1, pp. 289–300, 1995.

[157] J. H. Ward, “Hierarchical Grouping to Optimize an Objective Function,” *J. Am. Stat. Assoc.*, vol. 58, no. 301, pp. 236–244, 1963.

[158] Y. Chen, D. Cui, S. Zheng, S. Yang, J. YangTong, D. Yang, J. Fan, J. Zhang, B. Lou, X. Li, X. Zhuge, B. Ye, B. Chen, W. Mao, Y. Tan, G. Xu, Z. Chen, N. Chen, and L. Li, “Simultaneous detection of influenza A, influenza B, and respiratory syncytial viruses and subtyping of influenza A H3N2 virus and H1N1 (2009) virus by multiplex real-time PCR,” *J. Clin. Microbiol.*, vol. 49, no. 4, pp. 1653–1656, 2011.

[159] K. Suzuki, P. Bose, R. Y. Leong-Quong, D. J. Fujita, and K. Riabowol, “REAP: A two minute cell fractionation method.,” *BMC Res. Notes*, vol. 3, p. 294, 2010.

[160] M. S. Taha, K. Nouri, L. G. Milroy, J. M. Moll, C. Herrmann, L. Brunsveld, R. P. Piekorz, and M. R. Ahmadian, “Subcellular fractionation and localization studies reveal a direct interaction of the fragile X mental retardation protein (FMRP) with nucleolin.,” *PLoS One*, vol. 9, no. 3, p. e91465, 2014.

[161] P. L. Apopa, X. He, and Q. Ma, “Phosphorylation of Nrf2 in the transcription activation domain by casein kinase 2 (CK2) is critical for the nuclear translocation and transcription activation function of Nrf2 in IMR-32 neuroblastoma cells.,” *J. Biochem. Mol. Toxicol.*, vol. 22, no. 1, pp. 63–76, 2008.

[162] H. S. Y. Leung, O. T. W. Li, R. W. Y. Chan, M. C. W. Chan, J. M. Nicholls, and L. L. M. Poon, “Entry of influenza A Virus with a α2,6-linked sialic acid binding preference requires host fibronectin.,” *J. Virol.*, vol. 86, no. 19, pp. 10704–13, 2012.

[163] J. D. WATSON and F. H. CRICK, “The structure of DNA.,” *Cold Spring Harb. Symp. Quant. Biol.*, vol. 18, pp. 123–131, 1953.

[164] S. Y. Ow, M. Salim, J. Noirel, C. Evans, I. Rehman, and P. C. Wright, “iTRAQ underestimation in simple and complex mixtures: ‘the good, the bad and the ugly’.,” *J. Proteome Res.*, vol. 8, no. 11, pp. 5347–5355, 2009.

[165] A. K. Chakrabarti, V. C. Vipat, S. Mukherjee, R. Singh, S. D. Pawar, and A. C. Mishra, “Host gene expression profiling in influenza A virus-infected lung epithelial (A549) cells: a comparative analysis between highly pathogenic and modified H5N1 viruses.,” *Virol. J.*, vol. 7, p. 219, 2010.

[166] B. K. Dove, R. Surtees, T. J. H. Bean, D. Munday, H. M. Wise, P. Digard, M. W. Carroll, P. Ajuh, J. N. Barr, and J. a Hiscox, “A quantitative proteomic analysis of lung epithelial (A549) cells infected with 2009 pandemic influenza A virus using stable isotope labelling with amino acids in cell culture.,” *Proteomics*, vol. 12, no. 9, pp. 1431–6, 2012.

[167] Y. Yageta, Y. Ishii, Y. Morishima, H. Masuko, S. Ano, T. Yamadori, K. Itoh, K. Takeuchi, M. Yamamoto, and N. Hizawa, “Role of Nrf2 in host defense against influenza virus in cigarette smoke-exposed mice.,” *J. Virol.*, vol. 85, no. 10, pp. 4679–90, 2011.

[168] M. J. Kesic, S. O. Simmons, R. Bauer, and I. Jaspers, “Nrf2 expression modifies influenza A entry and replication in nasal epithelial cells.,” *Free Radic. Biol. Med.*, vol. 51, no. 2, pp. 444–53, 2011.

[169] B. Kosmider, E. M. Messier, W. J. Janssen, P. Nahreini, J. Wang, K. L. Hartshorn, and R. J. Mason, “Nrf2 protects human alveolar epithelial cells against injury induced by influenza A virus.,” *Respir. Res.*, vol. 13, p. 43, 2012.

[170] J. Kim, Y. N. Cha, and Y. J. Surh, “A protective role of nuclear factor-erythroid 2-related factor-2 (Nrf2) in inflammatory disorders,” *Mutation Research - Fundamental and Molecular Mechanisms of Mutagenesis*, vol. 690, no. 1–2. Elsevier B.V., pp. 12–23, 2010.

[171] S. K. Niture, R. Khatri, and A. K. Jaiswal, “Regulation of Nrf2-an update.,” *Free Radic. Biol. Med.*, vol. 66, pp. 36–44, 2014.

[172] A. Jacobs and M. Worwood, “Ferritin in serum. Clinical and biochemical implications.,” *N. Engl. J. Med.*, vol. 292, no. 18, pp. 951–956, 1975.

[173] G. A. Kaysen, “Biochemistry and biomarkers of inflamed patients: why look, what to assess.,” *Clin. J. Am. Soc. Nephrol.*, vol. 4 Suppl 1, pp. S56–63, 2009.

[174] P. Z. Soepandi, “Clinical Course of Avian Influenza A(H5N1) in Patients at the Persahabatan Hospital, Jakarta, Indonesia, 2005-2008,” *CHEST J.*, vol. 138, no. 3, p. 665, 2010.

[175] W. Zhang, H. Li, G. Cheng, S. Hu, Z. Li, and D. Bi, “Avian influenza virus infection induces differential expression of genes in chicken kidney,” *Res. Vet. Sci.*, vol. 84, no. 3, pp. 374–81, 2008.

[176] S. A. Chanas, Q. Jiang, M. McMahon, G. K. McWalter, L. I. McLellan, C. R. Elcombe, C. J. Henderson, C. R. Wolf, G. J. Moffat, K. Itoh, M. Yamamoto, and J. D. Hayes, “Loss of the Nrf2 transcription factor causes a marked reduction in constitutive and inducible expression of the glutathione S-transferase Gsta1, Gsta2, Gstm1, Gstm2, Gstm3 and Gstm4 genes in the livers of male and female mice.,” *Biochem. J.*, vol. 365, no. Pt 2, pp. 405–16, 2002.

[177] T. Hayakawa, “Glutathione S-transferases in the metabolism of foreign compounds.,” *Ecotoxicol. Environ. Saf.*, vol. 1, no. 3, pp. 305–9, 1977.

[178] W. B. Jakoby, “The glutathione S-transferases: a group of multifunctional detoxification proteins.,” *Adv. Enzymol. Relat. Areas Mol. Biol.*, vol. 46, pp. 383–414, 1978.

[179] P. Checconi, S. Salzano, L. Bowler, L. Mullen, M. Mengozzi, E.-M. Hanschmann, C. H. Lillig, R. Sgarbanti, S. Panella, L. Nencioni, A. T. Palamara, and P. Ghezzi, “Redox proteomics of the inflammatory secretome identifies a common set of redoxins and other glutathionylated proteins released in inflammation, influenza virus infection and oxidative stress.,” *PLoS One*, vol. 10, no. 5, p. e0127086, 2015.

[180] S. Aras, O. Pak, N. Sommer, R. Finley, M. Hüttemann, N. Weissmann, and L. I. Grossman, “Oxygen-dependent expression of cytochrome c oxidase subunit 4-2 gene expression is mediated by transcription factors RBPJ, CXXC5 and CHCHD2.,” *Nucleic Acids Res.*, vol. 41, no. 4, pp. 2255–66, 2013.

[181] M. Hüttemann, B. Kadenbach, and L. I. Grossman, “Mammalian subunit IV isoforms of cytochrome c oxidase.,” *Gene*, vol. 267, no. 1, pp. 111–23, 2001.

[182] The GeneCards Human Gene Database, “Fibronectin 1,” 2015. [Online]. Available: http://www.genecards.org/cgi-bin/carddisp.pl?gene=FN1&search=02f39e910110ffe000617406b6f2d659. [Accessed: 01-Jun-2015].

[183] P. Singh, C. Carraher, and J. E. Schwarzbauer, “Assembly of fibronectin extracellular matrix.,” *Annu. Rev. Cell Dev. Biol.*, vol. 26, pp. 397–419, Jan. 2010.

[184] J. Sottile and J. Chandler, “Fibronectin matrix turnover occurs through a caveolin-1-dependent process.,” *Mol. Biol. Cell*, vol. 16, no. 2, pp. 757–768, 2005.

[185] F. Shi and J. Sottile, “MT1-MMP regulates the turnover and endocytosis of extracellular matrix fibronectin.,” *J. Cell Sci.*, vol. 124, no. Pt 23, pp. 4039–50, 2011.

[186] A. M. Salicioni, K. S. Mizelle, E. Loukinova, I. Mikhailenko, D. K. Strickland, and S. L. Gonias, “The low density lipoprotein receptor-related protein mediates fibronectin catabolism and inhibits fibronectin accumulation on cell surfaces.,” *J. Biol. Chem.*, vol. 277, no. 18, pp. 16160–6, 2002.

[187] I. Z. A. Pawluczyk, S. R. Patel, and K. P. G. Harris, “Perindoprilat modulates the activity of lipoprotein receptor-related protein in human mesangial cells.,” *J. Biol. Chem.*, vol. 283, no. 8, pp. 4588–94, 2008.

[188] X. Wang, T. Oka, F. L. Chow, S. B. Cooper, J. Odenbach, G. D. Lopaschuk, Z. Kassiri, and C. Fernandez-Patron, “Tumor necrosis factor-alpha-converting enzyme is a key regulator of agonist-induced cardiac hypertrophy and fibrosis.,” *Hypertension*, vol. 54, no. 3, pp. 575–82, 2009.

[189] M. P. DeBerge, K. H. Ely, G.-S. Cheng, and R. I. Enelow, “ADAM17-mediated processing of TNF-α expressed by antiviral effector CD8+ T cells is required for severe T-cell-mediated lung injury.,” *PLoS One*, vol. 8, no. 11, p. e79340, 2013.

[190] M. P. DeBerge, K. H. Ely, P. F. Wright, E. B. Thorp, and R. I. Enelow, “Shedding of TNF receptor 2 by effector CD8+ T cells by ADAM17 is important for regulating TNF- availability during influenza infection,” *J. Leukoc. Biol.*, 2015.

[191] J. Li, X. Tang, and X. Chen, “Comparative effects of TGF-β2/Smad2 and TGF-β2/Smad3 signaling pathways on proliferation, migration, and extracellular matrix production in a human lens cell line.,” *Exp. Eye Res.*, vol. 92, no. 3, pp. 173–9, 2011.

[192] C. Li, S. Jiao, G. Wang, Y. Gao, C. Liu, X. He, C. Zhang, J. Xiao, W. Li, G. Zhang, B. Wei, H. Chen, and H. Wang, “The Immune Adaptor ADAP Regulates Reciprocal TGF-β1-Integrin Crosstalk to Protect from Influenza Virus Infection,” *PLOS Pathog.*, vol. 11, no. 4, p. e1004824, 2015.

[193] L. Jolly, A. Stavrou, G. Vanderstoken, V. A. Meliopoulos, A. Habgood, A. L. Tatler, J. Porte, A. Knox, P. Weinreb, S. Violette, T. Hussell, M. Kolb, M. R. Stampfli, S. Schultz-Cherry, and G. Jenkins, “Influenza Promotes Collagen Deposition via v 6 Integrin-mediated Transforming Growth Factor Activation,” *J. Biol. Chem.*, vol. 289, no. 51, pp. 35246–35263, 2014.

[194] S. L. Ashley, Y. Jegal, T. A. Moore, L. F. van Dyk, Y. Laouar, and B. B. Moore, “γ-Herpes virus-68, but not Pseudomonas aeruginosa or influenza A (H1N1), exacerbates established murine lung fibrosis.,” *Am. J. Physiol. Lung Cell. Mol. Physiol.*, vol. 307, no. 3, pp. L219–30, 2014.

[195] H. Fujiwara, Y. Hayashi, N. Sanzen, R. Kobayashi, C. N. Weber, T. Emoto, S. Futaki, H. Niwa, P. Murray, D. Edgar, and K. Sekiguchi, “Regulation of mesodermal differentiation of mouse embryonic stem cells by basement membranes.,” *J. Biol. Chem.*, vol. 282, no. 40, pp. 29701–11, 2007.

[196] D. Lan, C. Tang, M. Li, and H. Yue, “Screening and identification of differentially expressed genes from chickens infected with Newcastle disease virus by suppression subtractive hybridization.,” *Avian Pathol.*, vol. 39, no. 3, pp. 151–9, 2010.

[197] J. O. Humtsoe, M. Liu, A. B. Malik, and K. K. Wary, “Lipid Phosphate Phosphatase 3 Stabilization of -Catenin Induces Endothelial Cell Migration and Formation of Branching Point Structures,” *Mol. Cell. Biol.*, vol. 30, no. 7, pp. 1593–1606, 2010.

[198] A. Hillesheim, C. Nordhoff, Y. Boergeling, S. Ludwig, and V. Wixler, “β-catenin promotes the type I IFN synthesis and the IFN-dependent signaling response but is suppressed by influenza A virus-induced RIG-I/NF-κB signaling.,” *Cell Commun. Signal.*, vol. 12, p. 29, 2014.

[199] M. Hiyoshi, I. L. Indalao, M. Yano, K. Yamane, E. Takahashi, and H. Kido, “Influenza A virus infection of vascular endothelial cells induces GSK-3β-mediated β-catenin degradation in adherens junctions, with a resultant increase in membrane permeability.,” *Arch. Virol.*, vol. 160, no. 1, pp. 225–34, 2015.

[200] A. R. Grassian, F. Lin, R. Barrett, Y. Liu, W. Jiang, M. Korpal, H. Astley, D. Gitterman, T. Henley, R. Howes, J. Levell, J. M. Korn, and R. Pagliarini, “Isocitrate dehydrogenase (IDH) mutations promote a reversible ZEB1/microRNA (miR)-200-dependent epithelial-mesenchymal transition (EMT).,” *J. Biol. Chem.*, vol. 287, no. 50, pp. 42180–94, 2012.

[201] K. Kumari, S. Gulati, D. F. Smith, U. Gulati, R. D. Cummings, and G. M. Air, “Receptor binding specificity of recent human H3N2 influenza viruses.,” *Virol. J.*, vol. 4, no. 1, p. 42, 2007.

[202] E. Hatada, M. Hasegawa, J. Mukaigawa, K. Shimizu, and R. Fukuda, “Control of influenza virus gene expression: quantitative analysis of each viral RNA species in infected cells.,” *J. Biochem.*, vol. 105, no. 4, pp. 537–546, 1989.

[203] P. Stalmans, M. S. Benz, A. Gandorfer, A. Kampik, A. Girach, S. Pakola, and J. A. Haller, “Enzymatic Vitreolysis with Ocriplasmin for Vitreomacular Traction and Macular Holes,” *New England Journal of Medicine*, vol. 367, no. 7. pp. 606–615, 2012.

[204] ThromboGenics, “JETREA,” 2015. [Online]. Available: http://jetrea.com/healthcare-providers/. [Accessed: 27-Jun-2015].

[205] S. Hatakeyama, Y. Sakai-Tagawa, M. Kiso, H. Goto, C. Kawakami, K. Mitamura, N. Sugaya, Y. Suzuki, and Y. Kawaoka, “Enhanced expression of an alpha2,6-linked sialic acid on MDCK cells improves isolation of human influenza viruses and evaluation of their sensitivity to a neuraminidase inhibitor,” *J. Clin. Microbiol.*, vol. 43, no. 8, pp. 4139–46, 2005.

[206] N. Brument, R. Morenweiser, V. Blouin, E. Toublanc, I. Raimbaud, Y. Chérel, S. Folliot, F. Gaden, P. Boulanger, G. Kroner-Lux, P. Moullier, F. Rolling, and A. Salvetti, “A versatile and scalable two-step ion-exchange chromatography process for the purification of recombinant adeno-associated virus serotypes-2 and -5,” *Mol. Ther.*, vol. 6, no. 5, pp. 678–686, 2002.

[207] A. Sicard, M. Yvon, T. Timchenko, B. Gronenborn, Y. Michalakis, S. Gutierrez, and S. Blanc, “Gene copy number is differentially regulated in a multipartite virus.,” *Nat. Commun.*, vol. 4, p. 2248, 2013.

Chapter Eight – Appendix

8.1. Abbreviations

ARDS – Acute Respiratory Distress Syndrome

BME – Betam Meracptoethanol

BSA – Bovine Serum Albumin

CDC – Center for Disease Control and Prevention

DMSO – Dymethil Sulfoxyde

ECM – Extracellular Matrix

ESI – Electrospray Ionization

FBS – Fetal Bovine Serum

FLEUR – Focused Layout of Entities with Unbiased Relations

HA – Hemagglutinin

HAT – Human airway trypsin-like protease

HPAI – Highly Pathogenic Avian Influenza

HPLC – High performance liquid chromatography

IAV – Influenza A viruses

IPA – Ingenuity Pathway Analysis

ISGs – Interferon-stimulated genes

IVPI – Intravenous Pathogenicity Index

LPAI – Low pathogenicity avian influenza

LPS – Lipopolysaccharides

MALDI – Matrix-assisted Laser Desorption Ionization

MEM – Minimum Essential Media

MOI – Multiplicity of Infection

NA – Neuraminidase

PBS – Phosphate-buffered saline

PFU – Plaque Forming Unit

RNP – Ribonucleoprotein

SA – Sialic acid

SDS – Sodium dodecilsulfate

SOP – Standard Operating Procedure

TCID50 – Tissue Culture Infectious Dose 50%

TMPRSS2 – Transmembrane protease serine S1 member 2, AKA TMPRSS11D

TPCK – Tosyl phenylalanyl chloromethyl ketone

WHO – World Health Organization

8.2 Copyright authorizations

Figure 1.1. No authorization needed. Public domain image from the Public Health Image Library (PHIL) of the Center for Diseases Control and Prevention [29].

Figure 1.2. Copyright Clearance is attached

Figure 1.3. Copyright Clearance is attached

Figure 1.4. No authorization needed. Public domain work from Eurosurveillance.

Figure 1.5. Copyright Clearance is attached

Figure 1.6. No authorization needed. Educational use of WHO image.

Figure 1.7. No authorization needed. Public domain map.

Figure 1.8. Copyright Clearance is attached

Figure 1.9. No authorization needed. Public domain image.

Figure 1.10. No authorization needed as per the owners request

Figure 1.11. Personal authorization from Prof Angus Lamond (University of Dundee)

Figure 1.12. Copyright clearance is attached

Figure 1.13. Copyright clearance is attached

Figure 1.14. Copyright clearance is attached

Chapter 3 and 5. Copyright Clearance from Journal of Proteome Research pending for text and figures.

Chapter 4 and 5. Copyright Clearance from PNAS pending for text and figures.

Figure 5.1. Copyright clearance is attached

Figure 5.2. No authorization required as per Journal policies

ELSEVIER LICENSE
TERMS AND CONDITIONS

Apr 26, 2015

This is a License Agreement between Philippe F Simon ("You") and Elsevier ("Elsevier") provided by Copyright Clearance Center ("CCC"). The license consists of your order details, the terms and conditions provided by Elsevier, and the payment terms and conditions.

All payments must be made in full to CCC. For payment instructions, please see information listed at the bottom of this form.

Supplier	Elsevier Limited The Boulevard,Langford Lane Kidlington,Oxford,OX5 1GB,UK
Registered Company Number	1982084
Customer name	Philippe F Simon
Customer address	Dept. of Medical Microbiology Winnipeg, MB R3E0J9
License number	3616650511090
License date	Apr 26, 2015
Licensed content publisher	Elsevier
Licensed content publication	Cell
Licensed content title	Structure of the Hemagglutinin Precursor Cleavage Site, a Determinant of Influenza Pathogenicity and the Origin of the Labile Conformation
Licensed content author	Jue Chen,Kon Ho Lee,David A Steinhauer,David J Stevens,John J Skehel,Don C Wiley
Licensed content date	30 October 1998
Licensed content volume number	95
Licensed content issue number	3
Number of pages	9
Start Page	409
End Page	417
Type of Use	reuse in a thesis/dissertation
Portion	figures/tables/illustrations
Number of figures/tables/illustrations	1
Format	both print and electronic
Are you the author of this Elsevier article?	No

Will you be translating?	No
Original figure numbers	figure 2C-D
Title of your thesis/dissertation	Proteomic Host Responses and Growth Properties of Highly Pathogenic H5N1 and Novel H7N9 Avian Influenza Strains
Expected completion date	Aug 2015
Estimated size (number of pages)	150
Elsevier VAT number	GB 494 6272 12
Permissions price	0.00 USD
VAT/Local Sales Tax	0.00 USD / 0.00 GBP
Total	0.00 USD
Terms and Conditions	

INTRODUCTION

1. The publisher for this copyrighted material is Elsevier. By clicking "accept" in connection with completing this licensing transaction, you agree that the following terms and conditions apply to this transaction (along with the Billing and Payment terms and conditions established by Copyright Clearance Center, Inc. ("CCC"), at the time that you opened your Rightslink account and that are available at any time at http://myaccount.copyright.com).

GENERAL TERMS

2. Elsevier hereby grants you permission to reproduce the aforementioned material subject to the terms and conditions indicated.

3. Acknowledgement: If any part of the material to be used (for example, figures) has appeared in our publication with credit or acknowledgement to another source, permission must also be sought from that source. If such permission is not obtained then that material may not be included in your publication/copies. Suitable acknowledgement to the source must be made, either as a footnote or in a reference list at the end of your publication, as follows:

"Reprinted from Publication title, Vol /edition number, Author(s), Title of article / title of chapter, Pages No., Copyright (Year), with permission from Elsevier [OR APPLICABLE SOCIETY COPYRIGHT OWNER]." Also Lancet special credit - "Reprinted from The Lancet, Vol. number, Author(s), Title of article, Pages No., Copyright (Year), with permission from Elsevier."

4. Reproduction of this material is confined to the purpose and/or media for which permission is hereby given.

5. Altering/Modifying Material: Not Permitted. However figures and illustrations may be altered/adapted minimally to serve your work. Any other abbreviations, additions, deletions and/or any other alterations shall be made only with prior written authorization of Elsevier Ltd. (Please contact Elsevier at permissions@elsevier.com)

6. If the permission fee for the requested use of our material is waived in this instance, please be advised that your future requests for Elsevier materials may attract a fee.

7. Reservation of Rights: Publisher reserves all rights not specifically granted in the combination of (i) the license details provided by you and accepted in the course of this

licensing transaction, (ii) these terms and conditions and (iii) CCC's Billing and Payment terms and conditions.

8. License Contingent Upon Payment: While you may exercise the rights licensed immediately upon issuance of the license at the end of the licensing process for the transaction, provided that you have disclosed complete and accurate details of your proposed use, no license is finally effective unless and until full payment is received from you (either by publisher or by CCC) as provided in CCC's Billing and Payment terms and conditions. If full payment is not received on a timely basis, then any license preliminarily granted shall be deemed automatically revoked and shall be void as if never granted. Further, in the event that you breach any of these terms and conditions or any of CCC's Billing and Payment terms and conditions, the license is automatically revoked and shall be void as if never granted. Use of materials as described in a revoked license, as well as any use of the materials beyond the scope of an unrevoked license, may constitute copyright infringement and publisher reserves the right to take any and all action to protect its copyright in the materials.

9. Warranties: Publisher makes no representations or warranties with respect to the licensed material.

10. Indemnity: You hereby indemnify and agree to hold harmless publisher and CCC, and their respective officers, directors, employees and agents, from and against any and all claims arising out of your use of the licensed material other than as specifically authorized pursuant to this license.

11. No Transfer of License: This license is personal to you and may not be sublicensed, assigned, or transferred by you to any other person without publisher's written permission.

12. No Amendment Except in Writing: This license may not be amended except in a writing signed by both parties (or, in the case of publisher, by CCC on publisher's behalf).

13. Objection to Contrary Terms: Publisher hereby objects to any terms contained in any purchase order, acknowledgment, check endorsement or other writing prepared by you, which terms are inconsistent with these terms and conditions or CCC's Billing and Payment terms and conditions. These terms and conditions, together with CCC's Billing and Payment terms and conditions (which are incorporated herein), comprise the entire agreement between you and publisher (and CCC) concerning this licensing transaction. In the event of any conflict between your obligations established by these terms and conditions and those established by CCC's Billing and Payment terms and conditions, these terms and conditions shall control.

14. Revocation: Elsevier or Copyright Clearance Center may deny the permissions described in this License at their sole discretion, for any reason or no reason, with a full refund payable to you. Notice of such denial will be made using the contact information provided by you. Failure to receive such notice will not alter or invalidate the denial. In no event will Elsevier or Copyright Clearance Center be responsible or liable for any costs, expenses or damage incurred by you as a result of a denial of your permission request, other than a refund of the amount(s) paid by you to Elsevier and/or Copyright Clearance Center for denied permissions.

LIMITED LICENSE

The following terms and conditions apply only to specific license types:

15. **Translation**: This permission is granted for non-exclusive world **English** rights only unless your license was granted for translation rights. If you licensed translation rights you may only translate this content into the languages you requested. A professional translator

must perform all translations and reproduce the content word for word preserving the integrity of the article. If this license is to re-use 1 or 2 figures then permission is granted for non-exclusive world rights in all languages.

16. **Posting licensed content on any Website**: The following terms and conditions apply as follows: Licensing material from an Elsevier journal: All content posted to the web site must maintain the copyright information line on the bottom of each image; A hyper-text must be included to the Homepage of the journal from which you are licensing at http://www.sciencedirect.com/science/journal/xxxxx or the Elsevier homepage for books at http://www.elsevier.com; Central Storage: This license does not include permission for a scanned version of the material to be stored in a central repository such as that provided by Heron/XanEdu.

Licensing material from an Elsevier book: A hyper-text link must be included to the Elsevier homepage at http://www.elsevier.com . All content posted to the web site must maintain the copyright information line on the bottom of each image.

Posting licensed content on Electronic reserve: In addition to the above the following clauses are applicable: The web site must be password-protected and made available only to bona fide students registered on a relevant course. This permission is granted for 1 year only. You may obtain a new license for future website posting.

17. **For journal authors:** the following clauses are applicable in addition to the above:

Preprints:

A preprint is an author's own write-up of research results and analysis, it has not been peer-reviewed, nor has it had any other value added to it by a publisher (such as formatting, copyright, technical enhancement etc.).

Authors can share their preprints anywhere at any time. Preprints should not be added to or enhanced in any way in order to appear more like, or to substitute for, the final versions of articles however authors can update their preprints on arXiv or RePEc with their Accepted Author Manuscript (see below).

If accepted for publication, we encourage authors to link from the preprint to their formal publication via its DOI. Millions of researchers have access to the formal publications on ScienceDirect, and so links will help users to find, access, cite and use the best available version. Please note that Cell Press, The Lancet and some society-owned have different preprint policies. Information on these policies is available on the journal homepage.

Accepted Author Manuscripts: An accepted author manuscript is the manuscript of an article that has been accepted for publication and which typically includes author-incorporated changes suggested during submission, peer review and editor-author communications.

Authors can share their accepted author manuscript:

- immediately
    - via their non-commercial person homepage or blog
    - by updating a preprint in arXiv or RePEc with the accepted manuscript
    - via their research institute or institutional repository for internal institutional uses or as part of an invitation-only research collaboration work-group

- directly by providing copies to their students or to research collaborators for their personal use
- for private scholarly sharing as part of an invitation-only work group on commercial sites with which Elsevier has an agreement

- after the embargo period
  - via non-commercial hosting platforms such as their institutional repository
  - via commercial sites with which Elsevier has an agreement

In all cases accepted manuscripts should:

- link to the formal publication via its DOI
- bear a CC-BY-NC-ND license - this is easy to do
- if aggregated with other manuscripts, for example in a repository or other site, be shared in alignment with our hosting policy not be added to or enhanced in any way to appear more like, or to substitute for, the published journal article.

Published journal article (JPA): A published journal article (PJA) is the definitive final record of published research that appears or will appear in the journal and embodies all value-adding publishing activities including peer review co-ordination, copy-editing, formatting, (if relevant) pagination and online enrichment.

Policies for sharing publishing journal articles differ for subscription and gold open access articles:

Subscription Articles: If you are an author, please share a link to your article rather than the full-text. Millions of researchers have access to the formal publications on ScienceDirect, and so links will help your users to find, access, cite, and use the best available version.

Theses and dissertations which contain embedded PJAs as part of the formal submission can be posted publicly by the awarding institution with DOI links back to the formal publications on ScienceDirect.

If you are affiliated with a library that subscribes to ScienceDirect you have additional private sharing rights for others' research accessed under that agreement. This includes use for classroom teaching and internal training at the institution (including use in course packs and courseware programs), and inclusion of the article for grant funding purposes.

Gold Open Access Articles: May be shared according to the author-selected end-user license and should contain a CrossMark logo, the end user license, and a DOI link to the formal publication on ScienceDirect.

Please refer to Elsevier's posting policy for further information.

18. **For book authors** the following clauses are applicable in addition to the above: Authors are permitted to place a brief summary of their work online only. You are not allowed to download and post the published electronic version of your chapter, nor may you scan the printed edition to create an electronic version. **Posting to a repository:** Authors are permitted to post a summary of their chapter only in their institution's repository.

19. **Thesis/Dissertation**: If your license is for use in a thesis/dissertation your thesis may be

Commercial reuse includes:

- Associating advertising with the full text of the Article
- Charging fees for document delivery or access
- Article aggregation
- Systematic distribution via e-mail lists or share buttons

Posting or linking by commercial companies for use by customers of those companies.

20. **Other Conditions**:

v1.7

Questions? customercare@copyright.com or +1-855-239-3415 (toll free in the US) or +1-978-646-2777.

Gratis licenses (referencing $0 in the Total field) are free. Please retain this printable license for your reference. No payment is required.

NATURE PUBLISHING GROUP LICENSE
TERMS AND CONDITIONS

Apr 26, 2015

This is a License Agreement between Philippe F Simon ("You") and Nature Publishing Group ("Nature Publishing Group") provided by Copyright Clearance Center ("CCC"). The license consists of your order details, the terms and conditions provided by Nature Publishing Group, and the payment terms and conditions.

All payments must be made in full to CCC. For payment instructions, please see information listed at the bottom of this form.

License Number	3616721212056
License date	Apr 26, 2015
Licensed content publisher	Nature Publishing Group
Licensed content publication	Nature Reviews Microbiology
Licensed content title	Influenza A viruses: new research developments
Licensed content author	Rafael A. Medina and Adolfo García-Sastre
Licensed content date	Jul 11, 2011
Volume number	9
Issue number	8
Type of Use	reuse in a dissertation / thesis
Requestor type	academic/educational
Format	print and electronic
Portion	figures/tables/illustrations
Number of figures/tables/illustrations	1
High-res required	no
Figures	Figure 2
Author of this NPG article	no
Your reference number	None
Title of your thesis / dissertation	Proteomic Host Responses and Growth Properties of Highly Pathogenic H5N1 and Novel H7N9 Avian Influenza Strains
Expected completion date	Aug 2015
Estimated size (number of pages)	150
Total	0.00 USD
Terms and Conditions	

Terms and Conditions for Permissions

Nature Publishing Group hereby grants you a non-exclusive license to reproduce this material for this purpose, and for no other use,subject to the conditions below:

1. NPG warrants that it has, to the best of its knowledge, the rights to license reuse of this material. However, you should ensure that the material you are requesting is original to Nature Publishing Group and does not carry the copyright of another entity (as credited in the published version). If the credit line on any part of the material you have requested indicates that it was reprinted or adapted by NPG with permission from another source, then you should also seek permission from that source to reuse the material.

2. Permission granted free of charge for material in print is also usually granted for any electronic version of that work, provided that the material is incidental to the work as a whole and that the electronic version is essentially equivalent to, or substitutes for, the print version.Where print permission has been granted for a fee, separate permission must be obtained for any additional, electronic re-use (unless, as in the case of a full paper, this has already been accounted for during your initial request in the calculation of a print run).NB: In all cases, web-based use of full-text articles must be authorized separately through the 'Use on a Web Site' option when requesting permission.

3. Permission granted for a first edition does not apply to second and subsequent editions and for editions in other languages (except for signatories to the STM Permissions Guidelines, or where the first edition permission was granted for free).

4. Nature Publishing Group's permission must be acknowledged next to the figure, table or abstract in print. In electronic form, this acknowledgement must be visible at the same time as the figure/table/abstract, and must be hyperlinked to the journal's homepage.

5. The credit line should read:
   Reprinted by permission from Macmillan Publishers Ltd: [JOURNAL NAME] (reference citation), copyright (year of publication)
   For AOP papers, the credit line should read:
   Reprinted by permission from Macmillan Publishers Ltd: [JOURNAL NAME], advance online publication, day month year (doi: 10.1038/sj.[JOURNAL ACRONYM].XXXXX)

   Note: For republication from the *British Journal of Cancer,* the following credit lines apply.
   Reprinted by permission from Macmillan Publishers Ltd on behalf of Cancer Research UK: [JOURNAL NAME] (reference citation), copyright (year of publication)For AOP papers, the credit line should read:
   Reprinted by permission from Macmillan Publishers Ltd on behalf of Cancer Research UK: [JOURNAL NAME], advance online publication, day month year (doi: 10.1038/sj.[JOURNAL ACRONYM].XXXXX)

6. Adaptations of single figures do not require NPG approval. However, the adaptation should be credited as follows:

   Adapted by permission from Macmillan Publishers Ltd: [JOURNAL NAME] (reference citation), copyright (year of publication)

   Note: For adaptation from the *British Journal of Cancer,* the following credit line applies.
   Adapted by permission from Macmillan Publishers Ltd on behalf of Cancer Research UK: [JOURNAL NAME] (reference citation), copyright (year of publication)

7. Translations of 401 words up to a whole article require NPG approval. Please visit http://www.macmillanmedicalcommunications.com for more information.Translations of up to a 400 words do not require NPG approval. The translation should be credited as follows:

   Translated by permission from Macmillan Publishers Ltd: [JOURNAL NAME] (reference citation), copyright (year of publication).

   Note: For translation from the *British Journal of Cancer,* the following credit line

applies.

Translated by permission from Macmillan Publishers Ltd on behalf of Cancer Research UK: [JOURNAL NAME] (reference citation), copyright (year of publication)

We are certain that all parties will benefit from this agreement and wish you the best in the use of this material. Thank you.

Special Terms:

v1.1

Questions? customercare@copyright.com or +1-855-239-3415 (toll free in the US) or +1-978-646-2777.

Gratis licenses (referencing $0 in the Total field) are free. Please retain this printable license for your reference. No payment is required.

Order Completed

Thank you very much for your order.

This is a License Agreement between Philippe F Simon ("You") and Springer ("Springer"). The license consists of your order details, the terms and conditions provided by Springer, and the payment terms and conditions.

Get the printable license.

License Number	3638950749331
License date	May 30, 2015
Licensed content publisher	Springer
Licensed content publication	Springer eBook
Licensed content title	Evolution and Ecology of Influenza A Viruses
Licensed content author	Sun-Woo Yoon
Licensed content date	Jan 1, 2014
Type of Use	Thesis/Dissertation
Portion	Figures
Author of this Springer article	No
Original figure numbers	Figure 2
Title of your thesis / dissertation	Proteomic Host Responses and Growth Properties of Highly Pathogenic H5N1 and Novel H7N9 Avian Influenza Strains
Expected completion date	Aug 2015
Estimated size(pages)	150
Total	0.00 USD

CLOSE WINDOW

SIGMA-ALDRICH®

sigma-aldrich.com

3050 Spruce Street, St. Louis, MO 63103 USA
Tel. (800) 521-8956 (314) 771-5765 Fax: (800) 325-5052 (314) 771-5757

Request to Use Sigma-Aldrich Copyrighted Material

Part I – to be filled in by Requester:

Request Date 1 June 2015 Requester Signature [redacted]

Requester Information:

Name	Philippe Simon	Building	1015
Title	PhD Candidate	Street	Arlington
Department	Dept. of Medical Microbiology	City	Winnipeg
Organization	University of Manitoba	State	Manitoba
Phone	(204) 789 5066	Zip Code	R3E-3O2
Email	umsimonp@myumanitoba.ca	Country	Canada

Material Requested to be Used:

Form (check one) [ ] Printed [X] Electronic

Source Publ. Name or URL http://www.sigmaaldrich.com/content/dam/sigma-aldrich/life-science/metabolomics/enzyme-explorer/fibronectin.gif

Source Publ. Edition ——

Source Publ. Year ——

Source Publ. Volume ——

Single Gif image from your website

Description of Material and the intended use (Submit a photocopy or screen image of the context in which the copyrighted material will be used)

A single Gif image showing Fibronectin. It would be used in my PhD thesis

Type of Use (check one) [ ] For Profit [X] Not for Profit

If Material will be reproduced, how many copies will be made? 7

Part II – to be filled in by Sigma-Aldrich Authorizer

Sigma-Aldrich Co. LLC hereby grants permission for one-time use of the material described above for the purpose stated.

- provided a suitable acknowledgment is given, *e.g.*, "Reproduced with permission from Sigma-Aldrich Co. LLC" or "Reproduced with permission of Sigma-Aldrich Co. LLC from publication name, year, volume, issue and pages."
- ar[redacted]ons:

Authorized [redacted] Date 6/11/2015

Please submit completed form and any attachments to legal@sial.com

Rev. April 2014

Enabling Science to Improve the Quality of Life

ELSEVIER LICENSE
TERMS AND CONDITIONS

Apr 27, 2015

This is a License Agreement between Philippe F Simon ("You") and Elsevier ("Elsevier") provided by Copyright Clearance Center ("CCC"). The license consists of your order details, the terms and conditions provided by Elsevier, and the payment terms and conditions.

All payments must be made in full to CCC. For payment instructions, please see information listed at the bottom of this form.

Supplier	Elsevier Limited The Boulevard,Langford Lane Kidlington,Oxford,OX5 1GB,UK
Registered Company Number	1982084
Customer name	Philippe F Simon
Customer address	Dept. of Medical Microbiology Winnipeg, MB R3E0J9
License number	3616920309840
License date	Apr 27, 2015
Licensed content publisher	Elsevier
Licensed content publication	The Lancet
Licensed content title	Influenza
Licensed content author	Nancy J Cox,Kanta Subbarao
Licensed content date	9 October 1999
Licensed content volume number	354
Licensed content issue number	9186
Number of pages	6
Start Page	1277
End Page	1282
Type of Use	reuse in a thesis/dissertation
Portion	figures/tables/illustrations
Number of figures/tables /illustrations	1
Format	both print and electronic
Are you the author of this Elsevier article?	No
Will you be translating?	No

Original figure numbers	Figure 1
Title of your thesis/dissertation	Proteomic Host Responses and Growth Properties of Highly Pathogenic H5N1 and Novel H7N9 Avian Influenza Strains
Expected completion date	Aug 2015
Estimated size (number of pages)	150
Elsevier VAT number	GB 494 6272 12
Permissions price	0.00 USD
VAT/Local Sales Tax	0.00 USD / 0.00 GBP
Total	0.00 USD
Terms and Conditions	

INTRODUCTION

1. The publisher for this copyrighted material is Elsevier. By clicking "accept" in connection with completing this licensing transaction, you agree that the following terms and conditions apply to this transaction (along with the Billing and Payment terms and conditions established by Copyright Clearance Center, Inc. ("CCC"), at the time that you opened your Rightslink account and that are available at any time at http://myaccount.copyright.com).

GENERAL TERMS

2. Elsevier hereby grants you permission to reproduce the aforementioned material subject to the terms and conditions indicated.

3. Acknowledgement: If any part of the material to be used (for example, figures) has appeared in our publication with credit or acknowledgement to another source, permission must also be sought from that source. If such permission is not obtained then that material may not be included in your publication/copies. Suitable acknowledgement to the source must be made, either as a footnote or in a reference list at the end of your publication, as follows:

"Reprinted from Publication title, Vol /edition number, Author(s), Title of article / title of chapter, Pages No., Copyright (Year), with permission from Elsevier [OR APPLICABLE SOCIETY COPYRIGHT OWNER]." Also Lancet special credit - "Reprinted from The Lancet, Vol. number, Author(s), Title of article, Pages No., Copyright (Year), with permission from Elsevier."

4. Reproduction of this material is confined to the purpose and/or media for which permission is hereby given.

5. Altering/Modifying Material: Not Permitted. However figures and illustrations may be altered/adapted minimally to serve your work. Any other abbreviations, additions, deletions and/or any other alterations shall be made only with prior written authorization of Elsevier Ltd. (Please contact Elsevier at permissions@elsevier.com)

6. If the permission fee for the requested use of our material is waived in this instance,

Re: Permission to use a figure from your website

Carol Urquhart (Staff) <c.a.urquhart@dundee.ac.uk>

Tue 4/28/2015 7:32 AM

Inbox

To:Philippe Simon <umsimonp@myumanitoba.ca>;

Dear Phil

Thank you for your email. I have consulted with Professor Lamond and he agrees to you using the image below as you have described.

Good luck with your thesis.

Kind regards
Carol

Carol Urquhart
PA to Professor Angus I Lamond FRS FRSE FMedSci
Centre for Gene Regulation and Expression
College of Life Sciences
University of Dundee
JBC Complex
Dow Street
DUNDEE
DD1 5EH

Tel: +44 (0)1382 385811
Fax: +44 (0)1382 386375

From: Philippe Simon <umsimonp@myumanitoba.ca>
Sent: 28 April 2015 07:18
To: Carol Urquhart (Staff)
Subject: Permission to use a figure from your website

Greetings,

My name is Philippe Simon, I am finishing a PhD in Medical Microbiology at the University of Manitoba in Canada. As I write my thesis, I would like to include this image in the introduction of my thesis. I found it on your website and wanted to get your permission to do so. The work is academic, non-profit and will be available in press and electronically. Of course, this would be cited properly as originating form your website.

(http://www.lamondlab.com/MSResource/images/lcms/ChroSpectra.jpg)

Thank you!

Phil

Philippe Simon MSc McbA
-
PhD Candidate
Influenza Proteomics
FRSQ and MHRC Scholar
Medical Microbiology Dept.
University of Manitoba
Winnipeg, MB
-
www.philippesimon.ca

Title: Practical Implementation of 2D HPLC Scheme with Accurate Peptide Retention Prediction in Both Dimensions for High-Throughput Bottom-Up Proteomics

Author: Ravi C. Dwivedi, Vic Spicer, Michael Harder, et al

Publication: Analytical Chemistry
Publisher: American Chemical Society
Date: Sep 1, 2008

PERMISSION/LICENSE IS GRANTED FOR YOUR ORDER AT NO CHARGE

This type of permission/license, instead of the standard Terms & Conditions, is sent to you because no fee is being charged for your order. Please note the following:

- Permission is granted for your request in both print and electronic formats, and translations.
- If figures and/or tables were requested, they may be adapted or used in part.
- Please print this page for your records and send a copy of it to your publisher/graduate school.
- Appropriate credit for the requested material should be given as follows: "Reprinted (adapted) with permission from (COMPLETE REFERENCE CITATION). Copyright (YEAR) American Chemical Society." Insert appropriate information in place of the capitalized words.
- One-time permission is granted only for the use specified in your request. No additional uses are granted (such as derivative works or other editions). For any other uses, please submit a new request.

If credit is given to another source for the material you requested, permission must be obtained from that source.

Title:	H5N1 Virus Causes Significant Perturbations in Host Proteome Very Early in Influenza Virus-Infected Primary Human Monocyte-Derived Macrophages:
Author:	Chung Yan Cheung, Eric Y. Chan, Alexei Krasnoselsky, David Purdy, Arti T. Navare, Janine T. Bryan, Carolina K.L. Leung, Kenrie P.Y. Hui, Joseph Sriyal Malik Peiris, Michael G. Katze
Publication:	Journal of Infectious Diseases
Publisher:	Oxford University Press
Date:	09/01/2012

Order Completed

Thank you very much for your order.

This is a License Agreement between Philippe F Simon ("You") and Oxford University Press ("Oxford University Press"). The license consists of your order details, the terms and conditions provided by Oxford University Press, and the payment terms and conditions.

Get the printable license.

License Number	3617500901088
License date	Apr 28, 2015
Licensed content publisher	Oxford University Press
Licensed content publication	Journal of Infectious Diseases
Licensed content title	H5N1 Virus Causes Significant Perturbations in Host Proteome Very Early in Influenza Virus-Infected Primary Human Monocyte-Derived Macrophages:
Licensed content author	Chung Yan Cheung, Eric Y. Chan, Alexei Krasnoselsky, David Purdy, Arti T. Navare, Janine T. Bryan, Carolina K.L. Leung, Kenrie P.Y. Hui, Joseph Sriyal Malik Peiris, Michael G. Katze
Licensed content date	09/01/2012
Volume number	206
Issue number	5
Type of Use	Thesis/Dissertation
Requestor type	Academic/Educational institute
Format	Print and electronic
Portion	Figure/table
Number of figures/tables	1
Will you be translating?	No
Author of this OUP article	No
Order reference number	None
Title of your thesis / dissertation	Proteomic Host Responses and Growth Properties of Highly Pathogenic H5N1 and Novel H7N9 Avian Influenza Strains
Expected completion date	Aug 2015
Estimated size(pages)	150
Publisher VAT ID	GB 125 5067 30

NATURE PUBLISHING GROUP LICENSE
TERMS AND CONDITIONS

Apr 28, 2015

This is a License Agreement between Philippe F Simon ("You") and Nature Publishing Group ("Nature Publishing Group") provided by Copyright Clearance Center ("CCC"). The license consists of your order details, the terms and conditions provided by Nature Publishing Group, and the payment terms and conditions.

All payments must be made in full to CCC. For payment instructions, please see information listed at the bottom of this form.

License Number	3617510357218
License date	Apr 28, 2015
Licensed content publisher	Nature Publishing Group
Licensed content publication	Nature Reviews Immunology
Licensed content title	Modelling viral and immune system dynamics
Licensed content author	Alan S. Perelson
Licensed content date	Jan 1, 2002
Volume number	2
Issue number	1
Type of Use	reuse in a dissertation / thesis
Requestor type	academic/educational
Format	print and electronic
Portion	figures/tables/illustrations
Number of figures/tables/illustrations	1
High-res required	no
Figures	figure 1
Author of this NPG article	no
Your reference number	None
Title of your thesis / dissertation	Proteomic Host Responses and Growth Properties of Highly Pathogenic H5N1 and Novel H7N9 Avian Influenza Strains
Expected completion date	Aug 2015
Estimated size (number of pages)	150
Total	0.00 USD
Terms and Conditions	

Terms and Conditions for Permissions

Nature Publishing Group hereby grants you a non-exclusive license to reproduce this material for this purpose, and for no other use,subject to the conditions below: